UNIVERSITAT POLITÈCNICA DE CATALUNYA
BARCELONATECH
Departament de Física

Grup de Morfodinàmica de Costes
Departament de Física

DOCTORAL THESIS

On cross-shore beach profile morphodynamics

PhD thesis presented by
Àngels Fernàndez Mora
for the degree of Doctor

Supervisor:
Dr. Daniel Calvete Manrique

Co-Supervisor:
Prof. Albert Falqués Serra

Barcelona, November 2015

ABSTRACT

The nearshore zone is plenty of 3D morphodynamic patterns resulting from the interaction of waves, currents and sediments. The dynamics of formation and evolution of these patterns is at present a controversial point in coastal research. However, frequently nearshore zone shows a strongly persistent uniformity. In this situation, morphodynamic changes are dominated just by cross-shore processes. Remarkably, although this situation displays much less morphological complexity, cross-shore beach profile morphodynamics is still a research challenge, as sediment transport, in this case, is the result of a very subtle balance between onshore and offshore directed forces that still remain unsolved. The aim of this thesis is to get more insight on the physical processes involving cross-shore beach profile evolution and how relevant are them in the nearshore zone morphodynamics.

To this end, a 1D non-linear morphodynamical model for the evolution of the profile is developed to analyze some relevant aspects of cross-shore beach profile morphodynamics. The AMORFO70 model couples hydrodynamics, sediment transport and bottom changes to account for the morphodynamics feedback. The model considers the depth-integrated and wave-averaged momentum and mass conservation equations coupled with wave- and roller-energy conservation, Snell's law and the dispersion relation under the assumption of alongshore uniformity.

It is well-known that the intra-wave processes, particularly the near-bottom orbital velocity and acceleration, can lead to net onshore sediment transport. The model accounts for the most novel parameterization of the near-bed intra-wave velocity, to analyze the effects of the temporal distribution of the intra-wave near-bottom velocities and accelerations on cross-shore morphodynamics. It is found that accounting for both velocity and acceleration skewness in the sediment transport is essential to properly simulate onshore sandbar migration and the entire profile evolution. Results have shown a strong spatial dependence of sediment transport along the profile, in such a way that in the shoaling zone transport is mostly driven by bed-shear stress (velocity skewness) and the breaking and inner-zone transport is dominated by pressure gradients (acceleration skewness).

The accurate description of sediment transport is a key issue in morphodynamic modeling. The model has been complemented with several transport parameterizations to analyze the differences between morphodynamic predictions related to different sediment transport formulas for different sequences. Results evidenced several differences between the predicted transport rates and also between the predicted incipient bottom changes of the different sedi-

ment transport formulas. It is found that the cross-shore morphodynamic predictions depend strongly on the sediment transport formula that is used and not all of them capture the expected trends. Particularly, formulas that account directly for the effects of wave velocity and acceleration skewness lead to the best predictions, especially for accretionary sequences.

A common procedure on cross-shore beach profile morphodynamic modeling is to neglect the alongshore variability. This assumption has been analyzed for the prediction of the mean profile evolution on the short-, the mid- and the long-term. It has been proven that the model is able to reproduce short- and mid-term evolution of the mean profile with substantial accuracy. Thus, considering the mean profile as the average of the evolution of individual profiles along the shoreline leads to the best results, as 'a way to account for the alongshore variability'. In the long-term it is found that, although predictions may agree with measurements, they do not capture the real morphodynamics. This stresses the relevance of analyzing the behavior of the simulated morphodynamics during long-term evolution to avoid mistakes in the interpretation of the model capabilities.

RESUM

La zona costanera és plena de patrons morfodinàmics 3D que són el resultat de la interacció de l'onatge, els corrents i els sediments. La dinàmica de formació i evolució d'aquests patrons és un punt polèmic en la recerca de la dinàmica costanera. Tot sovint la zona costanera mostra una forta i persistent uniformitat longitudinal. En aquest cas, els canvis morfodinàmics són dominats pels processos transversals. Tot i que aquesta situació suposi una complexitat morfològica menor, la morfodinàmica del perfil transversal de platges és encara un repte científic, ja que, en aquest cas, el transport de sediment és el resultat d'un balanç molt subtil entre les forces onshore i offshore. L'objectiu d'aquesta tesis és obtindre una visió més clara dels processos físics involucrats en l'evolució del perfil transversal i com de importants són en la morfodinàmica costanera.

Amb aquesta finalitat, s'ha desenvolupat un model morfodinàmic 1D no lineal per a l'evolució del perfil transversal per tal d'analitzar alguns aspectes importants de la morfodinàmica del perfil. El model AMORFO70 acobla la hidrodinàmica, el transport de sediments i els canvis de fons per tal de tenir en compte el feedback morfodinàmic. El model compta amb les equacions de conservació de massa i de moment integrades en el temps i en la vertical, acoblades amb les equacions de conservació d'energia de l'onatge i dels rollers, la llei d'Snell i la relació de dispersió tot suposant uniformitat longitudinal.

Els processos entre-ona, i en particular la velocitat i l'acceleració orbitals a prop del fons, poden conduir al transport de sediments cap a terra. El model compta amb una nova parametrització de la velocitat a prop del fons per tal d'analitzar l'efecte de la distribució temporal de les velocitats i acceleracions a prop del fons en la morfodinàmica del perfil. S'ha provat que comptar amb l'skewness de la velocitat i de l'acceleració en el càlcul del transport és essencial per simular correctament la migració cap a terra de les barres de sorra i de l'evolució de tot el perfil. Els resultats mostren una forta dependència espacial del transport al llarg del perfil, de tal manera que a la zona de shoaling el transport és induït per esforços tallants (skewness de velocitats) i que la zona de rompents i de surf està dominada pels gradients de pressió (skewness d'acceleracions).

La descripció precisa del transport de sediments és clau en la modelització morfodinàmica. El model inclou múltiples fórmules del transport per tal d'analitzar les diferències en les prediccions morfodinàmiques de cadascuna d'elles per diferents seqüències. Els resultats evidencien moltes diferències entre els valors de transport i també entre els canvis de fons incipients predits per les diferents fórmules. S'ha provat que les prediccions de l'evolució del perfil de-

penen de la formula de transport emprada i que aquestes prediccions no sempre segueixen les tendències esperades. En particular, les fórmules que compten directament amb el efectes de l'skewness de la velocitat i de l'acceleració donen les millors prediccions, especialment en les seqüències acrecionals.

En la modelització de la morfodinamica del perfil transversal és una practica comuna el no considerar la variabilitat longitudinal. Aquest supòsit ha estat analitzat per a la predicció a curt, mig i llarg termini de l'evolució del perfil mig. S'ha demostrat que el model és capaç de predir acuradament l'evolució a curt i mig termini. El fet de considerar el perfil mig com el promig de les evolucions de diferents perfils al llarg de la costa porta als millors resultats, ja que es 'una manera de tenir en compte la variabilitat longitudinal'. A llarg termini s'ha provat que, tot i que les prediccions poden concordar amb les mesures, no capturen la morfodinamica real. Aquest fet destaca la importància de l'anàlisi de la morfodinàmica simulada durant les evolucions a llarg termini per tal d'evitar errors en la interpretació dels resultats.

ACKNOWLEDGEMENTS/AGRAÏMENTS

Enschede, 5 de Novembre de 2015

Fa poc vaig coneixer a algú que em va fer un símil perfecte sobre el que és fer una tesi: 'Una tesis es como un mono. Al principio es un monito pequeño, que lo llevas en el hombro, le vas dando cacahuetes y se lo enseñas a todo el mundo: 'Mirad que bonito y gracioso es mi monito! Mirad lo que hace!'. Tras cuatro años, el monito no es monito. Es gorila, y ya no lo llevas en el hombro...'. Doncs res, aquí està el meu goril·la. Una mica a contra cor per deixar una etapa que s'acaba... Però aquí estem...

Generalment, als agraïments de les tesis, sempre es parla dels supervisors com aquella font de sabiesa suprema que guia al doctorant. Crec que això está més que clar. He anat a parar a un grup de recerca, 'els morfos', amb una gent fabulosa. No només grans experts, sino, el que crec més important, grans persones. En aquesta aventureta meva m'han acompanyat els meus supervisors: l'Albert Falqués, i especialment en Daniel Calvete. Moltíssimes gràcies pel vostre esforç i dedicació.

Albert: No només ets un gran científic, sempre amb el llapis a la butxaca, sino que ets una de es persones més humanes que he conegut, amb la teva sabiduria, el teu equilibri i la teva empatia. Moltes gràcies per tot.

Daniel: 'los supervisores no tienen superpoderes'. Has sido quien más ha seguido esta tesis, y no solo como supervisor, con la cantidad de discusiones que hemos tenido y las prisas de última hora y las veces que nos hemos reido.... pero tambien me has ayudado y me has escuchado cuando no tenia animos o cuando algunas cosas se ponían difíciles. Has sido como un 'hermanito mayor'. Muchas, muchas gracias.

A la Cesca, pel seu suport, tot i que no hem pogut coincidir gaire, i pels ànims que m'ha donat durant la tesi. Al Niels i al Carles, que m'han acompanyat els primers anys, i també ara a 'Les Holandes'. I als dos nous morfos: en Nabil (Hooolaaaaa!) i en Jaime (que pasa wey!). A tot l'equip de Física Aplicada: Arantxa, Oriol, Àlvar, Fernando, Isabel, Paco,...,sempre m'han resultat molt divertides les vostres xerrades a la hora del café... A l'equip d'informatics del departament: en Toni i en Jordi, que fan una feina extraordinaria, i a l'equip de secretaria de Fisica Aplicada, que sempre m'han arreglat tots els problemes burocràtics (que generalment sempre son molts).

A Jorge Guillen, a qui he d'agraïr la possibilitat d'haver fet aquesta tesis i una frase que crec que no oblidaré mai: 'Una tesis és una carrera de fondo'. Pues será verdad...

To the team of the IMAU, specially, to Huib de Swart, Wim and Niels. The time I spent in Utrecht was a really great experience for me. Thanks!!!

To the team of the SINBAD project, for the chance to join the project and continue working on what I really love. Particularly to Jan Ribberink, Joep van der Zander and Jebbe van der Werf from the UTwente, that are sharing with me my day-by-day. To Tom O'Donoghe, Dominic van der A, Ivan Caceres, David Hurther, Ming Li, Justin Finn and Alan Davies.

A la meva mare, que a la seva manera ha fet la tesi com jo, la ha patit i la ha disfrutat. Al meu pare †, allà on sigui ('Eres el mas mejor.'). A les meves germanes i als meus cunyats, pel seu suport constant durant la tesi i ara més que estic fora. A la Familia Gascon, y especialmente a Inma Gascon, por estar siempre ahí.

A la Vilma, l'Anabella, la Lorena, en Martyn, el Toni, a Rotman padre i ara també, al Dylan, por todo su apoyo.

A la Tulli, per vetllar-me les moltes nits que he estat treballant.

Als 'tullits del Coll': Nuria, Laura, Pep i Pablo. Por mucho, muchísimo. Las charlas, las birrencas, las cenas, el Dixit,... Por vuestro apoyo y vuestros ánimos, por los skypes,... A la crew: Xavi, Ivan, Juanma, Marta y Sonia. Unos en Holanda, otros en Barcelona, pero no importa... Porque siempre puedo contar con vosotros. Make some noise!

A tota la colla de l'hora de dinar a la plaça de Camins (i espero no deixar-me ningú): Roger (peineeee), el Folch, el punki, la Paula, la Nuria, les Carmes, el Genís, l'Alba, el Ferran, la Gemma, la Sandra,... Als companys del Rotman de l'IDAEA: el Quimet, la Laura Scheiber, la Laura Trapote, l'Alex (les cates de vins i el bon menjar),... Als que estan voltant pel món: la Marta i l'Íñic, la Queraleta (i els skypes desde Liverpool), l'Andreu, el Jan,... Als companys d'E.G. i altres no E.G.: el Raulillo, la Roser, el Barberan, la MariCarmen, la Jana, el Julien, la Georgina, el Joshua, la Txell, el Ricard, a la Marta (Cayetano), la Mireia, la Nadia i la Anna i els respectius..., i els que em deixo...

Also, to all the people of the Water Engineering Department of the UTwente: the staff (Suzanne Hulscher, Pieter Roos, Bas Borsje, Denie Augustijn, Katherijna Wijnberg, Jord Warmink,...), the PhD students, my office-room mates, Geert and Leonardo (and Loreto), that make me feel like at home, to Juan Pablo (por todo tu apoyo y por el kapsalon...), Julietta (you are the next one!!!), Filipe, John, Pepijn, Ana Paula, Abebe, Wenglong, Koen, Joep,... and to Anke and Joke. It is being a really great experience for me. To Erik and Lianne, that althought they have leaved the WEM, they helped me a lot during my first months here in Enschede. To Daniel Chico, who told me the story about the thesis, the monkey and the gorilla.

Al Rotman, perquè ell també a fet aquesta tesi (i potser la ha patit més que jo...). Per haver-te trobat, per donar-me tantes forces i per ser una de les raons per seguir lluitant. A pesar de la distancia, sé que estás a mi lado. Gracias, sete.

(...) Allá muevan feroz guerra
ciegos reyes
por un palmo más de tierra,
que yo tengo aquí por mío
cuanto abarca el mar bravío
a quien nadie impuso leyes, (...)

'La canción del pirata', Jose de Espronceda, 1835.

CONTENTS

LIST OF FIGURES

LIST OF TABLES

A la meva familia de sang,
a la meva familia d'amics.
Arriba el telón!

CHAPTER 1

INTRODUCTION

1.1 GENERAL OVERVIEW

The nearshore zone is plenty of morphodynamic patterns resulting from the interaction of waves, currents and sediments. The dynamics of the formation and evolution of these patterns is at present a controversial point in coastal research, in spite of the amount of research that has been conducted during the last 30 years, showing that these patterns emerge essentially as a self-organized response of the coupling between water and sediment. Understanding the physical processes involved in this phenomena is essential not just in a scientific point of view but in their effects on human activities, such as beach nourishments, protection structures or harbors, and environmental issues.

Nearshore morphodynamics has a strong 3D nature that is linked to the wave-breaking induced horizontal circulation in the surf zone. The main sediment transport is driven by the currents: wave-driven longshore current (with possible meandering) and rips associated to 3D patterns. This patterns have been extensively studied by considering the bi-dimensional processes, disregarding the relevance of cross-shore processes in their formation and evolution. However, frequently nearshore zone shows a strongly persistent longshore uniformity persistence and in this situation, in absence of rips and longshore current meandering, morphodynamic changes are dominated just by cross-shore processes. This is the so-called cross-shore beach profile dynamics. In spite that this situation displays much less morphological complexity, cross-shore beach profile morphodynamics is still a research challenge, as sediment transport, in this case, is the result of a very subtle balance between onshore and offshore directed forces (wave-nonlinearities, undertow, gravity,...) that still remain unsolved.

The analysis of cross-shore beach profile dynamics is crucial to understand the global processes involved in near-shore zone evolution. The aim of this thesis is to get more insight on the physical processes involved in the cross-shore beach profile evolution and how relevant are them in the near-shore zone morphodynamics.

1.2 CROSS-SHORE BEACH PROFILE DYNAMICS ON NEARSHORE MORPHODYNAMICS

Nearshore morphodynamics has a strong temporal and three-dimensional variability, linked to the variations of the wave conditions. The interaction of waves, currents and sediments results into regular and well defined patterns both in the morphology and in the hydrodynamics (Wright & Short, 1984; Short & Aagaard, 1993; Blondeaux, 2001). These patterns cover a wide range of spatial and temporal scales. Examples are ripple, megaripples, beach cusps, megacusps, rip channels, sandbar systems, and shoreline sand waves. Each of them has its own characteristic length- and time-scale (Figure 1.1), ranging from cm and minutes such as ripples to km and decades, such as the shoreline sand waves.

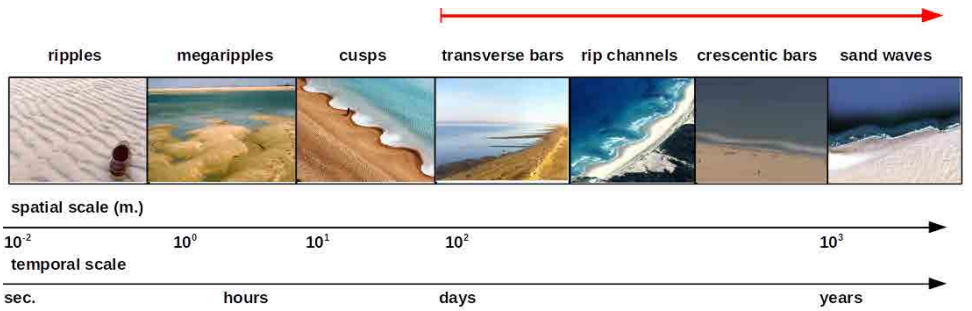

Figure 1.1: Scheme of representative rhythmic patterns and their corresponding time-scales.

Surf-zone sandbars are frequent observable near-shore patterns. These features have a strong effect over the near-shore hydrodynamics and are very sensitive to the wave conditions variations. Their position usually controls the wave-breaking zone and represents a natural barrier against high wave forcing (Figure 1.2). Longshore sandbars are alongshore uniform morphological features characterized by one or more lows (sandbar troughs) and highs (sandbar crests) parallel to the shoreline. They have an active behavior that depends on wave conditions . Longshore sandbars show a strong variability in terms on number of sandbars, position, horizontal and vertical shape and temporal persistence. Furthermore, under certain wave and bathymetric conditions longshore sandbars can become crescentic (rhythmic pattern). Crescentic sandbars are alongshore bars with periodic undulations in the along-shore direction. Their growing mechanism is linked to the 'bed-surf' instability feedback mechanism, in which wave breaking occurs more on the shoals that on the channels, developing onshore currents on the shoals and offshore currents at the channels (Calvete *et al.*, 2005, 2007; Garnier *et al.*, 2008; Castelle *et al.*, 2010*b*, among others). Transverse bars are usually series of sandbars that are steeply oblique or normal oriented with respect to the shoreline and they are usually attached to the coastline or to a longshore sandbar. The formation mechanism is considered from the feedback of an initial perturbation on the bottom with the wave-induced longshore currents (Falqués *et al.*, 1993, 1996; Caballeria *et al.*, 2001).

Despite the high three-dimensional complexity of nearshore morphodynamics, sometimes beach morphology shows an strong alongshore uniformity. In this conditions, cross-shore processes are the main players on near-shore zone evolution, and the cross-shore beach profile is then representative of the beach shape. But not only in these longshore uniform condi-

Figure 1.2: Video images from Castelldefels beach video station, southwest of Barcelona. The video station has been installed in the framework of the IMNOBE project (CTM2009-11892) undertaken by the research group. A, straight shore-parallel bar, 21/06/2010; B, crescentic sandbar, 22/06/2010; C, small oblique sandbars, 29/06/2010

tions the beach profile is considered as a reference of the beach state. The mean cross-shore profile, as the average of the profiles in the alongshore direction, is considered as the mean morphodynamical state of a beach and is an extended tool on beach morphodynamics research (Thornton & Humiston, 1996).

Surf-zone longshore sandbars are a common pattern in the beach states, particularly in the intermediate states and a relevant cross-shore beach profile feature. Their formation is observed when the wave forcing on dissipative beaches decreases or when it increases on reflective beaches (Short, 1999). The longshore sandbars formation has been a controversial issue last 20 years, since two main theories were widely accepted: the stationary long wave theory (Bowen, 1980) and the breaking point theory (Aagaard *et al.*, 2008). This last theory was consistent with the idea of the coupling between hydrodynamics and morphology, and at present the most accepted theory. Many efforts have been also conducted to elucidate the mechanism of migration and decay of sandbars. It is accepted that under low energy conditions sandbars tend to migrate onshore, and even grow, and under high energy conditions they migrate offshore and even decay (Gallagher *et al.*, 1998). This is also linked to the idea that they move to the 'equilibrium breaking point' (Plant *et al.*, 2006; Pape *et al.*, 2010). Also, during the last 10 years, it has been proven that the physical processes related to the skewness and asymmetry of near-bottom velocities, (i. e., bed-shear stress and pressure gradients), play a key role on cross-shore sediment transport and sandbar migration (Hoefel & Elgar, 2003; Foster *et al.*, 2006; Marino-Tapia *et al.*, 2007).

1.3 NUMERICAL MODELING OF BEACH PROFILE EVOLUTION

Previous modeling of the near-shore zone was focused into understanding the formation and evolution of bi-dimensional patterns (further reviewed in de Vriend *et al.*, 1993; Nicholson *et al.*, 1997). These models were lately extended to quasi-3D models by the addition of cross-shore processes, such as the undertow, the bed slope effects and wave non-linearities. Unfortunately, the predicted sediment transport and morphodynamics were very sensitive to small disturbances, as cross-shore sediment transport is the result of a narrow balance between onshore and offshore processes that were not fully understood and not fully implemented in the sediment transport parameterizations.

Recent improvements on near-shore hydrodynamics modeling allow to account for relevant processes involved on near-shore morphodynamics, such as the rollers effects on wave propagation (Reniers *et al.*, 2004; Ribas *et al.*, 2011), new parameterizations of the undertow (Kuriyama & Nakatsukasa, 2010; Nam *et al.*, 2013) or the parameterization of the near-bottom orbital velocity (Abreu *et al.*, 2010; Ruessink *et al.*, 2012). The latter parameterization has been recently implemented in cross-shore profile evolution models (Van der Werf *et al.*, 2012; Dubarbier *et al.*, 2013; Nam *et al.*, 2013). Furthermore, there is a number of sediment transport formulas that account for different processes. Most of these formulas have been widely used and implemented in different morphodynamic models (Ruessink *et al.*, 2007; Nam *et al.*, 2011; Dubarbier *et al.*, 2013). However, many of these parameterizations have been mainly compared and fitted to certain data (flume or field data). The amount of results and experimental conditions make difficult to elucidate which is the morphodynamical behavior related to each sediment transport formula. In summary, the wide range of types of models in terms of the hydrodynamics and the sediment transport processes they consider, makes difficult to

elucidate the relevance of each process on beach profile morphodynamics.

Many efforts has been driven to elucidate these processes by using numerical models of the evolution of the profile (i.e., Roelvink & Broker, 1993; Ribas, 2004; Ruessink *et al.*, 2007; Nam *et al.*, 2009; Castelle *et al.*, 2010*a*). Most of these models are developed to hind- and forecast the cross-shore evolution of the profile, and particularly the formation and migration of longshore sandbars. Although the results of these models are substantially encouraging, they are based on different physical concepts, not only in the hydrodynamics but also in the sediment transport, dismissing perhaps in this way some key processes.

1.4 AIM AND OBJECTIVES

As stated previously, understanding the cross-shore beach dynamics is essential to better understand the global near-shore processes.

The aim of this thesis is to get more insight in the cross-shore beach profile morphodynamics and how relevant are the cross-shore processes in the near-shore zone evolution. To this end, a new process-based model for the evolution of the profile has been developed that captures most processes involved in sediment transport by accounting for several sediment transport formulas and for novel improvements on hydrodynamics. These recent improvements, that have shown up during the development of this research (Abreu *et al.*, 2010; Ruessink *et al.*, 2012), have led to new research lines for this thesis, such as the analysis of the effects of velocity and acceleration skewness on beach profile morphodynamics.

The main research questions involved in this thesis are here detailed:

1. **Which is the morphodynamic prediction of beach profile evolution by using different sediment transport formulas? Which are the main differences and resemblances? Do the different predictions match with the expected trends for accretionary and erosive sequences?**

2. **In which way the addition of the intra-wave near-bottom velocities that account for the wave velocity and acceleration skewness improves cross-shore morphodynamics modeling? Which is the effect of wave velocity and acceleration skewness on nearshore morphodynamics?**

3. **Can we neglect alongshore variability on modeling the short-, mid- and long-term cross-shore profile evolution?**

1.5 OUTLINE OF THE THESIS

The thesis is divided into the following chapters:

- **Chapter 2:** describes the governing equations, parameterizations and numerical implementation of the new process-based model for the evolution of the profile: the AMORFO70 model.

- **Chapter 3:** details the sediment transport formulas implemented in the model.

- **Chapter 4:** addresses the analysis of the effects of neglecting the longshore variability of near-shore processes on modeling the short-, mid- and long-term evolution of the mean profile.
- **Chapter 5:** describes the concept of near-bottom wave velocity and acceleration skewness, their implementation in the model and their distribution along the profile.
- **Chapter 6:** deals with the effects of wave velocity and acceleration skewness on sediment transport and particularly in the onshore sand bar migration process.
- **Chapter 7:** addresses the dependence of the energy-based sediment transport of Hsu *et al.* (2006) on the wave shape in terms of wave velocity and acceleration skewness and the development of a proxy to the wave-related sediment transport.
- **Chapter 8:** contains the analysis of the morphodynamical evolution predicted by different sediment transport formulas.
- **Chapter 9:** gives the overall conclusions of this thesis, and details one-by-one the conclusions related to each research questions. Also, suggestions for further research are exposed.

CHAPTER 2

THE AMORFO70 MODEL

2.1 INTRODUCTION

To get more insight into the cross-shore processes occurring at the near-shore zone, a new process-based model for the cross-shore morphodynamics has been developed. The AMORFO70 model couples hydrodynamics, sediment transport and bottom changes under the assumption of alongshore uniformity. Its main application is to study the cross-shore profile morphodynamics considering different sediment transport mechanisms, as well as to examine the effects of the intra-wave processes on beach profile morphodynamics and on the equilibrium beach profile.

The AMORFO70 model is composed by three modules: the hydrodynamic module, the sediment transport module, and the morphodynamic module. The hydrodynamic module solves the depth-integrated and wave-averaged momentum and mass conservation equations coupled with wave- and roller-energy conservation, Snell's law and the dispersion relation. The hydrodynamic processes include the cross-shore wave transformation (shoaling, refraction, dissipation), the orbital motion and the time-averaged cross-shore and long-shore currents. In Section 2.3, the governing equations involved in this module are detailed. The sediment transport module allows to compute the sediment transport flux by considering different sediment transport parameterizations accounting for the effect of wave velocity and acceleration. Details of the sediment transport formulas that are implemented in the model are in Chapter 3. After the computation of the sediment transport rates, the bed level changes are computed from the gradients in the sediment flux (section 2.3.6) and the bottom is updated through the morphodynamic module. Figure 2.1 outlines the AMORFO70 model structure through the different modules and the main variables involved in each module. In the following sections, the AMORFO70 model is presented. Section 2.2 describes the frame of reference, the main assumptions and the variables considered in the numerical model. Governing equations for the hydrodynamics and the sediment mass conservation are detailed in Section 2.3, followed by the description of the velocities field in Section 2.4. Finally, the numerical implementation is described in Section 2.5.

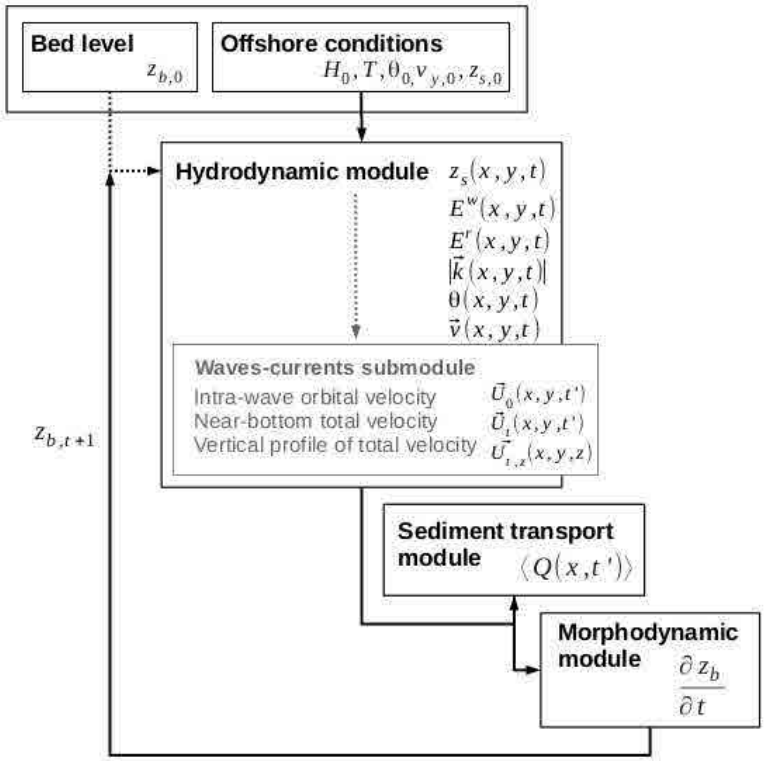

Figure 2.1: Overview of modules and model scheme. Variables are defined in the following sections.

2.2 COORDINATE SYSTEM, MODEL ASSUMPTIONS AND DYNAMICAL UNKNOWNS

We consider a Cartesian coordinate system located in the horizontal plane at the mean sea level, in which the x-axis is normal to the shoreline (here considered rectilinear) and points to the seaward direction, the y-axis is parallel to the shoreline, and the z-axis is the vertical dimension and increases upwards (see Figure 2.2). The coordinate axis is located at the mean sea level (MSL) point. Considering the vector notation of an arbitrary variable $\vec{\chi}_i$, the subscript i stands for the x and y components of the vector, where $i = 1, 2$. The fourth independent variable to be considered is the time t'.

Considering the spatial and temporal complexity of near-shore morphodynamics, the model is simplified by considering the following assumptions:

1. Alongshore uniformity assumption.

   The model assumes alongshore uniformity, so that the variables vary only in the vertical plane $x - z$, that corresponds to the cross-shore transects of the beach (Figure 2.2). This allows to drop out any derivative in the y direction ($\partial/\partial y = 0$).

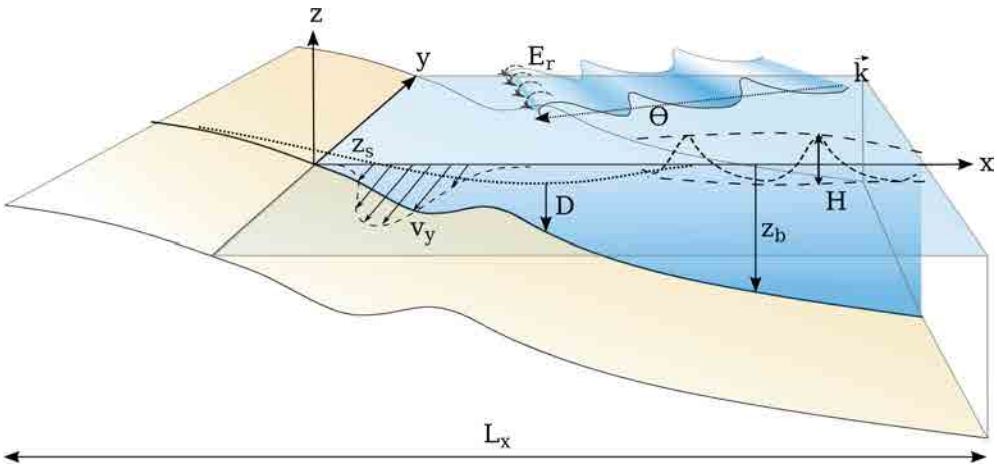

Figure 2.2: Cartesian coordinate system. Hydrodynamic variables are the mean free surface elevation z_s, the wave height H, the wave number $\vec{k}$ and wave incidence angle θ, the depth D and wave- and depth-averaged velocity $\vec{v}$ and the bottom depth z_b.

2. Time Scales

   Near-shore morphodynamics includes a wide range of time scales, from the intra-wave processes (seconds) to the bottom changes (hours, days, months,...). In the model, the rapid hydrodynamics variations are usually averaged over the wave period T. Thus, considering any arbitrary variable $f(t')$, the corresponding wave-averaged variable is defined as

$$f(t) = \langle f(t') \rangle = \frac{1}{T} \int_{t-T/2}^{t+T/2} f(t') dt' \tag{2.1}$$

   Hereinafter, the operator $\langle\rangle$ represents the wave-averaging of any variable. On the other hand, to account for the intra-wave processes that are relevant for bottom changes, the instantaneous time t' is also considered (Section 2.4). Furthermore, morphodynamical changes are considered to be slow respect to the instantaneous time (t') and the hydrodynamic time (t). This defines a 'slow' time variable τ at which the coupling between hydrodynamics and morphodynamics tales place.

3. Depth-averaged variables

   In the near-shore, the vertical length scales are smaller than the horizontal length scales. Thus hydrodynamic variables are considered averaged along the depth. For any arbitrary variable $\hat{f}(x, y, z, t)$, the corresponding depth-averaged variable is defined as

$$f(x, y, t) = \frac{1}{z_s - z_b} \int_{z_b}^{z_s} \hat{f}(x, y, z, t) dz \tag{2.2}$$

Near-shore dynamics can be studied in terms of a set of dependent unknowns in the x, y, z and t' domains, that are related to the wave propagation and the bottom evolution, These variables are the free surface elevation $\hat{z}_s(x, y, t')$, the bottom elevation $z_b(x, y, t')$ and the

fluid velocity field $\vec{U}_t(x, y, z, t')$ due to the intra-wave orbital motion along the water column and the horizontal circulation of currents. Considering the assumptions given above, the wave and depth-averaged velocities are defined as

$$\vec{v}(x, y, t) = \frac{1}{D}\langle \int_{z_b}^{z_s} \vec{U}(x, y, z, t')dz \rangle \qquad i = 1, 2 \quad (2.3)$$

where $D(x, y, t)$ is the water column height ($D = \langle \hat{z}_s \rangle - \langle \hat{z}_b \rangle$) including the tidal oscillation in the water level.

The free surface elevation $\hat{z}_s(x, y, t')$ can be divided into its mean and its fluctuating components $z_s(x, y, t)$ and $z'_s(x, y, t')$, respectively. This last term is the rapid oscillation of the surface related to the incoming waves and is a function of the wave phase $\Phi(x, y, t)$ and the root mean squared of the wave height $H(x, y)$ (Longuet-Higgins, 1952). During the wave propagation, the wave energy density $E^w(x, y, t)$ and the roller energy density $E^r(x, y, t)$ balances are considered. The wave phase Φ is related to the wave vector $\vec{k}(x, y, t)$ and the wave frequency ω. Furthermore, the wave vector is related to the wave number and the wave direction as $k = |\vec{k}|(\cos\theta, \sin\theta)$. The wave direction represents the incidence angle in which incoming waves propagate respect to the normal of the shoreline ($\theta = 0$ stands for the normal incidence respect to the shoreline).

Summarizing, the dynamical unknowns are:

- $z_s(x, y, t)$, the mean free surface elevation,
- $E^w(x, y, t)$ and $E^r(x, y, t)$, the wave and roller energy density, respectively.
- $\vec{v}(x, y, t)$, the depth- and wave-averaged horizontal velocity vector.
- $\vec{k}(x, y, t)$, the wave vector, or, $|\vec{k}|$, the wave number, and θ, the wave incidence angle.
- $z_b(x, y, \tau)$, the bed level.

2.3 GOVERNING EQUATIONS

The hydrodynamic module involves the set of partial equations of mass, momentum, wave energy and roller energy balance complemented with the dispersion relation and Snell's law, assuming periodic wave motion and the instantaneous accommodation of hydrodynamics to the bottom, which means that $\partial/\partial t = 0$ (Stive, 1986; Svendsen & Putrevu, 1995).

2.3.1 WATER MASS BALANCE

The water mass balance equation in a horizontal flow is (e.g. Mei, 1989)

$$\nabla \cdot (D\vec{v}) = 0 \quad (2.4)$$

where D is the total mean depth, $D = \langle z_s - z_b \rangle$ and z_s is the water elevation respect to the mean sea level (MSL) and z_b is the bottom elevation. The wave- and depth-average water mass flux $\vec{\mathcal{M}} = \rho\vec{v}D$ is defined across a vertical plane of unit width. This flux accounts for the onshore directed flux between the wave trough and crest (Stokes drift), and the offshore flux below the wave through (undertow).

2.3.2 WAVE PHASE: DISPERSION RELATION - REFRACTION

Under the assumption that the wave field spectrum is narrow in frequency and direction, the dispersion relation describes the wave propagation by defining the relation between the wave frequency and the wave number k. It reads

$$\sigma^2 = gk \tanh(kD) \tag{2.5}$$

in which σ is the intrinsic frequency and g is the acceleration due to gravity. Considering the waves and currents interaction, $\sigma = \omega_a - v_y k_y$, where the absolute wave frequency $\omega_a = 2\pi/T$ is constant because of the conservation of wave crests, T is the wave period, v_y is the wave and depth-averaged long-shore current and $k_y = k \sin\theta$ is the y component of the wave number $\vec{k}$.

Wave refraction during the propagation follows the Snell's law:

$$k \sin\theta = k_0 \sin\theta_0 \tag{2.6}$$

where θ is the incidence angle and the subscript 0 stands for the values of the variables at the seaward boundary.

2.3.3 WAVE ENERGY CONSERVATION

Under the assumption of alongshore uniformity and the quasi-steady conditions, the wave energy balance, that accounts for wave-current interactions, reads

$$\frac{\partial}{\partial x}(c_g E^w \cos\theta) + S^w_{xy}\frac{\partial v_y}{\partial x} = -\mathcal{D}_w \tag{2.7}$$

where c_g is the modulus of the group velocity, S^w_{xy} is the off-diagonal wave induced radiation stress $S^w_{i,j}$ (detailed in Section 2.3.7.1), and $\mathcal{D}^w$ is the wave breaking dissipation (see Section 2.3.7.2). The wave energy density E^w is approximated in terms of the root mean squared wave height H, by considering the random wave statistic formulation of Longuet-Higgins (1952). It reads

$$E^w = \frac{1}{8}\rho g H^2 \tag{2.8}$$

where ρ is the water density.

2.3.4 ROLLER ENERGY CONSERVATION EQUATION

In order to better describe the transformation of wave energy into turbulent energy at breaking, the roller formulation is adopted, accounting for the delay in the dissipation process and the shifting of the set-up region. The balance of roller energy E^r is modeled according to Ribas *et al.* (2011), as an extension of the one proposed by Reniers *et al.* (2004), which was adapted to account for wave-current interactions. It reads

$$\frac{\partial}{\partial x}(2cE^r \cos\theta) + S^r_{xy}\frac{\partial v_y}{\partial x} = -\mathcal{D}^r + \mathcal{D}^w \tag{2.9}$$

Here, E^r is the roller energy, c is the modulus of the phase velocity, S^r_{xy} is the off-diagonal component of the roller radiation stress tensor S^r_{ij} (detailed in Section 2.3.7.1) and D^r is the roller energy dissipation (detailed in Section 2.3.7).

2.3.5 MOMENTUM BALANCE

The depth- and wave-averaged Navier-Stokes equations lead to the momentum balance equation

$$v_j \frac{\partial v_i}{\partial x_j} = -g\frac{\partial z_s}{\partial x_i} - \frac{1}{\rho D}\frac{\partial}{\partial x_j}(S^w_{ij} + S^r_{ij}) - \frac{\tau_{bi}}{\rho D} \qquad i = 1, 2 \quad (2.10)$$

The $x-$component of the momentum balance equation governs the mean free surface level and represents the balance between the pressure and the radiation tensor gradients[i]:

$$0 = -g\frac{\partial z_s}{\partial x} - \frac{1}{\rho D}\frac{\partial}{\partial x}(S^w_{xx} + S^r_{xx}) \quad (2.11)$$

where S^w_{xx} and S^r_{xx} are the $x-$components of the wave and roller radiation stresses tensor respectively. On the other hand, the off-diagonal component of the momentum conservation equation governs the long-shore current through the balance between the driving forces (radiation stresses) and the frictional forces (bed-shear stresses):

$$0 = -\frac{1}{\rho D}\frac{\partial}{\partial x}(S^w_{xy} + S^r_{xy}) - \frac{\tau_{by}}{\rho D} \quad (2.12)$$

where S^w_{xy} and S^r_{xy} are the off-diagonal components of the radiation stresses tensor for waves and rollers respectively (see Section 2.3.7.1) and τ_{by} is the bed-shear stress (see section 2.3.7.3).

2.3.6 SEDIMENT MASS BALANCE

The morphodynamic module of the model accounts for the sediment depth-averaged mass balance equation as

$$\frac{\partial z_b}{\partial t} = -\frac{1}{(1-n)}\frac{\partial Q_x}{\partial x} \quad (2.13)$$

in which bed evolution is proportional to the divergence of the sediment transport rate Q_x in the cross-shore direction, and where t is the morphodynamic time (detailed in Section 2.2) and n is the porosity of sediment.

The sediment transport rate Q_x is computed using different parameterizations, according to different underlying physics accounted for in the formulas (energy-based models, bed-load transport models and suspended-load models). These parameterizations are detailed in Chapter 3.

[i] Note that the Reynolds turbulent stresses are neglected in the model (Longuet-Higgins & Stewart, 1964). This is a common simplification of hydrodynamics in cross-shore beach profile models.

2.3.7 MODEL PARAMETERIZATIONS

2.3.7.1 WAVE AND ROLLER RADIATION STRESSES

The momentum transfer due to the wave radiation stress tensor, S_{ij}^w, is parametrized using the expression of Longuet-Higgins & Stewart (1964):

$$S_{ij}^w = E^w \left(\frac{c_g}{c} \frac{k_i k_j}{k^2} + \left(\frac{c_g}{c} - \frac{1}{2} \right) \delta_{ij} \right) \qquad i = 1, 2 \quad (2.14)$$

where δ_{ij} is the Kronecker delta symbol. The components of the wave radiation stress tensor in equations 2.7, 2.11 and 2.12 that describe the transfer of momentum are the x component S_{xx}^w and the off-diagonal component S_{xy}^w:

$$\begin{cases} S_{xx}^w = E^w \left((1 + (\cos\theta)^2) \left(\frac{c_g}{c} \right) - \frac{1}{2} \right) \\ S_{xy}^w = \frac{c_g}{c} E^w \sin\theta \cos\theta \end{cases} \quad (2.15)$$

Following Svendsen (1984), the roller radiation stress tensor is given by

$$S_{ij}^r = 2E^r \frac{k_i k_j}{k^2} \quad (2.16)$$

The roller radiation stress x component S_{xx}^r and the off-diagonal component S_{xy}^r involved in equations 2.9, 2.11 and 2.12 are

$$\begin{cases} S_{xx}^r = 2E^r (\cos\theta)^2 \\ S_{xy}^r = 2E^r \cos\theta \sin\theta \end{cases} \quad (2.17)$$

The magnitudes of c and c_g are computed by using the linear wave theory and read

$$c = \sqrt{\frac{g}{k} \tanh(kD)} \quad (2.18)$$

$$c_g = \frac{c}{2} \left(1 + \frac{2kD}{\sinh 2kD} \right) \quad (2.19)$$

2.3.7.2 WAVE AND ROLLER ENERGY DISSIPATION

In the surf-zone, dissipation is mainly due to the energy transfer to turbulent eddies (Battjes *et al.*, 1990). According to Thornton & Guza (1983), the bottom friction contribution in this process is negligible, as well as the direct energy transfer into heat due to molecular viscosity. Thus, the model considers only the wave energy dissipation related to the wave breaking process, following the Thornton & Guza (1983) expression:

$$\mathcal{D}^w = \frac{3B^3 \rho g \sigma H_{rms}^5}{32\sqrt{\pi} {\gamma_b}^2 D^3} \left(1 - \left(1 + \left(\frac{H_{rms}}{\gamma_b D} \right)^2 \right)^{-2.5} \right) \quad (2.20)$$

where B describes the type of wave breaking, γ_b is the critical value of the normalized wave height and ρ is the water density. Parameters B and γ_b are the free variables used for the calibration of the hydrodynamics (see Appendix A).

The roller energy dissipation represents the roller energy transfer to turbulent kinetic energy and reads

$$\mathcal{D}^r = 2gE^r \frac{sin\beta_r}{c} \tag{2.21}$$

with the slope of the roller/wave front β_r set to 0.1 (Ruessink *et al.*, 2001).

2.3.7.3 BED-SHEAR STRESSES

The bed-shear stress in the momentum balance equation (Equation 2.12) is parametrized according Feddersen *et al.* (2000):

$$\tau_{by} = \rho c_d \frac{U_{rms}}{\sqrt{2}} v_y \left(1.16^2 + 2\frac{|\vec{v}|^2}{U_{rms}^2}\right)^{1/2} \tag{2.22}$$

where $c_d = [0.4/(\ln(D/z_0) - 1)]^2$ is the bed drag coefficient, U_{rms} is the root-mean-squared wave orbital velocity given by

$$U_{rms} = \frac{Hg}{2c} \frac{\cosh(kz_0)}{\cosh(kD)} \tag{2.23}$$

and z_0 is the bed-roughness length. The bed roughness is considered as a calibration parameter of the hydrodynamics (see Appendix A). Further details of the bed-roughness are described in Chapter 3.

2.3.8 BOUNDARY CONDITIONS AND FIXED PARAMETERS

Considering the set of partial differential equations eqs. (2.4) to (2.7), (2.9), (2.11) and (2.12), the boundary conditions are set at the offshore boundary and at the shoreline.

2.3.8.1 OFFSHORE BOUNDARY CONDITIONS

The offshore boundary is located at $x = L_x$, L_x being the span of the profile (see Figure 2.2). Boundary conditions are related to the drivers in hydrodynamics and are defined by the input parameters at this point, that are the wave height H_0, the wave period T, the sea surface elevation $z_{s,0}$ (tide level), the incidence angle θ_0 and the long-shore current $v_{y,0}$, where the subscript 0 denotes the offshore boundary. Usually the wave parameters are the offshore measured wave conditions. Considering the dynamical unknowns of the hydrodynamic equations (detailed in section 2.2), these are computed through the offshore wave conditions in the corresponding time-step t as follows:

- $z_{s,0}$, the free surface level that is directly given by the tidal conditions.

- E_0^w, the wave energy density that is computed through Equation 2.8 and the offshore wave height H_0.
- E_0^r, the roller energy density, set to $E_0^r = 0$ at this point.
- $\vec{v}_0$, the depth- and wave-averaged horizontal velocity vector that is given by the offshore current conditions.
- $k_0 = |\vec{k}_0|$, the magnitude of the wave number, that is computed by solving the wave dispersion relation (Equation 2.5).
- θ_0, the offshore wave incidence angle.
- $z_{b,0}$, the bed level at the x_0 point.

2.3.8.2 SHORELINE TREATMENT

Near the shoreline, surf-zone hydrodynamics and sediment transport interact with the swash zone processes. The AMORFO70 model does not account for the description of these processes, since the morphodynamic time involved with the swash zone is smaller than that of the surf-zone.

For the hydrodynamics, the model stops the computation at the last point where the depth $D \geq 0.15$ m. This point is named 'last wet point' x_{wet}. On the other hand, an special treatment of the sediment transport and the bottom changes in the shoreline zone is considered, that is further detailed in Chapter 3.

2.3.8.3 OTHER PARAMETERS

Other parameters to be set as model inputs are those related to the sediment characteristics (the grain size, the specific weight and the equilibrium friction angle ϕ_{eq}), the hydrodynamics calibration parameters (B^3, γ_b and z_0) and the roller/wave front slope β_r.

2.4 WAVE AND CURRENT VELOCITY

Water motion in the near-shore is a complex system of fluxes, with several time and length scales. These fluxes are related to the wave orbital motion and the mean currents that interact with the bed driving the sediment transport processes. The fluid velocities considered in the model are here detailed.

2.4.1 MEAN STEADY CURRENTS

The mean current $\vec{U}$ is defined as $\vec{U}(x,y) = U_{tow}(x)\hat{\imath} + v_y(x)\hat{\jmath}$, in which U_{tow} is the offshore directed undertow and v_y is the long-shore mean current.

2.4.1.1 STOKES DRIFT - UNDERTOW

As a result of the mass conservation and the balance of the cross-shore momentum in terms of radiation stresses and set-up, there is a shoreward flux above the wave trough level and an offshore directed flux (undertow) below the wave trough level. In the wave direction, the vertical profile resulting from the Stokes drift and the bed returning flow is parameterized through the Van Rijn (1993) formula

$$U_m(z) = \frac{\omega k H^2}{8 sinh^2(kD)} F(z)$$

$$F(z) = cosh(2k(z-D)) + \frac{3}{2} + \frac{kD}{2} sinh\left(2kD\left(3\frac{z^2}{D^2} - 4\frac{z}{D} + 1\right)\right) +$$

$$+\frac{3}{2}\left(\frac{sinh(2kD)}{2kD} + \frac{3}{2}\right)\left(\frac{z^2}{D^2} - 1\right) \tag{2.24}$$

At the bottom, the last expression leads to the linear theory expression of undertow:

$$U_{tow} = \frac{\omega k H^2}{8 sinh^2(kD)} \tag{2.25}$$

The undertow parameterization is still a sticky point in near-shore hydrodynamic modeling, as, although being recognized as an offshore directed current, existing parameterizations are not able to approximate these currents properly enough. It must be pointed out that these parameterizations are really approximated for flume experiments in which there is no horizontal circulation, but in the case of field conditions, undertow is believed to be strongly influenced by three-dimensional processes. Nevertheless, recently new insights on these parameterizations allow to improve the prediction of the undertow. A recent improvement is the one given by Kuriyama & Nakatsukasa (2010) and Nam *et al.* (2013), that determines the undertow from the mass fluxes due to waves and rollers.

$$U_{tow}(x) = \frac{-(Q^w + Q^r)}{D - |min(\mu_s)|} \tag{2.26}$$

in which $Q^w = E^w/(\rho c)\cos\theta$ and $Q^r = 2E^r/(\rho c)\cos\theta$ are the mass fluxes due to wave motion and surface rollers, respectively, $D - |min(\mu_s)|$ is the water depth below wave trough, and μ_s is determined by the Abreu *et al.* (2010) approximation (Equation 2.31).

2.4.1.2 WAVE DRIVEN CURRENTS

The momentum balance accounts for the depth-averaged cross-shore radiation stress S_{xx}, the pressure and the wave set-up in the x direction and for the balance of the S_{xy} radiation stress, the bed-shear stresses and the depth- and wave-averaged long-shore current in the long-shore direction.

The vertical distribution of a steady current (in this case, the radiation stress related long-shore current v_y) is generally presented as a logarithmic profile. Waves propagating into shallow

waters interacts with currents in such a way that the turbulence generated inside the wave boundary layer affect the velocity profile. Following Van Rijn (1993), the effects on $\vec{v}_{y,z}$ of the wave action is given by

$$\vec{v}_{y,z}(z) = \frac{v_y ln(30z/k_a)}{-1 + ln(30D/k_s)}, \text{for } z \geq \delta$$

$$\vec{v}_{y,z}(z) = \frac{v_{m,\delta} ln(30z/k_s)}{ln(30D/k_s)}, \text{for } z < \delta \tag{2.27}$$

where $\vec{v}_{y,z}(z)$ is the vertical profile of the depth-averaged long-shore current v_y at a certain level z and $v_{m,\delta}$ is the prescribed velocity at the near-bed mixing layer level $\delta = 3\delta_w$, given by:

$$v_{m,\delta} = \frac{v_y ln(30\delta/k_a)}{-1 + ln(30D/k_a)} \tag{2.28}$$

Here, k_s is defined as the effective bed roughness, k_a is the apparent bed roughness and δ_w the thickness of the wave boundary layer (detailed in Chapter 3).

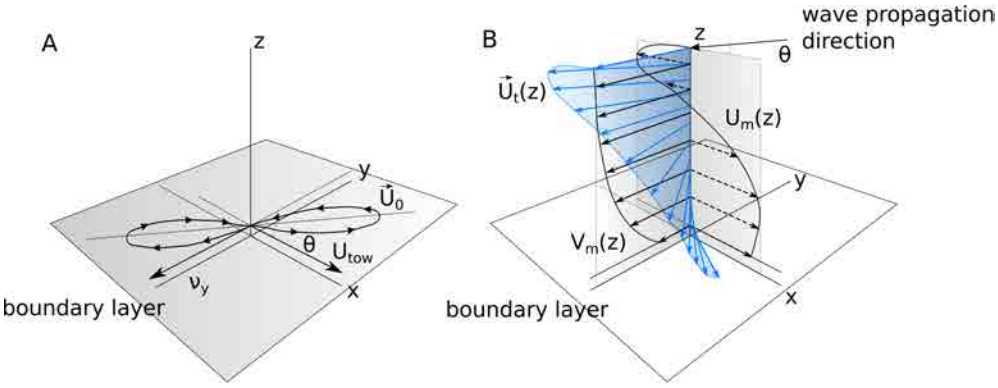

Figure 2.3: Sketch of: A, total near-bottom velocity components: undertow $U_{tow}(x,t)$, long-shore current $v_y(y,t)$ and wave orbital velocity $U_0(x,y,t')$, and B, vertical distribution of the total velocity $\vec{U}_{t,z}(x,y,z,t)$ and the corresponding components: the long-shore current $v_{y,z}(y,z,t)$ (accounting for waves effects) and the Stokes drift $\overline{U}_m(x,y,z,t)$

2.4.2 INTRA-WAVE MOTION DESCRIPTION

As waves approach the coast and wave surface changes from a sinusoidal to a pitched-forward face shape, wave-induced velocities become skewed. Furthermore, as waves get closer to the breaking point, wave velocity asymmetry increases, driving strong near-bottom accelerations. The evolution of the near-bottom velocities that affects to sediment transport (see Figure 2.4). The recent intra-wave near-bottom velocity and acceleration approximation of Abreu *et al.* (2010), improved by Ruessink *et al.* (2012), is incorporated to the model, in order to consider more realistically the shape of near-bottom velocities and, particularly, to consider the effects

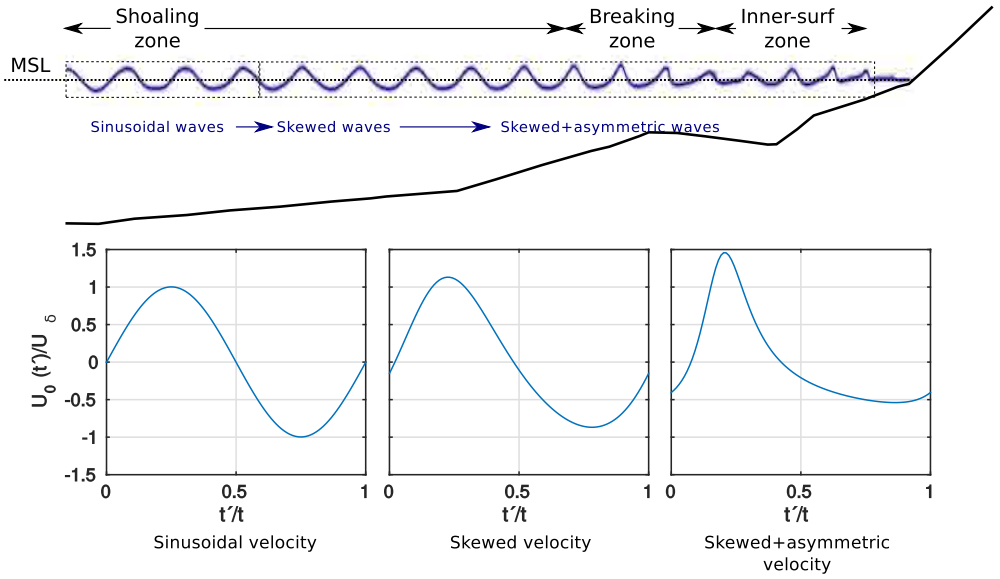

Figure 2.4: Sketch of free surface transformation along the profile and normalized near-bottom velocities shape.

of wave velocity skewness and asymmetry, that play a key role on the near-shore morphodynamics,

This approximation is given by

$$U_0(t') = U_\delta \sqrt{1-r^2}\frac{\left[\sin(\omega t') + \frac{r\sin\phi}{1+\sqrt{1-r^2}}\right]}{[1-r\cos(\omega t'+\phi)]} \tag{2.29}$$

in which $U_\delta = \pi H\{Tsinh(kD)$ is the amplitude of orbital velocity given by the linear theory. Parameters ϕ and r control the wave velocity shape in terms of the phase and non-linearities. They are function of the Ursell number $U_r = 3Hk/8(kD)^3$ and are computed by following the Ruessink *et al.* (2012) approximation.

The corresponding intra-wave acceleration $a(t')$ is given by:

$$a(t') = U_\delta \omega \sqrt{1-r^2}\frac{\cos(\omega t') - r\cos\phi - \frac{r^2}{1+\sqrt{1-r^2}}\sin\phi\sin(\omega t'+\phi)}{[1-r\cos(\omega t'+\phi)]^2} \tag{2.30}$$

and the corresponding wave surface elevation $\mu_s(t')$:

$$\mu_s(t') = \frac{1}{2}H\sqrt{1-r^2}\frac{\sin(\omega t') + \frac{r\sin\phi}{1+\sqrt{1-r^2}}}{1-r\cos(\omega t'+\phi)} \tag{2.31}$$

The wave velocity $U_0(t')$ and $a(t')$ are represented in the wave direction $\vec{k}$.

The wave velocity skewness is defined as $Sk = \langle U_0^3(t')\rangle/\sigma_{U_0}^3$ and wave velocity asymmetry is defined as $As = \langle Hilb(U_0(t'))^3\rangle/\sigma_{U_0}^3$ in which the operator $Hilb$ is the Hilbert transform (Elgar, 1987). (see Chapter 5 for further information)

2.4.3 TOTAL VELOCITY

The total near-bottom velocity vector is defined as $\vec{U}_t = \vec{U}_0 + \vec{U}$, where $\vec{U}_0$ is the intra-wave near-bottom oscillatory velocity vector and $\vec{U}$ is the mean current vector.

The wave-averaged vertical profile of the total velocity $\vec{U}_{t,z}(x, y, z, t)$ is the resultant of the vertical profile of the long-shore steady current $\vec{v}_{yz}$ (Equation 2.27) and the vertical distribution of the Stokes drift (Equation 2.24), as follows

$$\vec{U}_{t,z}(x, y, z, t) = \vec{U}_m(x, y, z, t) + \vec{v}_{yz}(y, z, t) \tag{2.32}$$

Figure 2.3 a) and b) sketches the near-bottom velocity $\vec{U}_t(x, y, t')$ and its components, and the vertical velocity distribution $\vec{U}_{t,z}(x, y, z, t)$.

2.5 NUMERICS

Finite difference methods are used to approximate the solution of the governing equations by approximating the differential equations by other simpler algebraic expressions. These methods need transforming the continuous space in a finite number of elements (grid), at which the variables are calculated.

2.5.1 SPATIAL DISCRETIZATION

The computational domain is set in the $x - z$ plane, and defined at $t = 0$ by the bottom contour given by the initial bathymetry $z_b(x, 0)$, that extends from the initial point of the profile to the most seaward point, in the cross-shore axis x, and from the value of $z_b(x, 0)$ at each cross-shore position, to the free surface level $z_s(x, 0)$, in the vertical axis z.

Figure 2.5 sketches the computational domain and grid.

2.5.1.1 X-SPACE DISCRETIZATION

Given a bathymetry as initial condition $z_b(x, 0)$, (i.e. surveyed bathymetry), it is defined in a finite difference grid with respect to the cross-shore axis x.

Considering that most of morphodynamics changes are located in the surf-zone, and in order to speed up the computations, a non-uniform grid spacing Δx in the x axis is considered, that refines with rising the bottom elevation z_b through the following expression:

$$\begin{aligned}\Delta x(i) = \frac{\Delta x_{max}}{\arctan(l\frac{z_{b,max}-z_{b,med}}{\pi/2})}(\arctan(l\frac{z_{b,i-1}-z_{b,med}}{\pi/2}) \\ + \arctan(l\frac{z_{b,min}+z_{b,med}}{\pi/2})) + \Delta x_{min}\end{aligned} \tag{2.33}$$

where Δx_{max} is an input parameter defining the maximum spacing at the cross-shore position defined by the input parameter $z_{b,max}$ (seaward depth in which $\Delta_x = \Delta x_{max}$); Δx_{min} defines the minimum spacing at the cross-shore position in which bottom depth is defined by

the input parameter $z_{b,min}$ (shoreward depth in which $\Delta_x = \Delta x_{min}$), $z_{b,med}$ is the medium depth ($z_{b,med} = (z_{b,max} + z_{b,min})/2$) and l defines the steepness of the arc-tangent function. The bottom depth z_{b_i} at the new grid point $x_i = x_{i-1} + \Delta x_i$ is computed by a cubic interpolation considering the original bathymetry $z_b(x, 0)$ (defining n_x nodes along the profile). The first node x_0 is located in the offshore boundary. This grid is maintained during all the computational steps. Figure 2.5 A shows a sketch of the grid spacing Δx dependence on the bottom elevation z_b.

2.5.1.2 Z-SPACE DISCRETIZATION

In order to compute velocities and concentration profiles, the model needs a discretization of the z space. To this end, a σ_z coordinate discretization is considered. This kind of grid allows an equal number of vertical levels in the water column, irrespective of its depth. In this way, each level follows the bathymetry (see Figure 2.5 B. The grid spacing is uniform for each vertical line and is defined by the input variable n_z that indicates the number of nodes in the vertical domain.

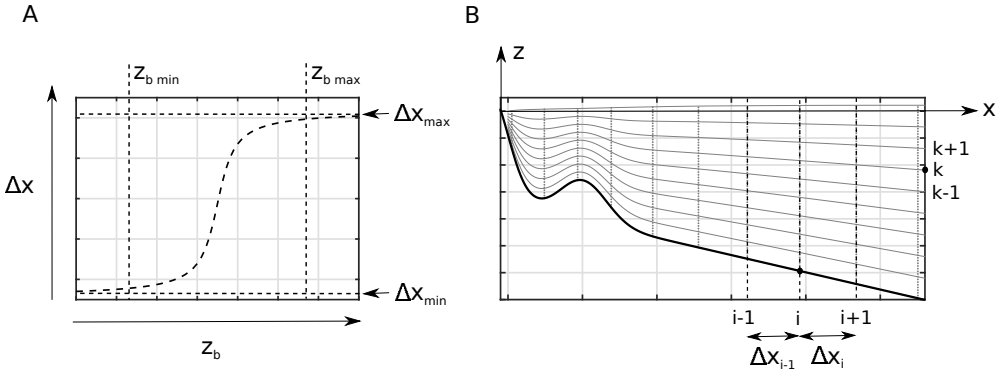

Figure 2.5: Sketch of: A, the non-uniform grid in the x space where Δx_{max} is the maximum value of Δx (in the offshore region of the x space), Δx_{min} is the minimum value of Δx (in the shore-ward zone of the x space), z_{max} is the maximum bottom elevation in which $\Delta x = \Delta x_{max}$, z_{min} is the minimum bottom elevation in which $\Delta x = \Delta x_{min}$, and B, the computational domain in the horizontal and vertical directions.

2.5.1.3 TEMPORAL DISCRETIZATION

Similarly to the spatial coordinates, the time domain must be discretized. The basis of this discretization is the same of the spatial discretization but considering that, whereas a variable in a spatial grid can influence to the flow at any spatial point, forcing in a given instant will affect the flow only in the future (no backward influence). The morphodynamic time-step dt is an input parameter of the model and it is considered uniform in all the computational steps.

On the other hand, to compute the intra-wave time dependent variables (such as $\vec{U}_0$, and its related variables) the instantaneous time domain t', defined within the wave period T, is

adopted. This secondary domain is discretized by using an equispaced grid as a function of n_t, defined as the number of nodes considered in the t' domain which is an input of the model.

2.5.2 SPATIAL DERIVATIVES $\partial/\partial x$: FINITE DIFFERENCE APPROXIMATION

Finite difference methods for the approximation of spatial derivatives rely on approximating the partial derivatives by Taylor expansions series.

There are different schemes to approximate to the spatial derivative at a point: backwards (BD), forward (FD) and centered schemes (CD). These approximations can be used in flow problems: when flow is from node x_{i-1} to x_i the scheme used is BD approximation, and FD when is in the inverse direction. These schemes are also known as *upwind schemes*. Particularly, two finite difference approximations are used in the model: the backwards and centered schemes. The hydrodynamics module needs to use the BD scheme because the forward points are unknowns. The transport module can use both BD and CD schemes to compute the spatial derivatives of the transport variable.

In both cases, the approximation can be considered by an arbitrary m order of derivatives, considering $m+1$ points before or around the computing node (BD or CD). Although high order derivatives approximation requires more computational resources, they are more accurate.

In the hydrodynamic module, the derivatives are approximated via a BD scheme of the kind $(\partial f/\partial x)_i = f(f_i, f_{i-1}, ..., f_{i-n})$, where $f(x)$ is an arbitrary function. For instance, the 2^{nd} order BD for the approximation of the spatial derivative $(\partial f/\partial x)_i$ in a non-uniform grid leads to:

$$\frac{\partial f}{\partial x} = \frac{(\Delta x_{i-1}^2 + \Delta x_i^2) f_i - (\Delta x_i + \Delta x_{i-1})^2 f_i + \Delta x_i^2 f_{i-1}}{\Delta x_{i-1} \Delta x_i (\Delta x_{i-1} + \Delta x_i)} \tag{2.34}$$

where f_i, f_{i-1} and f_{i-2} are the value of the function $f(x)$ at x_i, x_{i-1} and x_{i-2}, respectively, and $\Delta x_i = x_i - x_{i-1}$ and $\Delta x_{i-1} = x_{i-1} - x_{i-2}$. This scheme is used in the evaluation of the spatial derivatives involved in equations eqs. (2.7), (2.9), (2.11) and (2.12).

In the sediment transport and the morphodynamic modules, derivatives are considered by an n order centered differences scheme of the kind $(\partial f/\partial x)_i = f(f_{i+n/2}, ..., f_i, .., f_{i-n/2})$. For instance, the approximation of the 2^{nd} order CD scheme for a non-uniform grid follows

$$\left(\frac{\partial f}{\partial x}\right)_i = \frac{f_{i+1}(\Delta x_i)^2 - f_{i-1}(\Delta x_{i+1})^2 + f_i[(\Delta x_{i+1})^2 - (\Delta x_i)^2]}{\Delta x_{i+1} \Delta x_i (\Delta x_i + \Delta x_{i+1})} \tag{2.35}$$

This approximation is used in the evaluation of the $\partial Q_x/\partial x$ term in equation 2.13.

2.5.3 SOLVER OF THE INITIAL VALUE PROBLEM

The initial value problem is set by the sediment mass conservation equation, which was presented in section 2.3.6:

$$\frac{\partial z_b}{\partial t} = \frac{1}{(1-n)} \frac{\partial Q_x}{\partial x} \tag{2.36}$$

and it is solved by a a Predictor-Corrector multi-point method, a combination of explicit and implicit methods in such a way that the explicit method predicts an approximation to $z_{b,t+1}$, and the implicit method corrects this prediction. Furthermore, multi-point methods use the solution of previous time steps $(t_0, t_1, ..., t_i)$ to find the solution in the time step t_{i+1}.

Particularly, the model uses a combination of the 4^{th} order explicit Adams-Bashforth method and the 4^{th} order implicit Adams-Moulton method.

Considering the initial value problem for the ODE

$$\frac{\partial y}{\partial t} = f(t, y) \tag{2.37}$$

for which y^{n+1} is the arbitrary variable to be solved in the time-step t^{n+1} ($y^{n+1} = y(t^{n+1})$), the Adams-Bashforth method uses the Lagrange polynomial approximation for p^{n+1} based on previous time-steps, where p^{n+1} is the prediction of the unknown y^{n+1}. The scheme of the $4th$ order Adams-Bashforth method follows

$$p^{n+1} = y^n + dtf(t^n, y^n) \qquad n = 0$$

$$p^{n+1} = y^n + \frac{dt}{2}(3f(t^n, y^n) - f(t^{n-1}, y^{n-1})) \qquad n = 1$$

$$p^{n+1} = y^n + dt\left(\frac{23}{12}f(t^n, y^n) - \frac{4}{3}f(t^{n-1}, y^{n-1}) + \frac{5}{12}f(t^{n-2}, y^{n-2})\right) \qquad n = 2$$

$$p^{n+1} = y^n + dt\left(\frac{55}{24}f(t^n, y^n) - \frac{59}{24}f(t^{n-1}, y^{n-1}) + \frac{37}{24}f(t^{n-2}, y^{n-2}) - \frac{3}{8}f(t^{n-3}, y^{n-3})\right) \qquad n \geq 3 \tag{2.38}$$

where dt is the time step. The predicted value p^{n+1} is used as a term for the implicit $4th$ order scheme of Adams-Moulton that follows

$$y^{n+1} = y^n + dtf(t^{n+1}, p^{n+1}) \qquad n = 0$$

$$y^{n+1} = y^n + \frac{dt}{2}(f(t^{n+1}, p^{n+1}) - f(t^n, y^n)) \qquad n = 1$$

$$y^{n+1} = y^n + dt\left(\frac{5}{12}f(t^{n+1}, p^{n+1}) + \frac{2}{3}f(t^n, y^n) - \frac{1}{12}f(t^{n-1}, y^{n-1})\right) \qquad n = 2$$

$$y^{n+1} = y^n + dt\left(\frac{3}{8}f(t^{n+1}, p^{n+1}) + \frac{19}{24}f(t^n, y^n) - \frac{5}{24}f(t^{n-1}, y^{n-1}) + \frac{1}{24}f(t^{n-2}, y^{n-2})\right) \qquad n \geq 3 \tag{2.39}$$

Several methods has been tested previously in the model for the temporal evolution of the profile. Simple explicit methods, such as Euler methods or the Adams-Bashforth method, are low computational demanding but can drive to numerical instabilities (particularly due to using a non-uniform grid). Implicit methods, such as the Adams-Moulton method, are the most stable methods but the Newton scheme to solve the hydrodynamics and sediment transport in the AMORFO70 model requires the solution of an internal Newton for the intra-wave near-bottom velocity at each iteration. This results on high computational cost and can lead to no-solution for complex sediment transport formulas.

2.5.4 NUMERICAL INTEGRATION METHOD: TRAPEZOIDAL RULE

Considering an arbitrary function $f(x)$ over the domain $[a, b]$ discretized in n equispaced nodes, the averaged value of the function is computed by the trapezoidal rule

$$\begin{aligned}\langle\Phi(x)\rangle|_a^b &= \frac{1}{b-a}\sum_{j=1}^{n}\int_{x_{j-1}}^{x_j} f(x)dx = \sum_{j=1}^{n}\left\{\frac{h}{2}[f(x_{j-1}) + f(x_j)]\right\} \\ &= \frac{1}{b-a}(f(x_o) + 2f(x_1) + 2f(x_3) + \cdots + 2f(x_{n-1}) + f(x_n))\end{aligned} \tag{2.40}$$

This formula is used several times in the model,to average in the instantaneous time domain $[0, T]$ the near-bottom velocity $\langle U_t\rangle$ and the sediment transport $\langle Q\rangle$ and the depth-averaged value of suspended transport in the vertical domain $[0, D]$.

CHAPTER 3

SEDIMENT TRANSPORT PARAMETERIZATIONS

3.1 INTRODUCTION

The difficulty on properly predict the morphodynamical changes of beach profile relies on the way the processes involved in sediment transport are accounted for on computing sediment transport rates.

The sediment transport includes two main transport modes, the bed-load transport and the suspended-load transport. The bed-load transport is mainly due to the interaction between particles near the bottom and bed-shear stresses due to fluxes. Suspended-load transport is supported by the turbulence of the fluid and is present primary for fine sediments. It is considered that under different conditions, sediment is mobilized by one or other process. In the alongshore uniformity framework (and normal wave incidence), sediment transport is the results of the differences between the onshore and the offshore hydrodynamic processes. A more exhaustive discussion about sediment transport processes in the nearshore zone can be found in the literature, such as Fredsoe & Deigaard (1992); Nielsen (1992); Van Rijn (1993); Soulsby (1997, among others)

To examine the relevance of the different cross-shore processes involved in sediment transport and their implication on the morphodynamical evolution of the profile under the same forcing, the AMORFO70 model incorporates several sediment transport parameterizations to compute the cross-shore directed sediment transport rate Q_x. In this chapter, the sediment transport formulas used in the model are detailed.

3.2 ENERGY-BASED MODELS

The energy-based models are based on the idea of Bailard & Inman (1981) by considering both the bed-load and the suspended-load processes as the result of the energy transfer of wave motion over the sediment. Bed-load transport is accounted for as interaction between the particles at the bottom, and suspended transport is considered by the advection due to the currents of the turbulent sediment concentration.

3.2.1 HOEFEL & ELGAR (2003) ACCELERATION-BASED TRANSPORT

The Hoefel & Elgar (2003) transport formula is an extension of the Drake & Calantoni (2001) bed-load transport approximation. This parameterization considers that sediment transport is the result of the horizontal pressure gradients on the sediment, that are strongly related to the acceleration skewness of near-bottom orbital motion. Hoefel & Elgar (2003) extended this parameterization to account for the action of random waves as follows

$$Q = \begin{cases} K_a(a_{spike,x} - sign(a_{spike,x})a_{cr}) & a_{spike,x} \geq a_{cr} \\ 0 & a_{spike,x} < a_{cr} \end{cases} \tag{3.1}$$

where, K_a is a constant (set in $1.40 \cdot 10^{-4}\ m\,s$), a_{cr} is the threshold acceleration ($0.5\ \mathrm{m/s^2}$) and $a_{spike} = \langle a(t)^3 \rangle / \langle a(t)^2 \rangle$ is the dimensional acceleration skewness. Subscript x indicates the cross-shore coordinate. The acceleration $a(t)$ is the local temporal derivative of the total velocity U_t. In their approximation, suspended-load transport and currents action are neglected.

Hoefel & Elgar (2003) simulated properly the onshore sandbar migration event during the Duck94 experiment at the FRF-Duck, NC (Gallagher *et al.*, 1998; Elgar *et al.*, 2001), by using the near-bottom current-meters data during the experiment.

3.2.2 HSU *et al.* (2006) ENERGETICS TOTAL LOAD TRANSPORT MODEL

Hsu *et al.* (2006) modified the total-energy based formula of Bailard & Inman (1981) by considering separately the wave action from the current action as follows

$$Q_W = \frac{C_w}{(s-1)g} \left(\frac{\varepsilon_B}{\tan\varphi} \langle |\vec{U}_0|^2 U_{0,x} \rangle + \frac{\varepsilon_S}{W_0} \langle |\vec{U}_0|^3 U_{0,x} \rangle \right) \tag{3.2}$$

$$Q_C = \frac{C_c}{(s-1)g} \left(\frac{\varepsilon_B}{\tan\varphi} \langle |\vec{U}_t|^2 \rangle U_x + \frac{\varepsilon_S}{W_0} \langle |\vec{U}_t|^3 \rangle U_x \right) \tag{3.3}$$

$$Q = Q_W + Q_C \tag{3.4}$$

Here, subscripts W and C indicate the wave term and the wave+currents term respectively, s is the specific gravity (set to 2.65), g is acceleration due to gravity, φ is the friction angle ($\tan\varphi = 0.63$); ε_B and ε_S are the bed-load and the suspended-load transport efficiency parameters (set to $\varepsilon_B = 0.135$ and $\varepsilon_S = 0.015$ (Thornton & Humiston, 1996; Gallagher *et al.*, 1998)), W_0 is the sediment fall velocity (set to $W_0 = 0.025\ \mathrm{ms^{-1}}$, considering an uniform grain size along the profile of $d_{50} = 0.2\ \mathrm{mm}$ (Hsu *et al.*, 2006)) , $\vec{U_0}$ is the near-bottom orbital velocity, $\vec{U_t}$ is the total velocity vector (waves plus currents) and $\vec{U}$ is the mean currents velocity (see Section 2.4). Subscript x indicates the cross-shore component. Vertical

bars indicate the magnitude of the vector. Values of the waves and current friction coefficients C_w and C_c were set to 0.048 and 0.053 in Hsu *et al.* (2006).

This transport formula has been used in morphodynamic models to accurately predict different laboratory and field experiments of the evolution of the cross-shore profile (Hsu *et al.*, 2006; Dubarbier *et al.*, 2013; Fernandez-Mora *et al.*, 2013, 2015*b*, under review).

3.3 BED-LOAD TRANSPORT FORMULAS

Bed-load transport models usually consider that the bed-load transport process is the result of the action of bed-shear stresses on the sediment (Meyer-Peter & Mueller, 1948). The general expression of the volumetric bed-load transport rate Q_b $[m^2/s^{-1}]$ is usually defined as a function of the dimensionless bed-load transport rate Φ:

$$Q = \langle\Phi\rangle\sqrt{(g(s-1)d_{50}^3)} \tag{3.5}$$

where $\langle\Phi\rangle$ is function of the Shields parameter θ', and d_{50} is the grain size and the subscript b indicates bed-load transport mode.

The various bed-load transport formulas based on bed-shear stresses differ in the way that the relation $\Phi(t) = f(\theta'(t))$ is defined. In the following, the bed-load transport parameterizations implemented in the model are detailed.

3.3.1 RIBBERINK (1998) BED-LOAD TRANSPORT

Ribberink (1998) proposed a widely used bed-load transport formula that accounts for the non-linear interaction of the near-bottom velocities and steady currents on defining the Shields parameter θ'. The dimensionless instantaneous bed-load transport rate Φ accounting for the effects of gravity (Ruessink *et al.*, 2007) in the cross-shore direction reads

$$\Phi(t) = m\frac{\beta_s}{(1-\rho)}[|\theta'_{cw}(t)| - \theta_{cr,s}]^n\frac{\theta'_{cw}(t)}{|\theta'_{cw}(t)|} \tag{3.6}$$

where θ_{cw} is the Shields parameter related to both waves and currents action and and $\theta_{cr,s}$ is the critical Shields parameter, m and n are calibration parameters (set to 9.1 and 1.8 respectively). The non-dimensional critical shear stress representing the threshold of motion of sediment is function of the non-dimensional grain size D_* following Van Rijn (1993) (see Section 3.7.1). The Bagnold parameter β_s increases the transport rate in case of downslope transport, and decreases it in case of up slope transport and is defined as

$$\beta_s = \frac{tan\varphi}{tan\varphi + \frac{dz_b}{ds}} \tag{3.7}$$

where $dz_b/ds = (U_x/|\vec{U}|)dzb/dz$.

This formula has been tested under several hydrodynamic and sediment conditions and implemented in many morphodynamical models (Ruessink *et al.*, 2007; Van der A *et al.*, 2010*b*; Van der Werf *et al.*, 2012).

3.3.2 CAMENEN & LARSON (2005) BED-LOAD TRANSPORT

The bed-load transport formula of Camenen & Larson (2005), based on Meyer-Peter & Mueller (1948) and Ribberink (1998) formulas, separates the onshore directed component of the Shields parameter θ_{on} from the offshore directed component θ_{off}. In this way, sediment transport is the result of the balance between onshore directed velocities and offshore currents.

The wave and current related non-dimensional transport of Camenen & Larson (2005) follows

$$\Phi_w = a_w \sqrt{\theta_{cw,on} + \theta_{cw,off}} \theta_{cw,m} \exp\left(-b \frac{\theta_{cr}}{\theta_{cw}}\right) \tag{3.8}$$

$$\Phi_n = a_n \sqrt{\theta_{cn}} \theta_{cw,m} \exp\left(-b \frac{\theta_{cr}}{\theta_{cw}}\right) \tag{3.9}$$

where the w subindex points at the wave direction and the n subindex at the normal direction of waves motion and a_w, a_n and b are calibrating parameters.$\theta_{cw,on}$ and $\theta_{cw,off}$ are the half-period time-averaged values of the waves and currents Shields parameter $\theta_{cw}(t) = 0.5|\vec{U}_0 + \vec{U}\cos\phi|(\vec{U}_0 + \vec{U}\cos\phi)(s-1)gd_{50}$, given by:

$$\theta_{cw,on} = \frac{1}{T_{w,c}} \int_0^{T_{w,c}} \theta'_{cw}(t) dt \tag{3.10}$$

$$\theta_{cw,off} = \frac{1}{T_{w,t}} \int_{T_{w,c}}^{T_{w,t}} \theta'_{cw}(t) dt \tag{3.11}$$

where T_{wc} and T_{wt} are the half-periods in which the instantaneous velocity $\vec{U}_t(t)$ is directed onshore (< 0 in the coordinate system) or offshore (> 0 in the coordinate system). $\theta_{cw,m}$ and θ_{cw} are the mean and maximum combined Shields parameters. ϕ is the angle between waves and currents.

Camenen & Larson (2005) tested the formula and compared it with different bed-load transport formulas by using the data of laboratory experiments, and comparing the amount of sediment transport predicted by the formulas. It has been also used, complemented with suspended transport formulas, by Nam *et al.* (2011) in a morphological evolution model to predict the bottom evolution of beaches around near-shore structures.

3.4 SUSPENDED LOAD TRANSPORT FORMULAS

Suspended transport is classically computed as depth-average of the product of the sediment concentration profile along the water column and the vertical profile of velocities.

$$Q = \int_{-h}^{0} \mathcal{C}(z) \vec{U}_{t,z} dz \tag{3.12}$$

where $\mathcal{C}(z)$ is the time-averaged vertical profile of sediment concentration, $\vec{U}_{t,z}$ is the vertical profile of total velocities along the water column and the subscript s indicates the suspended-load transport mode.

The time-averaged concentration profile follows the solution of the advection-diffusion equation given by

$$\frac{d\mathcal{C}}{dz} = -\frac{\mathcal{C}\omega_s}{\varepsilon_{s,cw}} \tag{3.13}$$

where ω_s is the sediment fall velocity, $\varepsilon_{s,cw}(z)$ is the wave and currents mixing coefficient. Suspended transport parameterizations differ on the definition of the concentration profile in terms of the reference concentration and the mixing coefficient model. In the following, the parameterizations considered by the model are detailed.

3.4.1 BIJKER (1967) CONCENTRATION PROFILE

Following Bijker (1967), the time-averaged suspended sediment concentration profile is given by

$$\frac{\mathcal{C}}{\mathcal{C}_a} = \left[\frac{k_s}{D-k_s}\frac{D-z}{z}\right]^{\frac{w_s}{(\kappa u_{*,cw})}} \tag{3.14}$$

where $\mathcal{C}_a$ is the time-averaged reference concentration at $z = k_s$ (the boundary layer level), that follows

$$\mathcal{C}_a = \frac{b\rho_s d_{50}}{6.34 k_s} exp\left[-\frac{0.27(\rho_s-\rho)g d_{50}}{\nu\tau_{b,cw}}\right] \tag{3.15}$$

where b is an empirical coefficient (set to 5) and $\tau_{b,cw}$ is the total bed-shear stress due to waves and currents (Equation 3.30).

3.4.2 VAN RIJN (1993) SUSPENDED-LOAD CONCENTRATION PROFILE APPROXIMATION

Van Rijn (1993) considered an extended eddy diffusivity profile to account for both wave and current action on computing suspended transport. Considering the equation 3.13, the Van Rijn (1993) parameterization for the concentration profile $C(z)$ is obtained via the numerical integration of

$$\frac{dC}{dz} = \frac{(1-C)^5 C W_0}{\varepsilon_{s,cw}(1+(C/0.65)^{0.5}-2(C/0.65)^{0.4})} \tag{3.16}$$

where C is the vertical concentration, $\varepsilon_{s,cw}$ is the mixing coefficient for waves and currents. In the boundary layer, the reference concentration is

$$\mathcal{C}_a = 0.015\rho_s \frac{d_{50}}{k_s}\frac{T_a^{1.5}}{D_*^{0.3}} \tag{3.17}$$

where T_a is the bed-shear stress parameter defined as $T_a = (\tau_{b,cw}-\tau_{cr})/\tau_c r$, $\tau_{b,cw}$ is the bed-shear stress due to waves and currents and $\tau_{cr} = (\rho_s-\rho)g d_{50}\theta_{cr}$ is the critical bed-shear stress (further detailed in Section 3.7).

The sediment mixing coefficient ε_{cw} related to currents and waves can be written as a function of the current related sediment mixing coefficient ε_c and the wave related sediment mixing coefficient ε_w (Van Rijn, 1993), by

$$\varepsilon_{cw} = \sqrt{\varepsilon_c^2 + \varepsilon_w^2} \tag{3.18}$$

where the current-related mixing coefficient ε_c follows the parabolic-constant approximation:

$$\begin{aligned} \varepsilon_c =& \kappa u_* D \frac{z}{D}(1 - \frac{z}{D}), && z/D < 0.5 \\ \varepsilon_c =& 0.25\kappa u_* D, && z/D > 0.5 \end{aligned} \tag{3.19}$$

and the wave-related mixing coefficient is

$$\begin{aligned} \varepsilon_w =& \varepsilon_{w,bed}, && z \leq \delta_s \\ \varepsilon_w =& \varepsilon_{w,bed} + (\varepsilon_{w,max} - \varepsilon_{w,bed}) \left(\frac{z - \delta_s}{0.5D - \delta_s} \right), && \delta_s < z < 0.5D \\ \varepsilon_w =& \varepsilon_{w,max}, && z \geq 0.5D \end{aligned} \tag{3.20}$$

3.4.3 CAMENEN & LARSON (2008) SUSPENDED-LOAD TRANSPORT APPROXIMATION

Following a similar concept as the Camenen & Larson (2005) bed-load formula, Camenen & Larson (2008) simplifies the suspended-load transport by using the solution for the total suspended load transport of Madsen & Grant (1976) and considering the difference between the onshore and the offshore directed velocities as stirring term. Assuming an exponential profile for the sediment concentration and a uniform value over depth for the time-averaged current velocity, the resulting sediment transport rate can be estimated as

$$Q = \vec{U}_t \mathcal{C}_a^{CL} \frac{\varepsilon}{W_0} \left[1 - exp\left(-\frac{W_0 D}{\varepsilon} \right) \right] = \overline{U} F(\mathcal{C}_a^{CL}.\varepsilon) \tag{3.21}$$

Considering the action of waves and currents separately, equation 3.21 can be written as follows:

$$Q_w = (U_{cw,on} - U_{cw,off}) F(\mathcal{C}_a^{CL}.\varepsilon)$$

in the wave direction

$$Q_c = U_c F(\mathcal{C}_a^{CL}.\varepsilon) \tag{3.22}$$

normal to wave direction. The velocity $U_{cw} = U_0 + U_c \cos\phi$ is the near-bottom velocity in the waves direction (ϕ is the angle between waves and currents) and $U_{cw,on}$ and $U_{cw,off}$ are the corresponding half period-averaged of U_{cw} for which $U_t^w > 0$ and $U_t^w < 0$ respectively.

The sediment diffusivity is given by

$$\varepsilon_{s,w} = \left(\frac{\mathcal{D}}{\rho} \right)^{1/3} D \tag{3.23}$$

where $\mathcal{D}$ is the total effective dissipation here considered as $\mathcal{D} = \mathcal{D}^w + \mathcal{D}^r$.

3.5 TOTAL LOAD TRANSPORT FORMULAS

Energy-based models account for the action of bed-load and suspended-load transport processes (Bailard & Inman, 1981; Hsu *et al.*, 2006). At present, most common used near-shore morphodynamic models (Ruessink *et al.*, 2007; Van der A *et al.*, 2010*b*; Nam *et al.*, 2011; DHI, 2004, among others) combines bed-load and suspended-load transport formulas to account for both sediment transport processes. The AMORFO70 model also allows to combine different bed-load transport parameterizations with suspended-load transport models considering that the total load transport $Q_t = Q_b + Q_s$. The combinations used in the model are

1. Ribberink (1998) and Van Rijn (1993) model, in which Q_b is the bed-load transport formula given in equation 3.6 and Q_s is the suspended-load transport resulting from using the concentration profile given by equation 3.16.

2. Camenen & Larson (2005) and Camenen & Larson (2008) model, in which Q_b is the bed-load transport formula given by equations 3.8 and 3.9, and Q_s is the suspended-load transport given by the equation 3.21.

Also the Soulsby (1997) total transport formula is implemented in the model. This formula combines the action of waves and currents in the bed-load and suspended-load transport processes following

$$Q_t = A_s \vec{U} \left[\left(\vec{U}^2 + \frac{0.018}{C_D} U_\delta^2 \right)^{0.5} - U_{cr} \right]^{2.4} (1 - 1.6 \tan\beta) \tag{3.24}$$

where $A_s = A_{sb} + A_{ss}$ is the wave stirring factor, and

$$\begin{aligned} A_{sb} =& \frac{0.005 D (d_{50}/D)^{1.2}}{[(s-1) g d_{50}]^{1.2}} \\ A_{ss} =& \frac{0.012 d_{50} D_*^{-0.6}}{[(s-1) g d_{50}]^{1.2}} \end{aligned} \tag{3.25}$$

in which A_{sb} is the bed-load stirring factor and A_{ss} is the suspended-load stirring factor. The threshold current velocity U_{cr} is here defined as

$$\begin{aligned} U_{cr} =& 0.19 (d_{50})^{0.1} \log_{10} \left(\frac{4D}{d_{90}} \right) && 0.1 \leq d_{50} < 0.5mm \\ U_{cr} =& 8.5 (d_{50})^{0.6} \log_{10} \left(\frac{4D}{d_{90}} \right) && 0.5 \leq d_{50} < 2mm \end{aligned} \tag{3.26}$$

3.6 DIFFUSIVE TRANSPORT

Most of the sediment transport formulas do no account for gravity effects on the transport rate (Hoefel & Elgar, 2003; Hsu *et al.*, 2006; Camenen & Larson, 2005, among others). To consider these effects, the model introduces a transport term that represents the diffusive transport

resulting from the tendency of sand to move downslope combined with the effect of the turbulence induced by the dissipation of energy from waves and rollers. Following Bagnold (1963), this sediment transport component is represented as

$$Q_D = \lambda_d \, \nu(x) \left[\left(\frac{1}{\tan\varphi - dz_b/dx} \right) \left(\frac{dz_b/dx}{\tan\varphi} \right) \right] \tag{3.27}$$

where the last term is related to the gravity effects, in which dz_b/dx is the bottom slope and φ is the friction angle ($\tan\varphi = 0.63$). The coefficient λ_d is a calibration parameter. The second term ν ($\mathrm{m^2 s^{-1}}$) stands for the effects of the wave and roller energy density, so that diffusive transport is enhanced over steep bottoms on the breaking zone. It is given by

$$\nu(x) = M(E^w + E^r) \left(\frac{\mathcal{D}_w + \mathcal{D}_r}{\rho} \right)^{1/3} \tag{3.28}$$

where M is a scaling parameter set to $M = 1 \ \mathrm{s^2 kg^{-1} m^{-1}}$. Other options on the definition of ν were explored, but this was found to be the most convenient to avoid unrealistic growth and shapes of sandbars.

3.7 SHIELDS PARAMETER, WAVE AND CURRENTS BED-SHEAR STRESS AND MOTION THRESHOLD

The Shields parameter $\theta'_{cw}(t)$ is the instantaneous dimensionless effective shear stress related to currents and waves that forces the sediment movement. The Shields parameter $\theta'_{cw}(t)$, in the bed-load transport formula of Ribberink (1998) (Equation 3.6), is computed via a quadratic friction law using intra-wave near-bed velocities of the combined wave-current motion:

$$\theta_{cw}(t)' = \frac{\tau'_{cw}}{(\rho_s - \rho) g d_{50}} \tag{3.29}$$

where the effective bed-shear stress τ'_{cw} represents the transfer of bed-shear stresses to the grains from skin friction. This parameter is temporal and spatial dependent since it depends on the time-dependent value of the near-bottom velocity $U_t(x, y, t')$ according to:

$$\tau_{b,cw} = \frac{1}{2} \rho f'_{cw} |U_t| U_t \tag{3.30}$$

where $|U_t| = \sqrt{U_{t,x}^2 + U_{t,y}^2}$. Following Madsen & Grant (1976), the wave and currents friction factor f'_{cw} is computed as a linear combination of the wave friction factor f'_w and the currents friction factor f'_c:

$$f'_{cw} = \alpha f'_c + (1 - \alpha) f'_w \tag{3.31}$$

where $\alpha = \langle U_t \rangle / \langle U_t \rangle + U_\delta$. The wave friction factor is defined as $f_w = \exp[-6 + 5.2 (A_\delta / k_s)^{-0.19}]$ and the currents friction factor f'_c is $f'_c = 2(0.4/\ln(\delta/z_0))$.

In the case of the Camenen & Larson (2005) bed-load formula (Equations 3.8 and 3.9), the Shields parameter is given in terms of the wave direction and the normal direction respect to the waves motion. The instantaneous Shields parameter in the wave direction reads

$$\theta_{cw}(t) = \frac{\frac{1}{2} |U_0(t) + v \cos\phi| (U_0(t) + v \cos\phi)}{(s-1) g d_{50}} \tag{3.32}$$

where ϕ is the angle between waves and currents. Also we define, in one hand, the mean combined Shields parameter $\theta_{cw,m} = (\theta_c^2 + \theta_{w,m}^2 + 2\theta_{w,m}\theta_c \cos\varphi)^{1/2}$ and, in the other hand, the maximum combined Shields parameter $\theta_{cw} = (\theta_c^2 + \theta_w^2 + 2\theta_w\theta_c \cos\varphi)^{1/2}$, where φ is the angle between waves and currents. Subscripts w and c indicates the Shields parameter in the waves and the normal to waves directions respectively.

3.7.1 THRESHOLD OF MOTION θ_{cr}

The non-dimensional critical shear stress representing the threshold of sediment motion is given by the relation of Van Rijn (1993):

$$\begin{aligned}
\theta_{cr} &= 0.24 D_*^{-1} && 1 < D_* < 4 \\
\theta_{cr} &= 0.14 D_*^{-0.64} && 4 < D_* < 10 \\
\theta_{cr} &= 0.04 D_*^{-0.1} && 10 < D_* < 20 \\
\theta_{cr} &= 0.013 D_*^{0.29} && 20 < D_* < 150 \\
\theta_{cr} &= 0.055 D_*^{-1} && 150 < D_* \qquad (3.33)
\end{aligned}$$

where D_* is the non-dimensional grain $D_* = d_{50}(g(\rho_s - \rho)/\rho/\nu^2)^{1/3}$, and ν is the kinematic water viscosity.

Ruessink *et al.* (2007) modified the Ribberink (1998) transport considering the effect of gravity on the critical shields parameter, increasing or decreasing the threshold of movement depending on the direction (upslope or downslope) of the motion. θ'_{cr} is modified introducing the Schoklitsh factor as follows:

$$\theta_{cr,s} = \frac{sin\left(\varphi + arctan\left(\frac{dz_b}{ds}\right)\right)}{sin\varphi}\theta_{cr} \qquad (3.34)$$

3.7.2 THE BOUNDARY LAYER

Under the action of wave and currents, the bed roughness increases the resistance of bed over the flow due to the pressure forces induced by vorticity of the onshore-offshore fluxes. Bed roughness z_0 varies over different orders of magnitude, from the grain size diameter to mega-ripples and affects directly the vertical distribution of velocities. There are a number of parametrization to compute the bed roughness, but there is a large uncertainty on it. In the model, z_0 is an input parameter involved in the hydrodynamics calibration (see Appendix A).

The effective bed roughness is defined as $k_s = 30z_0$ (Van Rijn, 1993; Soulsby, 1997), and it represents the resistance of the seabed over the flow motion.

The effects of bed roughness over the flux extents from the bed to approximately the position where the amplitude of the wave orbital motion U_δ is maximum. It is defined as the wave boundary layer δ_w and computed following Van Rijn (1993):

$$\frac{\delta_w}{\hat{A}_\delta} = 0.072\left(\frac{\hat{A}_\delta}{k_s}\right)^{-0.25} \qquad (3.35)$$

where $\hat{A}_\delta$ is the peak value of the orbital excursion given by the linear wave theory.

3.8 SHORELINE TREATMENT OF BOTTOM CHANGES

As it has been stated in Chapter 2, the model does not account for the description of the processes near the shoreline, such as the interaction of surf-zone hydrodynamics and sediment transport with the swash zone processes. Furthermore, some hydrodynamics model variables, particularly the free-stream velocity, show an unrealistic behaviour at small water depths that lead to high gradients of the sediment transport rates and thus unrealistic bottom changes.

To avoid this problem near the shoreline, a smoother function is applied to the spatial derivative of the sediment transport dQ/dx for depths $D < 0.5$ m. This function follows

$$\left.\frac{dQ_x}{dx}^{*}\right|_i = \left.\frac{dQ_x}{dx}\right|_i \arctan\left(\frac{\frac{\pi}{2}(D_i - D_{wet})}{D_{0.5\mathrm{m}} - D_{wet}}\right) \tag{3.36}$$

where $(dQ_x/dx)^*|_i$ is the smoothed spatial derivative of Q_x at point x_i, D_{wet} is the water depth at the 'last wet point' x_{wet} (detailed in Section 2.3.8.2), $D_{0.5\mathrm{m}}$ is the depth at the first point in which $D < 0.5$ m ($x_{0.5\mathrm{m}}$) and D_i is the depth at point x_i. The point x_i is bounded spacially by the location of the point $x_{0.5\mathrm{m}}$ and x_{wet}.

CHAPTER 4

ON THE PREDICTABILITY OF CROSS-SHORE PROFILE EVOLUTION[i]

4.1 INTRODUCTION

The long-term prediction of beach evolution is still a challenge not only for coastal managers but also for the scientific community. A commonly-used tool for the analysis of long-term beach morphodynamics is the equilibrium profile concept. Citing Dean (1991), *'an equilibrium beach profile might be one which would occur if the forcing were held constant for a sufficiently long time for the sediment transport resulting from the force imbalance to mold the profile to one in which the forces are in balance'*. Obtaining equilibrium profiles can be done both experimentally, from the analysis of the bathymetry, and theoretically, from the balance between offshore-directed sediment fluxes (e.g., gravity and undertow) and onshore-directed fluxes (e.g., wave shear stresses and pressure gradients) or by considering the stable profile resulting from the long-term evolution under steady wave conditions ($dz_b/dt \overset{t\to\infty}{\approx} 0$). A widely used definition of the equilibrium profile is that one that represent the mean state of a beach during a period of time, and usually computed as the mean profile of a set of observed profiles. It is based on the idea that the equilibrium profile can be defined by averaging the cross-shore beach profiles along the beach over a long period of time. All these approaches assume a degree of uniformity along the coast and neglect alongshore processes. Despite their simplicity, equilibrium profiles are useful for interpreting beach processes and for engineering applications (Dean, 2002).

In the short term (from days to a few weeks), several cross-shore profile models are able to predict trends in the evolution of beach profiles (Henderson *et al.*, 2004; Hsu *et al.*, 2006; Ruessink *et al.*, 2012). This type of models usually assume alongshore uniformity and, recently, they account for wave non-linearities in the sediment transport. However, to simulate the mid- and long-term evolution of the cross-shore beach profile (from months to several years), these models face up with a number of challenges. In addition to numerical limi-

[i]This chapter is based on the work in Fernandez-Mora *et al.* (2013): Fernandez-Mora, A., Calvete, D., Falques, A., Ribas, F. and Idier, D. 2013. On the predictability of mid-term cross-shore profile evolution. Proceedings 12th International Coastal Symposium(Plymouth, England), Journal of Coastal Research SI 65 (476-481), iSSN 0749-0208.

tations, such as numerical instabilities, error propagations or long computational times, the absence of the longshore physical processes, neglected in this kind of models, can lead to significant errors in the predictions. In the surf-zone, the hydrodynamics and the morphodynamic features lead to three-dimensional dynamics that breaks the alongshore uniformity and may result in longitudinal gradients of the sediment transport. Furthermore, in the long term, the climate variability, in terms of the directional spread, results on bi-dimensional hydrodynamics (longshore currents) that should be also considered.

A common procedure to avoid the alongshore morphological variability on modeling the long-term beach evolution is to integrate the existing bathymetry in the alongshore direction (see Thornton & Humiston, 1996).

In this chapter, the model capability on simulating the short-, mid- and long-term morphodynamics of the beach profile by neglecting the alongshore variability is studied. To this end, the 151-days evolution simulation of a real beach is studied by comparing the evolution of 8 individual profiles and the corresponding mean profile with measurements. First, the field data and the experimental setup are described. After that, the numerical results are then detailed and the discussion is presented, followed by the conclusions.

4.2 DATA

The data used in the present study was obtained at the Field Research Facility FRF Duck at Duck, North Carolina, from August to December 1997 (151 days) during the SandyDuck97 experiment (Birkemeier *et al.*, 2001). Surveys were conducted over a series of 26 cross-shore lines, which extend from the dune to approximately $950\ \mathrm{m}$. offshore by using the Coastal Research Amphibious Buggy (CRAB). In the present analysis, 8 survey lines have been selected, situated at the northern zone of the FRF pier. The location of the FRF Duck facility and the cross-shore profiles are shown in Figure 4.1 A and B. The initial profiles were measured on 15^{th} August 1997, and the final date of simulation has been set to 13^{th} January 1998. For the analysis of the results, the bathymetries of the intermediate dates 16^{th} September, 25^{th} October and $16\mathrm{th}$ December 1997 are also considered, dates in which survey measurements were available.

The offshore wave conditions were measured by a $3\ \mathrm{km}$ offshore wave rider buoy, in service since 1986, that covers the full event and provides the 3-hours record of the significant wave height $H_s\ (\mathrm{m})$, the wave period $T\ (\mathrm{s})$ and wave direction θ_0. The tide was provided by the NOAA tide station at Duck (operating since 1981). Figure 4.2 A to D show the offshore wave conditions and tides during the study period.

The sequence can be divided in three stages. In the first stage (from 16^{th} August to 16^{th} September), the mean shore-parallel sand bar, initially placed at $x \approx 370\ \mathrm{m}$ an the crest at $\approx 3.30\ \mathrm{m}$ depth, is forced with of low-intermediate energy waves and migrates approximately $30\ \mathrm{m}$ onshore while the shoreline becomes less steep. During the second stage from 16^{th} September to 25^{th} October, that includes several storms, the sandbar decays and a 100 m-long terrace is formed. In the third stage, characterized by high energy waves (from 25^{th} October to 13^{th} January 1998), a sandbar detaches from the terrace and migrates $\approx 60\ \mathrm{m}$ offshore while the outer sandbar totally disappears.

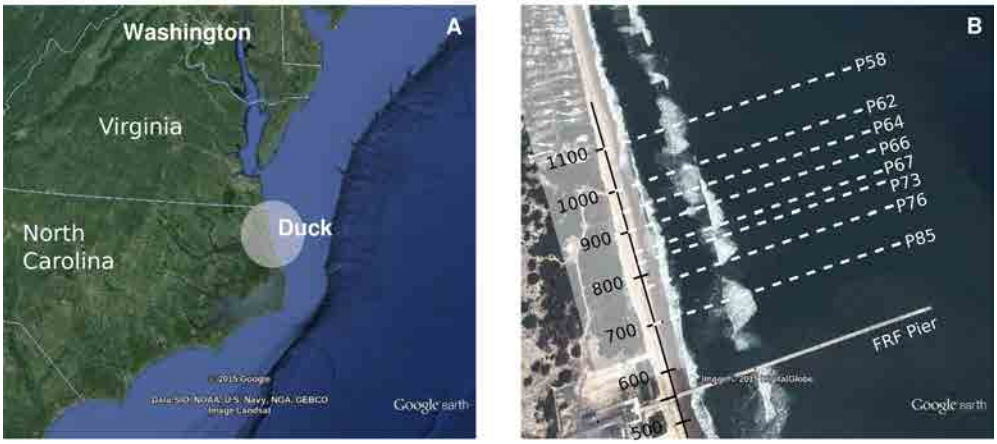

Figure 4.1: A, Location of the Field Research Facility (red box) at Duck, North Carolina, USA, and, B, position of the study profiles (source: *Google Earth*).

4.3 NUMERICAL MODELING AND EXPERIMENTAL SET-UP

The AMORFO70 model, detailed in Chapters 2 and 3, is used to compute the long-term evolution of the 8 individual profiles during the 151-days event. The Hsu *et al.* (2006) sediment transport formula has been selected to compute the sediment transport rate. The model is forced with the offshore wave and tide conditions during the whole event. A continuous $150-$days simulation has been computed for each profile, considering a non-uniform grid and a time-step of 300 s for the bottom changes.

In order to analyze the effects of neglecting alongshore variabilities on modeling the evolution of the mean cross-shore profile, two different approaches are considered: i), the simulation of the evolution of the initial mean profile (hereinafter Method A), and ii) the analysis of the mean evolution of the individual profiles, (hereinafter Method B). Figure 4.3 shows the mean profile at the initial, intermediate and final times and the corresponding standard deviation.

The model skill is quantified through a 'Brier skill score' type parameter (Van Rijn *et al.*, 2003; Ruessink, 2005) defined as

$$S = 1 - \frac{\int_{x_1}^{x_2}(z_b(x) - z_{b,obs}(x))^2 dx}{\int_{x_1}^{x_2}(z_{b,obs}(x) - z_{b0,obs}(x))^2 dx} \tag{4.1}$$

where $z_b(x)$ is the bottom elevation computed by the model at a selected time, $z_{b,obs}(x)$ is the observed bottom elevation at that date, $z_{b0,obs}(x)$ is the observed elevation at $16^{th}August$ along the cross-shore direction x, and x_1 and x_2 limit the cross-shore profile zone where the skill is computed. To account for measurement errors, a threshold on the calculation of $(z_b(x) - z_{b,obs}(x))^2$ is considered, in such a way that $(z_b(x_i) - z_{b,obs}(x_i))^2 = 0$ if $(z_b(x_i) - z_{b,obs}(x_i)) < \sigma_m$, where x_i is the measure point in the interval $[x_1 x2]$ and $\sigma_m = 0.1$ m is the estimated measurement error Gallagher *et al.* (1998). The values of the skill *S* range within $[-\infty < S \leq 1]$. Perfect agreement between results and observations is given by a $S = 1.0$.

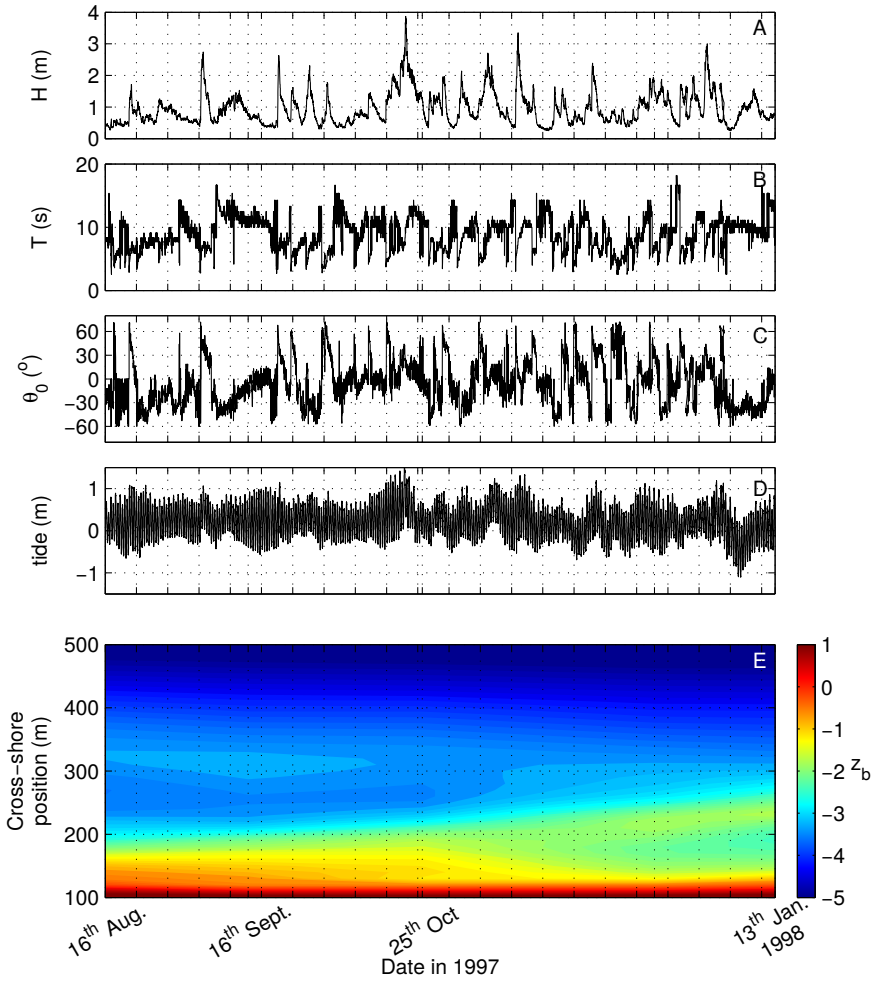

Figure 4.2: Wave climate registered by the 3−km offshore buoy versus time at Duck (from 15^th August 1997 to 13^th January 1998): A) the root mean squared wave height H (m), B) the peak period T_p, C) the wave incidence angle θ_0 (with respect to the shore normal) and D) the registered tide range (m). Mean profile evolution during the sequence (panel E).

Values $0 < S < 1$ stand for better simulations than assuming no-bottom change ($S = 0$).

The model skill is computed for each individual profile, for the evolutions of the mean profile (Method A) and for the average of the evolution of the individual profiles (Method B) respect to the initial profile. The offshore zone of the profile, ($x > 500$ m), where there is hardly any morphological change, is not accounted for on computing the model skill. Likewise, cross-shore points at $x < 150$m have been excluded to avoid swash and the inter-tidal zones, whose dynamics is not captured by the model.

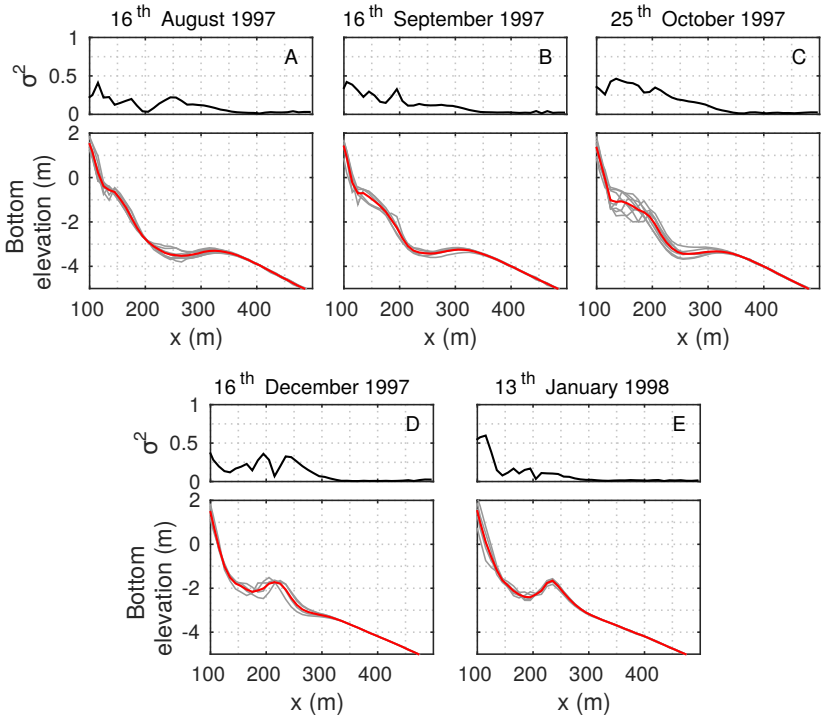

Figure 4.3: Measured profiles (gray lines) and mean profiles (red lines), and the corresponding standard deviation (upper plots), for: A, the initial time 16^{th} August; B, 16^{th} September; C, 27^{th} October; D, 16^{th} December, and E, 13^{th} January 1998.

4.4 RESULTS AND DISCUSSION

The predicted evolution of the individual profiles and the methods A and B are shown in Figures 4.4 and 4.5. Table 4.1 summarizes the model skill S computed at the end of each stage (16^{th} September, 25^{th} October and 13^{th} January 1998).

Regarding the first stage, in which the mean outer sandbar migrates slightly onshore, there is an overall agreement between the model results and measurements for each individual profile and for the methods A and B, particularly in the sandbar zone. However, the simulations fail to predict the accretion of the inner-surf zone. The model skill of the individual profiles for the first 30 days are good ($0.66 \leq S \leq 0.78$). Similarly, the evolution of the mean profile (method A) and the average of evolutions (method B) also reach properly the onshore migration. The addition of the wave velocity skewness effects on sediment transport through the intra-wave near-bottom oscillatory flow allows to perform net onshore sediment transport fluxes (further examined in Chapters 5, 6 and 7.

The results of the second stage evidence more discrepancies between the measurements and the simulation of the mid-term evolution of the profile. The model is not able to reproduce

Table 4.1: Model Skill at the intermediate time (16th September 1997) and at the final computational time (27th October 1997) for each single profile and for the methods AC and DC.

Survey	First stage 1997/09/16	Second stage 1997/10/27	Third stage 1998/01/13
Line 58	0.66	0.36	0.79
Line 62	0.78	0.60	0.57
Line 64	—	0.24	0.68
Line 66	0.77	0.22	0.78
Line 67	0.73	0.31	0.80
Line 73	—	0.34	0.62
Line 76	0.75	0.65	0.77
Line 85	—	0.84	0.68
Mean	0.74	0.45	0.70
Method A	0.73	0.61	0.57
Method B	0.85	0.74	0.85

the accretion of the inner-surf zone, specially the formation of an inter-tidal sandbar (in the individual profiles). The result of the method B agree with the position of the outer sandbar, although dismiss the formation of the terrace. In contrast, the evolution of the mean profile (method A) maintains the onshore migration trend, opposite to the offshore migration trend expected in this stage. The model skill decreases for all the simulations, particularly for the individual profiles. Note that the model does not update the bathymetry in the intermediate control time with the measured bathymetry.

The final profile (13^{th} January 1998) shows a sandbar located at ≈ 200 m offshore. Most of the simulations results in a similar barred profile, but differ from the measurements in terms of the height of the sandbar, the position of the sandbar crest, and in the erosion of the beach face. The model skill increases respect the end of the second stage for almost all the individual profiles and the Methods A and B, with a mean value for the individual profiles of $S = 0.70$ and a maximum for the Method B of $S = 0.85$. Despite these good results, the evolution predicted by the model is not the real one. This is evidenced in Figure 4.6. Measurements indicate that the sandbar is detached from the terrace and further migrates offshore during the third stage (Figure 4.6 A), while the model reproduces a full onshore migration of the outer sandbar for the whole 150-days simulation for both methods A and B (Figure 4.6 B and C). This points out that although long-term predictions may match measurements, simulations do not always capture the real processes. In addition, the sandbar detached from the terrace is apparently the result of swash and inter-tidal processes. The model does not account for this dynamics and thus, can not fully reproduce beach face changes or sandbar generation near the shoreline.

Also, note that at the end of the second interval (25^{th} October) and at the middle of the third interval ($16[th]$ December), morphodynamics are highly three-dimensional. This is evidenced by the high values of the standard deviation of the mean profile (see Figure 4.3) that point to a dispersion on the sandbar crest position due to a possible presence of a crescentic sandbar. This is also observable through the shape of the measured individual profiles. In these conditions, the mean profile is not representative of the beach profile along the shore.

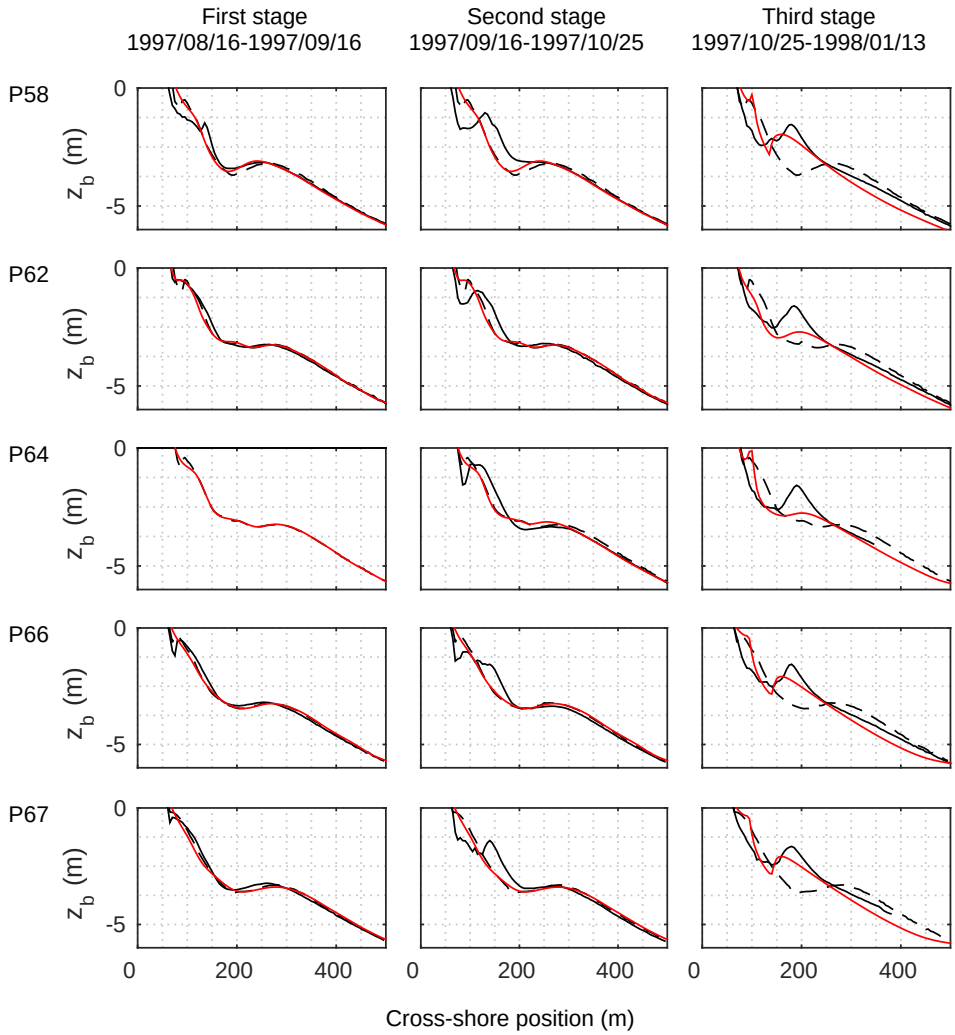

Figure 4.4: Predicted profiles at the end of each sequence (red solid line). The profile line is indicated in the left upper corner of each panel. Initial measured profiles are indicated by the dotted lines and the final measured profiles by the dashed lines.

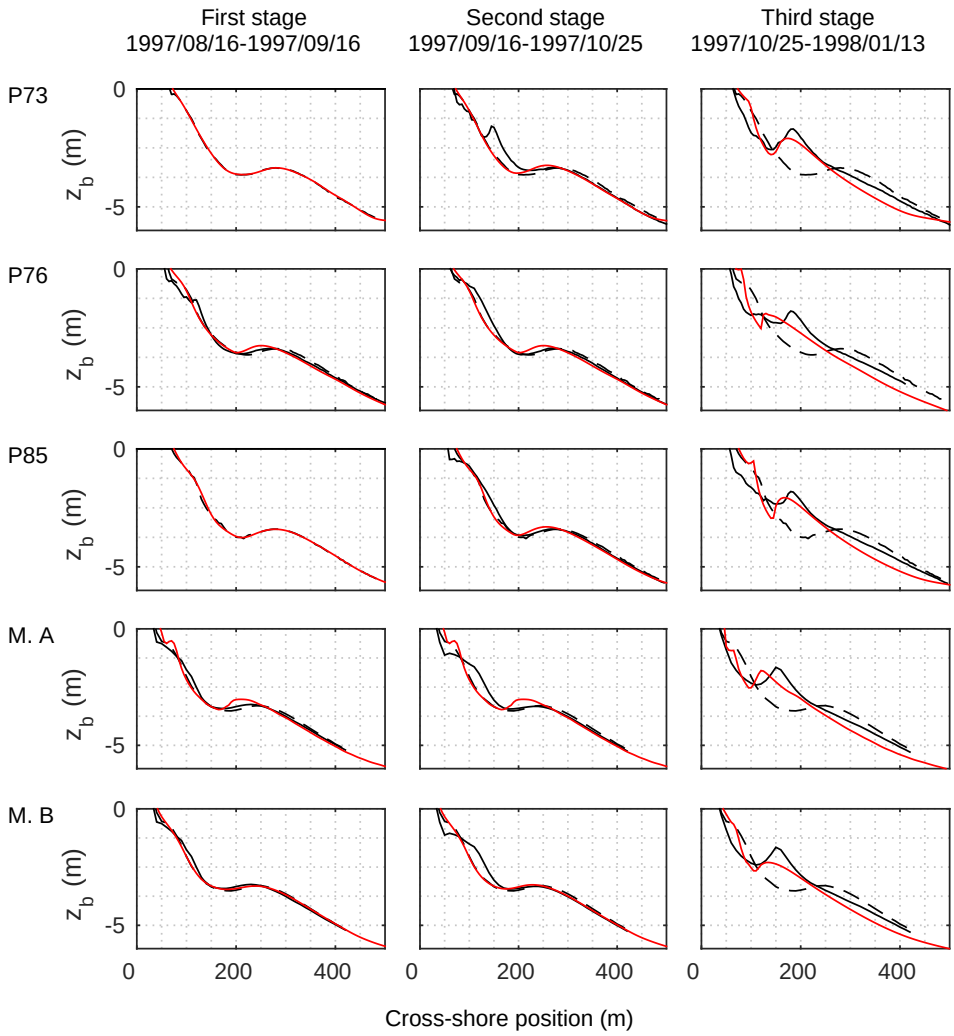

Figure 4.5: Idem Figure 4.4

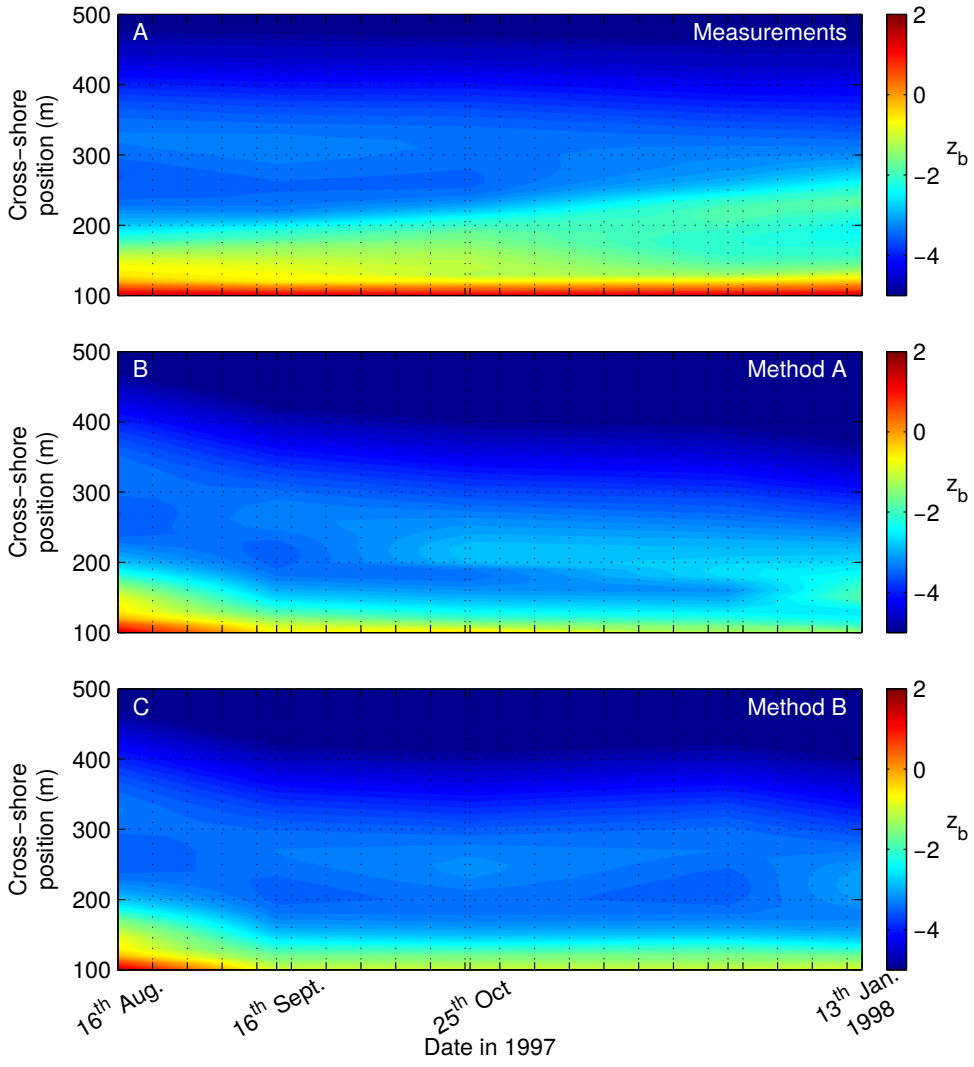

Figure 4.6: Profile evolution during the sequence for: A, the mean measured profile; B, the evolution of the mean profile (Method A); and C, the average of the evolution of the individual profiles (Method B)

4.5 CONCLUSIONS

In this chapter, the hypothesis that the alongshore processes can be neglected for the prediction of the mean profile evolution has been analyzed through the simulation of a long-term (150 days) event at Duck, North Carolina, for multiple profiles along the beach and for the corresponding mean profile.

The event has been divided in three stages according to the morphodynamics described by the mean profile. In the first stage, the onshore sandbar migration is properly simulated by the model for the individual profiles, the evolution of the mean profile (method A) and the average of the evolution of the individual profiles (method B). Thus, the process-based model is able to reproduce this kind of short-term events. The introduction of the effects of wave velocity and acceleration skewness, through the parameterization of Abreu *et al.* (2010) and Ruessink *et al.* (2012), allows to simulate net onshore sediment transport fluxes and thus, the onshore migration of the sandbar.

For the mid-term evolution the best results are given by averaging the evolution of the individual profiles (method B). This method is a way to account for the longshore variability of the cross.shore beach profiles.

In the long-term, although the predictions for the individual profiles and the A and B methods agree with the measurements, the morphodynamics described by the model are not realistic. This stresses the necessity of analyzing the behavior of the simulated morphodynamics during long-term evolution, as not considering intermediate time-steps to control the evolution can lead to mistakes in the interpretation of the model capabilities. These differences between real and modeled morphodynamics can be due to the dismissing of swash-zone and inter-tidal processes that cause the formation of a sandbar and its further offshore migration towards the surf-zone. The addition of inter-tidal dynamics in the model might improve the long-term predictions.

Finally, note that, opposite to previous works on the long-term evolution of the profile (Ruessink *et al.*, 2003; Ruessink, 2005; Ruessink *et al.*, 2007; Dubarbier *et al.*, 2015), the model has neither been calibrated for the conditions of the event, nor updated in the intermediate dates, and the free parameters set to the original values given by the authors.

CHAPTER 5

NEAR-BOTTOM WAVE VELOCITY AND ACCELERATION SKEWNESS

5.1 INTRODUCTION

As it has been stated in Chapter 2, waves approaching to the shore evolve from a sinusoidal shape to a 'pitched-forward-sawtooth' shape. The intra-wave velocity distribution changes in a similar way. In the offshore zone, near-bottom velocities are assumed to be sinusoidal with a zero balance between onshore and offshore-directed fluxes. When approaching to the coast, the onshore-directed velocities are stronger than the offshore-directed velocities (skewed profile). This net balance drives sediment onshore. Furthermore, in the vicinity of the breaking point, wave velocity asymmetry increases, producing strong accelerations that enhances the onshore sediment flux (Doering & Bowen, 1995). It is well known that these changes of the velocity and acceleration profiles, that take place during the wave period (in the instantaneous time t'), play a key role on onshore sediment transport (Hoefel & Elgar, 2003; Hsu *et al.*, 2006; Austin *et al.*, 2009; Van der A *et al.*, 2010*a*; Silva *et al.*, 2011, among others). An accurate description of the near-bottom wave motion is then crucial to predict the near-shore sediment transport, and furthermore, the cross-shore beach profile morphodynamics.

Isobe & Horikawa (1992) and Elfrink *et al.* (2006) developed approximations of the intra-wave near-bottom oscillatory flow as a function of time-averaged variables. These formulas were the first to account for the skewness and asymmetry on computing the intra-wave near-bottom velocity. Unfortunately, the skewness and asymmetry of these parameterizations was not precise enough to perform accurate specific morphodynamical predictions. Abreu *et al.* (2010) gave an approximation for the intra-wave oscillatory flow as a function of non-linearity parameters and fitted it with different flume experiment measurements. Ruessink *et al.* (2012) improved this approximation and found a direct relation with the Ursell number. They also compared the approximation with measurements of the DUCK94 experiment (Gallagher *et al.*, 1998; Elgar *et al.*, 2001). These parameterizations were further compared with data of other field experiments to set their applicability for several wave and bathymetric conditions (Rocha *et al.*, 2013). The Ruessink *et al.* (2012) approximation showed a good agreement with measurements, particularly for beaches and wave conditions similar to the ones used on developing this parameterization (significant wave height H_s ranging from 0.05 to 3.99 m, periods T

from 3.1 to 13.9 s, water depths D from 0.25 to 11.2 m, U_r ranging from 0.004 to 24.8 and bed slopes lower than 1 : 30).

At present, many morphodynamic models (Bosboom *et al.*, 2000; Van Rijn, 2007*a*,*b*; Deltares-Delft Hydraulics, 2007; Van der Werf *et al.*, 2012; Dubarbier *et al.*, 2015, among others) use the Ruessink *et al.* (2012) parameterization to consider the effects of wave velocity and acceleration skewnesses on computing the sediment transport rates. In this chapter, this parameterization is analyzed in order to get more insight in the interdependence between the non-linearity parameters in the formula (further detailed in next sections), the predicted intra-wave velocity and acceleration and their distribution along the profile for different wave and bathymetric conditions.

5.2 THE FREE-STREAM VELOCITY APPROXIMATION

The approximation for the near-bottom intra-wave velocity of Abreu *et al.* (2010) is given by

$$U_0(t') = U_\delta \sqrt{1-r^2}\,\frac{\left[\sin(\omega t') + r\sin\phi/1+\sqrt{1-r^2}\right]}{\left[1-r\cos(\omega t'+\phi)\right]} \tag{5.1}$$

where $U_\delta = \pi H/(T sinh(kD))$ is the amplitude of the near-bed orbital velocity given by the linear theory. Parameters ϕ and r describe the intra-wave velocity distribution in terms of the phase and non-linearities. They are computed as a function of the Ursell number $U_r = 3Hk/8(kD)^3$, following the Ruessink *et al.* (2012) approximation. The phase parameter ϕ is defined by

$$\begin{aligned}\psi &= -90^0 + 90^0\tanh(\frac{p_5}{U_r^{p_6}})\\ \phi &= -\psi - \pi/2\end{aligned} \tag{5.2}$$

and the non-linearity parameter r follows from:

$$\begin{aligned}b &= r/(1+\sqrt{1-r^2})\\ B &= \frac{3b}{\sqrt{2(1-b^2)}}\\ B &= p_1 + \frac{p_2-p_1}{1+\exp(p_3-\log U_r/p_4)}\end{aligned} \tag{5.3}$$

where the coefficients p_1 to p_6 are fitting shape parameters set to: $p_1 = 0$, $p_2 = 0.857 \pm 0.016$, $p_3 = -0.471 \pm 0.025$, $p_4 = 0.297 \pm 0.021$, $p_5 = 0.815 \pm 0.055$ and $p_6 = 0.672 \pm 0.073$ (for further details, see Ruessink *et al.*, 2012).

Figure 5.1 shows both parameters as a function of the Ursell number. They have been computed considering different bathymetries (detailed in Appendix B), and a wide range of offshore wave conditions (wave heights H_0 from 0.5 to 3.5 m and periods T from 5 to 15 s). Both parameters increases by increasing the Ursell number (as waves approach to the shore). This parameterization bounds the values of r and ϕ between 0 and 0.67, and between $-\pi/2$ and 0, respectively. Besides, it sets a one-to-one relationship between r and ϕ (see Figure 5.2).

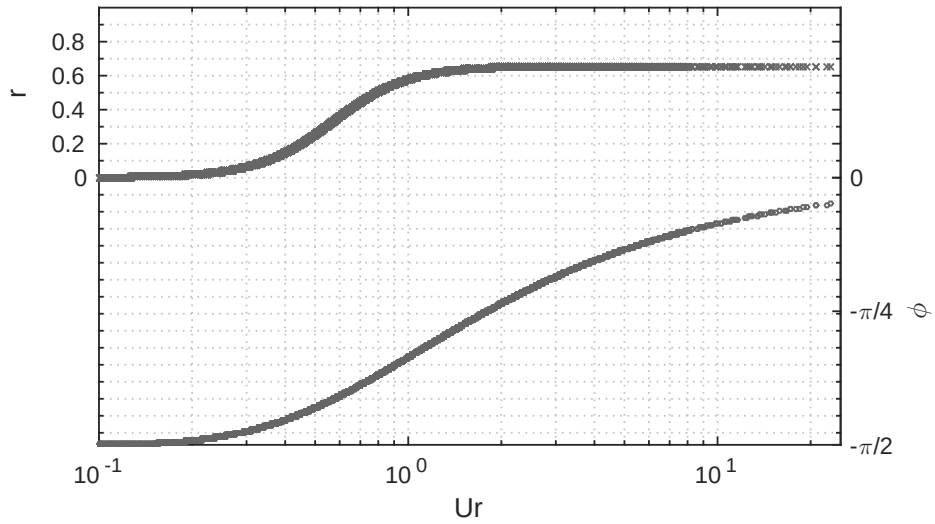

Figure 5.1: Predicted non-linearity parameter r and phase parameter ϕ as a function of the Ursell number given by the Ruessink *et al.* (2012) approximation for 420 individual cases.

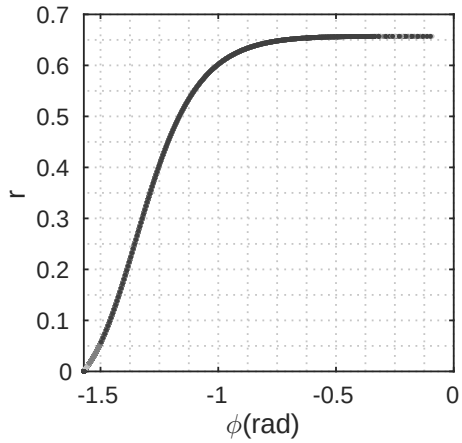

Figure 5.2: Relation between r and ϕ parameters given by the expression of Ruessink *et al.* (2012).

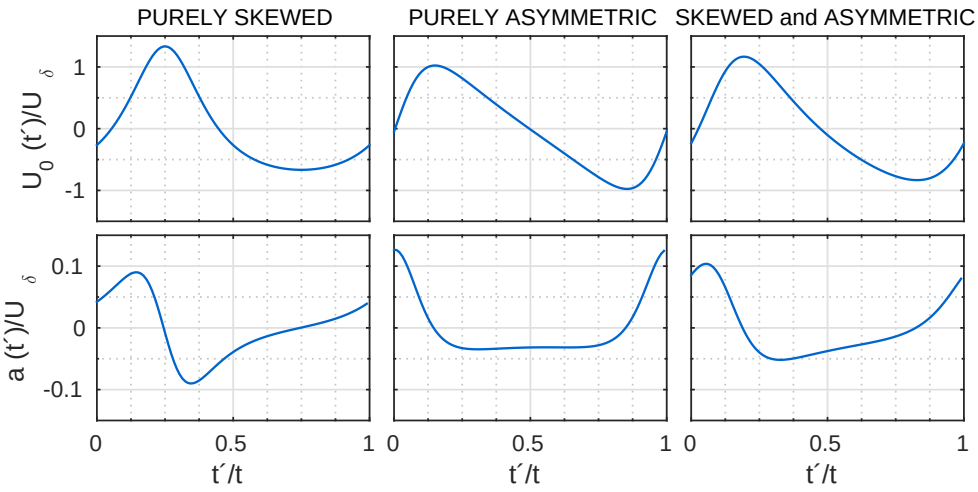

Figure 5.3: Normalized free-stream velocity and the corresponding acceleration for solely skewed (left panel), asymmetric velocity (middle panel), and for both skewed and asymmetric waves (right panel).

5.3 WAVE VELOCITY AND ACCELERATION SKEWNESS

Parameters r and ϕ in Equation 5.1 control the resulting wave velocity and acceleration intra-wave distribution. High values of r combined with low values of ϕ ($\phi << 0$) result in pure skewed velocity profiles. These are characterized by a short onshore directed velocity (short crest) and long offshore directed (long through). The corresponding acceleration shows a fast decrease followed by a long soft acceleration (left panels in Figure 5.3). In the opposite case, for $r = 0$ and $\phi = 0$, the velocity shape is asymmetric (sawtooth shape), characterized by a strong rapid increase of the velocity and a long velocity decrease period. Note that asymmetric near-bottom velocities lead to skewed accelerations (middle panels in Figure 5.3). In natural waves, both characteristics are present together, leading to both skewed and asymmetric velocities (right panels in Figure 5.3). These shape characteristics are usually defined by the skewness and asymmetry. The velocity skewness, as a statistical measure, is usually computed as

$$\mathrm{SkV} = \frac{\langle \mathrm{U_0(t)^3} \rangle}{\sigma^2_{\mathrm{U_0}}} \tag{5.4}$$

in which σ is the standard deviation of $U_0(t)$. Wave acceleration skewness (SkA) is defined by substituting $U_0(t)$ by $a(t)$ in Equation 5.4. Similarly, the asymmetry is defined as $\mathrm{AsV} = \langle \mathrm{Hilb(U_0(t)^3)} \rangle / \sigma^2_{\mathrm{U_0}}$, where the $Hilb$ operator stands for the Hilbert transform of the velocity (Elgar, 1987).

5.3.1 RELATIONSHIPS BETWEEN THE r AND ϕ PARAMETERS AND THE PREDICTED VELOCITY AND ACCELERATION SHAPES

In this section, the predicted SkV and SkA are analyzed with respect to the non-linearity and the phase parameters for several bathymetries and wave conditions. Figure 5.4 shows the distribution along the profile of the simulated wave height, the Ursell number Ur, the intra-wave velocity, the velocity and acceleration skewness and the parameters r and ϕ for a barred profile forced with $H_0 = 1.5$ m and $T = 5$ s. It is shown, in this particular case, that the SkV and SkA have a similar behavior along the profile, with the local maximums located in the vicinity of the sandbar crest. Also note that the velocity skewness and the r parameter have similar shapes, similarly to the SkA and ϕ. These relations are further evidenced by extending the analysis for several wave conditions and bathymetries. An almost linear relation between the non-linearity parameter r and the wave velocity skewness SkV is evidenced (see Figure 5.4 D). Note that both values have a one-to-one relation, except in the region of maximum r. These points are located in the reforming waves zone and close to the shoreline. In the shoreline zone, the approximation of the free-stream velocity is likely not valid because the processes involved in this zone are not captured by the model (swash zone processes). Similarly to the SkV and the r parameter, there is a one-to-one relation between the wave acceleration skewness SkA and the phase parameter ϕ, but not following a totally linear trend (Figure 5.5 D). This is shown also in the relation of SkV and SkA with the Ursell number (Figure 5.6). Similarly to the r and ϕ parameters, the SkV and SkA are bounded between 0 and 0.67, and between 0 and $\pi/2$, respectively. In the case of the SkV, it increases up to its maximum located at $Ur \approx \mathcal{O}(1)$, similarly to the r parameter, but it decreases for higher values of the Ursell number.

Despite these resemblances between the distribution of the r and ϕ parameters and the distribution of SkV and SkA, the one-to-one relation between r and ϕ is not reproduced by both skewnesses (see Figure 5.7), in which a parabolic relation is evidenced.

5.3.2 CROSS-SHORE DISTRIBUTION OF WAVE VELOCITY AND ACCELERATION SKEWNESS

As it is shown in Figure 5.4, the velocity and acceleration skewness have similar spatial distribution along the profile. In this section, this distribution is analyzed for several wave conditions and bathymetries.

Figure 5.8 A shows the cross-shore distribution along a barred profile of both velocity and acceleration skewness for different wave heights and a fixed period ($T = 5$ s). It is shown that the cross-shore distribution of both skewnesses are similar, with the local maximum in the vicinity of the bar crest, and a local minimum in the inner surf-zone. Both skewness values increases on increasing the wave height. Further differences on the cross-shore distribution of these parameters are evidenced for different wave periods (see Figure 5.8 B). It is shown that wave acceleration skewness increases gradually on increasing the wave period, while the wave velocity skewness distribution becomes more complex. As the wave period increases, the maximum value of the skewness is reached further offshore ($SkV = 0.67$), with a local minimum placed in the bar crest position, and a second local maximum is placed in the inner-surf zone.

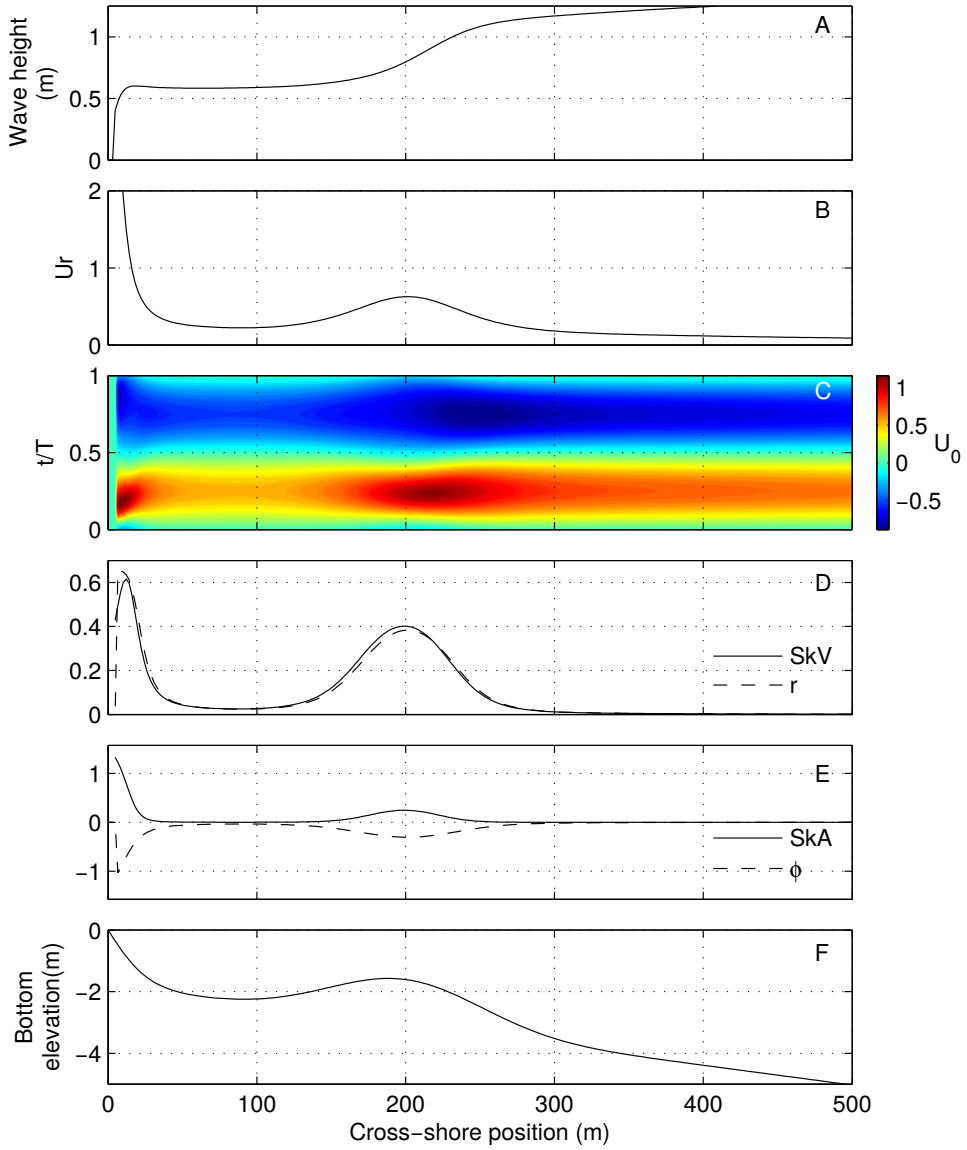

Figure 5.4: Cross-shore distribution of: A, wave height H; B, the Ursell number Ur; C, intra-wave near-bottom velocity U_0; D, wave velocity skewness SkV and non-linearity parameter r; E, acceleration skewness SkA and phase parameter ϕ. Lower panel shows the bathymetry. The offshore wave conditions for this example were $H_0 = 1.5$ m and $T = 5$ s.

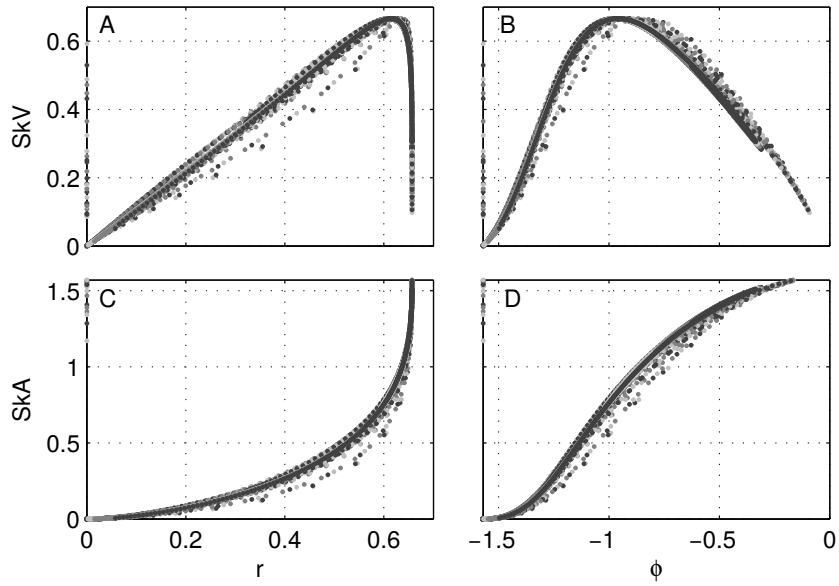

Figure 5.5: Wave velocity skewness versus the parameters r and ϕ (panels A and B, respectively) and wave acceleration skewness versus the parameters r and ϕ (panels C and D, respectively).

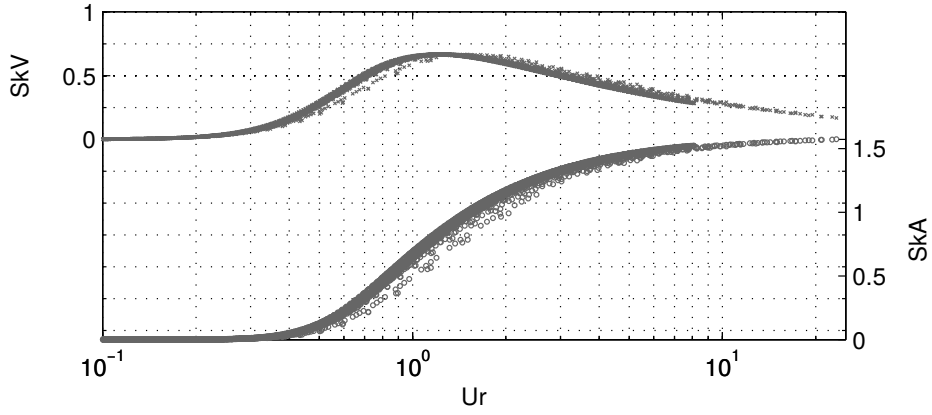

Figure 5.6: Predicted wave velocity and acceleration skewness SkV and SkA as a function of the Ursell number.

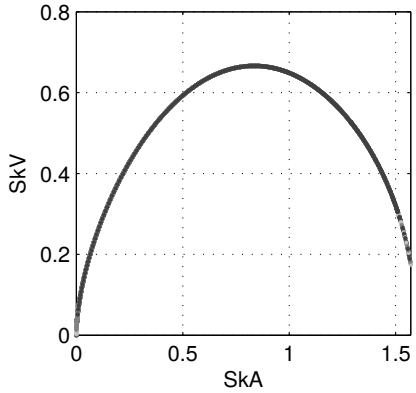

Figure 5.7: Relation between predicted SkV and SkA for several wave and bathymetric conditions.

This analysis has been extended for other wave height and period conditions. Figure 5.9 shows the distribution of both velocity and acceleration skewness along the barred profile for different wave heights and periods. By increasing wave height and period, velocity skewness increases faster and reaches the first local maximum in the shoaling zone. As stated before, for longer waves ($T > 8$ s), a local minimum is placed over the sand bar crest, and a second local maximum is observable in the inner-surf zone. Opposite to the complex behavior of the SkV, the acceleration skewness SkA shows a more regular trend. The local maximum is always placed in the vicinity of the sandbar, which value increases in the measure that the wave height and period increase.

These spatial differences of the distribution of both skewness are a key issue to find out which physical processes dominates sediment transport along the profile (bed-shear stresses or pressure gradients) (Fernandez-Mora *et al.*, 2015*b*). This will be addressed in Chapter 6.

5.4 CONCLUSIONS

In this chapter, the predicted wave velocity and acceleration skewness related to the Ruessink *et al.* (2012) parameterization for the free-stream wave velocity has been analyzed. For almost all the Ursell number values, both wave velocity and acceleration skewness distributions are similar to the distributions of the non-linear parameter r and the phase parameter ϕ, respectively. Furthermore, it is found a strong linear relation between the non-linearity parameter r and the wave velocity skewness SkV.

Moreover, the distribution of both skewnesses along a barred profile has been analyzed for several wave heights and periods. It is found that for short waves, their cross-shore distributions are similar (maximum values in the bar crest). This resemblance disappears for longer waves, for which SkV distribution becomes more complex.

The effects of wave velocity and acceleration skewness on cross-shore beach profile morphodynamics are further analyzed in the next chapter.

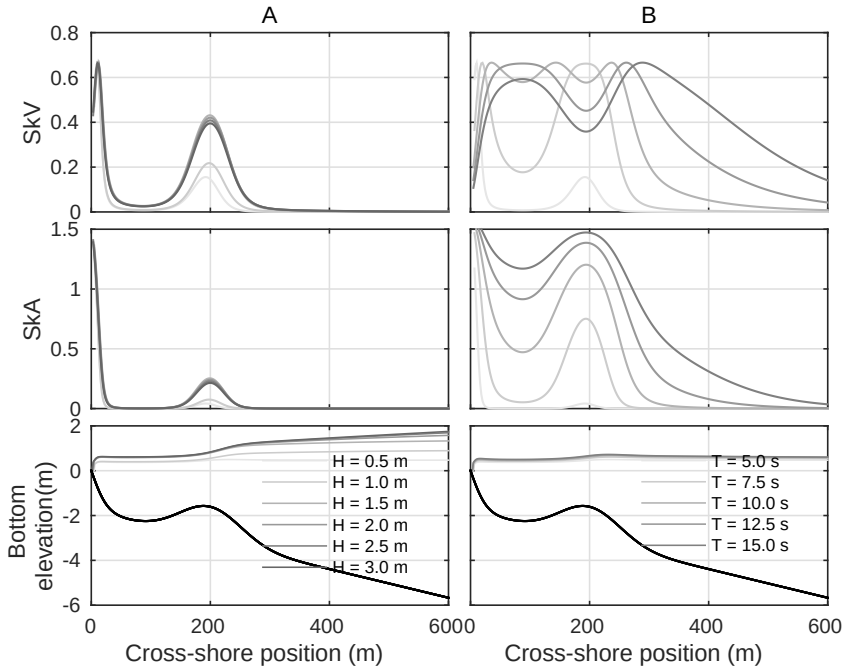

Figure 5.8: A. Cross-shore distribution of velocity skewness (upper panel) and acceleration skewness (middle panel) for different wave heights H_0 and fixed period ($T = 5$ s). The lower panel shows the bathymetry and the distribution of wave heights along the profile. B. Cross-shore distribution of velocity skewness (upper panel) and acceleration skewness (middle panel) for different periods T and fixed wave height ($H_0 = 0.5$ m). The lower panel shows the bathymetry and the distribution of wave heights along the profile.

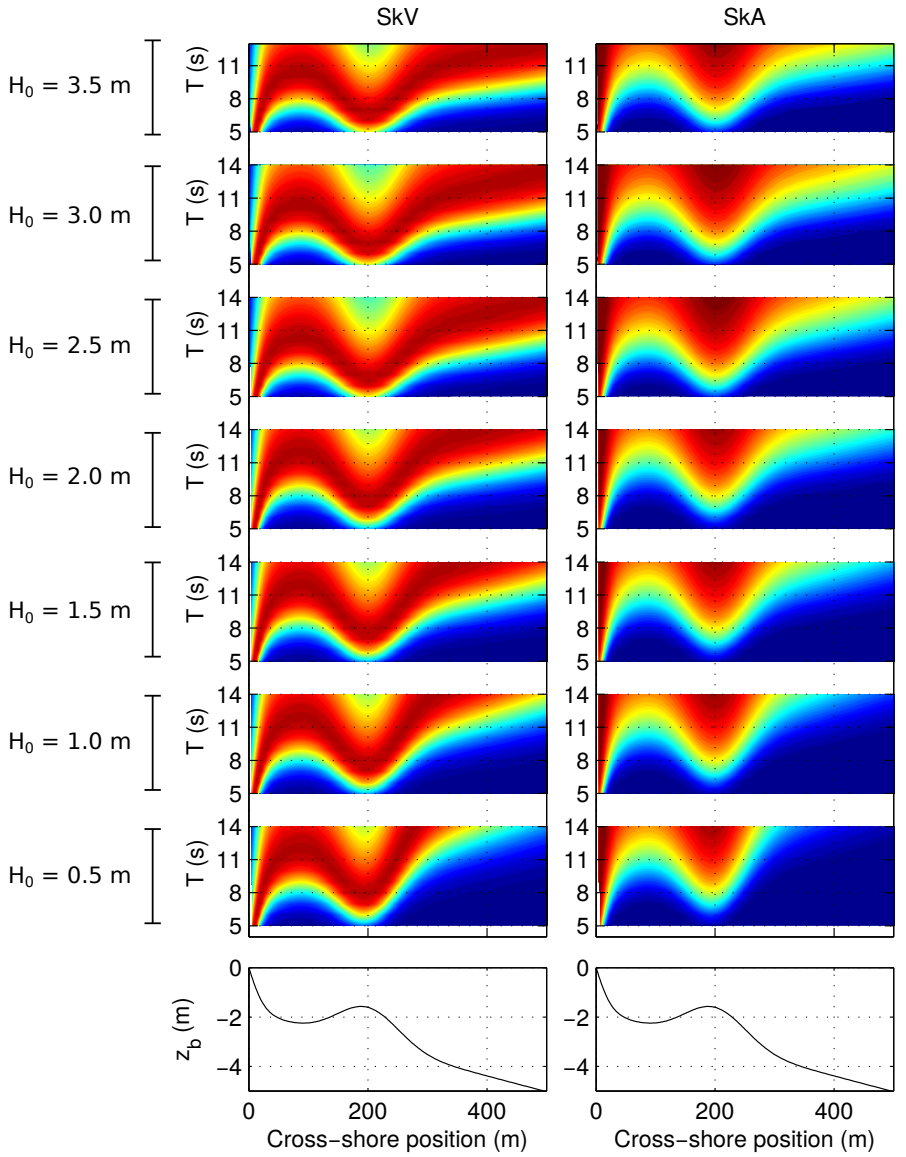

Figure 5.9: Cross-shore distribution of predicted wave velocity skewness SkV (left panels) and predicted wave acceleration skewness SkA (right panels) for several offshore wave conditions.

CHAPTER 6

WAVE VELOCITY AND ACCELERATION SKEWNESS EFFECTS ON ONSHORE SANDBAR MIGRATION MECHANISM[i]

6.1 INTRODUCTION

Surf zone sandbars are of primary importance for the persistence of sandy shores, as they protect the beach during storms causing wave dissipation through wave breaking. They also constitute a reservoir for the exchange of sand between the submerged and the dry beach. Since the morphology of sandbars and the surf zone hydrodynamics are intrinsically coupled, understanding sandbar dynamics is important for coastal protection, human activities (eg. industry, tourism, surfing, etc) or environmental issues (water quality, pollutant dispersion, biologic activity, etc). Sandbar morphodynamics has a strong three-dimensional nature which is linked to wave-breaking, inducing horizontal circulation in the surf zone (longshore current, rip currents). Despite the 3D nature of nearshore morphodynamics, in many cases sandbars are remarkably longshore uniform and it is assumed that cross-shore, rather than longshore processes, control the formation and migration of bars.

There is general consensus with regard to the underlying mechanisms causing the offshore migration of sandbars: during storms, strong waves drive near-bottom intense offshore directed flow (undertow) that moves bars offshore (Short, 1999). In contrast, the mechanics of onshore sandbar migration is still a controversial topic. Under low energetic conditions, currents are weak, and sediment transport is driven mostly by near-bottom wave orbital motion. However, early attempts to simulate onshore sandbar migration using wave-averaged sediment transport parameterizations based on bottom stresses (e.g. Meyer-Peter and Müller power law) were not successful (Roelvink & Stive, 1989; Wright *et al.*, 1991; Thornton & Humiston, 1996; Rakha *et al.*, 1997; Gallagher *et al.*, 1998). It was argued by Elgar *et al.* (2001) that this discrepancy was due to the sediment transport formulation, which considers velocity skewness but no acceleration skewness (skewness is here defined as the wave-averaging of the third power of a variable). This was confirmed by Hoefel & Elgar (2003) who used a bedload sediment transport proxy based on the acceleration skewness developed by Drake & Calantoni (2001)

[i]This chapter is based on the work in Fernandez-Mora *et al.* (2015*b*): Fernandez-Mora, A., Calvete, D., Falques, A. and de Swart H. E. 2015. Onshore sandbar migration in the surf zone: New insights into the wave induced sediment transport mechanisms. Geophysical Research Letters, ISSN 1944-8007, DOI: 10.1002/2014GL063004

to successfully model an observed onshore sandbar migration event during the Duck94 experiment at the Field Research Facility - USACE Army at Duck, North Carolina, USA. The contribution of Hoefel & Elgar (2003) suggested that acceleration skewness was indispensable to correctly model onshore bar migration.

Interestingly, Hsu *et al.* (2006) were also able to model onshore migration for the same event using a modified energetic-based sediment transport model that distinguishes the action of the wave stirring in sediment transport from the action of waves plus currents. As a result, it is unclear which mechanism, velocity or acceleration skewness, is the main driver of onshore sandbar migration. Hoefel & Elgar (2003) and Hsu *et al.* (2006) obtained their results by calculating the sediment transport from measured near bottom velocities (3 hours averaged) of current meters at 40-100 cm from the bottom during the Duck94 experiment. These models use the hydrodynamic measurements taken on the real bathymetry to compute bottom changes. As real and computed bathymetry may diverge, these models do not address the morphodynamic coupling and thus lack on the forecasting abilities of fully process-based morphodynamical models.

Such process-based models are nowadays available and they include a detailed description of the intra-wave motion. In the framework of wave-averaged and depth-integrated models, a parametrization that accurately describes that motion is a key factor. Ruessink *et al.* (2012) used an adjusted version of the parameterization for orbital motion of Abreu *et al.* (2010) to compute the morphological change of a cross-shore profile by using the CROSMOR model (Van Rijn, 2007*a*,*b*) for a 5 days simulation under steady wave forcing. They succeeded to model onshore sandbar migration patterns and, in this sense, their results encourage the use of this approximation as a plausible way to include wave skewness and asymmetry effects on sediment transport computation in beach evolution models. Van der Werf *et al.* (2012), using the Ruessink *et al.* (2012) parameterization, tested a total load transport formula against experimental data (Roelvink & Reniers, 1995; Grasso *et al.*, 2011). In this line, Fernandez-Mora *et al.* (2013) considered the extended energetic model of Hsu *et al.* (2006) and the intra-wave parameterization of Ruessink *et al.* (2012) to model bar migrations during 72 days at Duck, North Carolina, USA. Similarly, Dubarbier *et al.* (2013), also by using the approach for the intra-wave motion, combined the transport of Hoefel & Elgar (2003) and Hsu *et al.* (2006), to model the observed migration of a bar in a flume. However, those papers did not examine the joint action of both wave velocity and wave acceleration skewness comparing the role of each one on onshore sandbar migration mechanism.

In this chapter we examine the relevance of wave velocity and acceleration skewness on the onshore sandbar migration mechanism. To this end, the morphodynamic process-based model AMORFO70 is used by considering the intrawave orbital velocity approximation of Ruessink *et al.* (2012) and including the two main drivers of sediment transport, i.e., velocity skewness and acceleration skewness. A third sediment transport formulation that combines the two energy-based formulas above indicated is presented as well. Following the research of Hoefel & Elgar (2003) and Hsu *et al.* (2006), the process-based model is used to model the onshore migration event of Duck94. The three sediment transport formulas are calibrated separately to obtain the best fit for this event. A comparison of the results of the three formulas is done for two main purposes. The first is to confirm the results of Hoefel & Elgar (2003) and Hsu *et al.* (2006) with a process-based model. That is, sediment transport formulations based on either velocity skewness or on acceleration skewness can reproduce the onshore sandbar migration,

and, therefore, both wave properties may act in nature with similar effects. The second purpose is to elucidate which is the role of velocity skewness and acceleration skewness on the mechanism of onshore sandbar migration. First, the sediment transport parameterizations will be introduced. Data and experimental set-up will be described in the following section. Afterward, numerical results and a discussion will be presented, followed by the conclusions.

6.2 NUMERICAL MODEL AND SET-UP

To determine which is the governing mechanism driving onshore sandbar migration, sediment transport is computed considering two transport formulas, one directly related to velocity skewness and the currents (Hsu *et al.*, 2006) and the other one related to acceleration skewness (Hoefel & Elgar, 2003) (described in Chapter 3).

6.2.1 SEDIMENT TRANSPORT FORMULAS

6.2.1.1 THE VELOCITY SKEWNESS TRANSPORT (SKV)

The velocity skewness transport (hereinafter SkV transport) follows the sediment transport description given by Hsu *et al.* (2006) (Equation 3.4) complemented with a diffusive transport term Q_D (Equation 3.27). It is defined as

$$Q_{SkV} = Q_V + Q_C + Q_D \tag{6.1}$$

in which Q_V and Q_C are the net sediment transport due to waves and currents given by Hsu *et al.* (2006), respectively:

$$Q_V = \frac{C_w}{(s-1)g}\left(\frac{\varepsilon_B}{\tan\varphi}\langle|\vec{U}_0|^2 U_{0,x}\rangle + \frac{\varepsilon_S}{W_0}\langle|\vec{U}_0|^3 U_{0,x}\rangle\right) \tag{6.2}$$

$$Q_C = \frac{C_c}{(s-1)g}\left(\frac{\varepsilon_B}{\tan\varphi}\langle|\vec{U}_t|^2\rangle U_x + \frac{\varepsilon_S}{W_0}\langle|\vec{U}_t|^3\rangle U_x\right) \tag{6.3}$$

where the subscript x indicates the cross-shore component. Note that these sediment transport terms neglect settling lag effects, and thus, the transport related to the Stokes drift is not considered, as was done in Henderson *et al.* (2004). Values of the waves and currents friction coefficients C_w and C_c will be calibrated by fitting the SkV transport model results with observations, to verify that a sediment transport formula based on velocity skewness can explain the onshore migration of the bar.

6.2.1.2 THE ACCELERATION SKEWNESS TRANSPORT (SKA)

The acceleration skewness transport model (hereinafter SkA transport) is based on the model of Hoefel & Elgar (2003) (Equation 3.1), complemented with the transport due to mean currents (Q_C) and the diffusive transport (Q_D) as are given in equations 6.3 and 3.27, respectively, to provide a more accurate description of the physics involving sediment transport processes. The SkA transport reads

$$Q_{SkA} = Q_A + Q_C + Q_D \tag{6.4}$$

Although the original expression of the Hoefel & Elgar (2003) formula accounted just for the bed-load contribution, in the present work it is assumed that the K_a constant accounts for the contribution of both bedload and suspended load. Subscript x indicates the cross-shore component. The acceleration $\vec{a}(t)$ is computed as the local time derivative of the total velocity $\vec{U}_t$. Similarly as for the SkV transport, K_a, C_c and λ_d are parameters to be calibrated by fitting results of the SkA transport model with observations, in order to address that acceleration skewness can explain the onshore migration.

6.2.1.3 THE COMBINED TRANSPORT (MIX)

In order to account for all previous transport terms, a new sediment transport formulation is considered that combines the SkV and the SkA transport formulas and therefore contains the terms Q_V, Q_A, Q_C and Q_D of equations (6.2), (6.3), (3.27) and (3.1). To systematically analyze the relative importance of the velocity skewness and the acceleration skewness on onshore sandbar migration, the new sediment transport model (hereinafter MiX transport) is defined in terms of the SkV and the SkA transports as follows:

$$\begin{aligned} Q_{MiX} = \alpha_V Q_V^{\mathrm{SkV}} + \alpha_A Q_A^{\mathrm{SkA}} + \beta[\alpha_V Q_C^{\mathrm{SkV}} + \alpha_A Q_C^{\mathrm{SkA}}] \\ +\gamma[\alpha_V Q_D^{\mathrm{SkV}} + \alpha_A Q_D^{\mathrm{SkA}}] \end{aligned} \tag{6.5}$$

In the expression above, the superscripts SkV and SkA denote, respectively, the sediment transport terms from the SkV and the SkA models once they have been calibrated separately. The coefficients α_V, α_A, β and γ are four independent coefficients that weight the different transport terms. The coefficients α_V and α_A weight the amount of the action of velocity skewness and acceleration skewness on the MiX transport, in such a way that the set $[\alpha_V, \alpha_a, \beta, \gamma] = [1, 0, 1, 1]$ is the calibrated SkV transport, and the set $[\alpha_V, \alpha_a, \beta, \gamma] = [0, 1, 1, 1]$ leads to the calibrated SkA transport. The optimum values of the four coefficients $[\alpha_V, \alpha_A, \beta, \gamma]$ will result from a calibration with observed onshore sandbar migration.

6.2.2 DATA, EXPERIMENTAL SETUP AND CALIBRATION

The test period concerns the onshore sandbar migration event during the Duck94 field experiment at the Field Research Facility (FRF) at Duck, NC (Gallagher *et al.*, 1998; Elgar *et al.*, 2001). This sequence is characterized by a $30\ \mathrm{m}$ onshore migration of the sandbar under relatively low energy wave conditions from 21st to 28th September 1994. The hydrodynamics of the model are initialized with the cross-shore profile bathymetry of 21st September and are driven with the wave data sampled by the 8-m water depth, $925\ \mathrm{m}$ offshore FRF pressure gauges that supply the RMS wave heights, period and direction each 3 hours during the Duck94 experiment, and the water level is given by the NOAA pressure gauge at the end of the FRF pier (sampled each 6 minutes).

The hydrodynamics and the morphological change are computed every 300 s over a non-uniform grid. Sand grain diameter is considered constant along the profile and set to $d_{50} = 0.2$ mm with the corresponding settling velocity $W_0 = 0.025\ \mathrm{ms}^{-1}$ (Hsu *et al.*, 2006). Hydrodynamic parameters are set according to hydrodynamic calibration, using the wave height, set-up and longshore current data along 10 cross-shore profiles for 39 wave conditions during the SandyDuck'97 experiment at the FRF-Duck, NC (see Appendix A).

The model skill is quantified through a 'Brier skill score' type parameter (Van Rijn *et al.*, 2003; Ruessink, 2005) defined in Equation 4.1. The measured bathymetry on 28th September 1994 is fixed the end of the event, and the initial elevation at 21st September 1994. The values of the skill *S* range within $[-\infty < S \leq 1]$. Perfect agreement between results and observations is given by a $S = 1.0$. Values $0 < S < 1$ correspond to better simulations than assuming no-bottom change ($S = 0$).

As the aim of the present work is focused on sandbar morphodynamics, the skill *S* is considered along the bar zone $S_{bar} = S(185\ \mathrm{m}, 265\ \mathrm{m})$. In addition, the *S* related to the inner zone $S_{in} = S(155\ \mathrm{m}, 185\ \mathrm{m})$, the offshore zone $S_{off} = S(265\ \mathrm{m}, 335\ \mathrm{m})$ and the entire profile $S_{tot} = S(155\ \mathrm{m}, 335\ \mathrm{m})$ will be considered as well.

The SkV and SkA transports are calibrated to maximize the skill S_{bar} for the Duck94 onshore sandbar migration event. The sediment transport parameters are considered in the following ranges: the wave and current friction coefficients C_w and C_c from 0 to 5×10^{-3}, the K_a constant from 0 to 1×10^{-3} m s and the coefficient λ_d from 0 to 1×10^{-2}. The set of parameters achieving the global maximum value of S_{bar} are considered the best fitting parameters for the SkV and SkA transport models. Using these parameters, the MiX transport is calibrated ranging the weighting parameters α_V, α_A, β, and γ from 0 to 1.50 to get the maximum value of S_{bar}.

6.3 RESULTS AND DISCUSSION

6.3.1 PROFILE MORPHODYNAMICS

With the best fits for the SkV transport ($C_w = 3.9 \times 10^{-4}$, $C_c = 1.0 \times 10^{-5}$, $\lambda_d = 3.0 \times 10^{-3}$) and for the SkA transport ($K_a = 1.4 \times 10^{-5}$ m s, $C_c = 1.4 \times 10^{-4}$, $\lambda_d = 4.2 \times 10^{-4}$) , both bar crest position and growth are properly reproduced (see Figures 6.1A and 6.1B). In terms of the skill of each model, the result for the SkV transport is slightly more accurate than the one obtained with the SkA transport ($S_{bar}^{SkV} = 0.965$ and $S_{bar}^{SkA} = 0.955$). This yields to our first and second key results: i) the process-based model confirms the findings of Hoefel & Elgar (2003) and Hsu *et al.* (2006) and, ii) supports the considerations of Hsu *et al.* (2006) that indeed both sediment transport mechanisms can yield the onshore bar migration.

Note that each transport mechanism leads to different behavior outside the sandbar zone. The SkA transport performs quite better in the inner region, reproducing the near-shore erosion, but overestimates the erosion on the bar seaward face. On the contrary, the SkV performs better in the outer region, although it is not able to simulate the near-shore erosion and the trough shape. These behaviors have been quantified (see Table 6.1) by the skill in the inner surf zone (S_{in}), the shoaling zone (S_{out}) and for the entire profile (S_{tot}). Beach profile evolution for the Duck94 onshore event is also computed using the MiX transport.

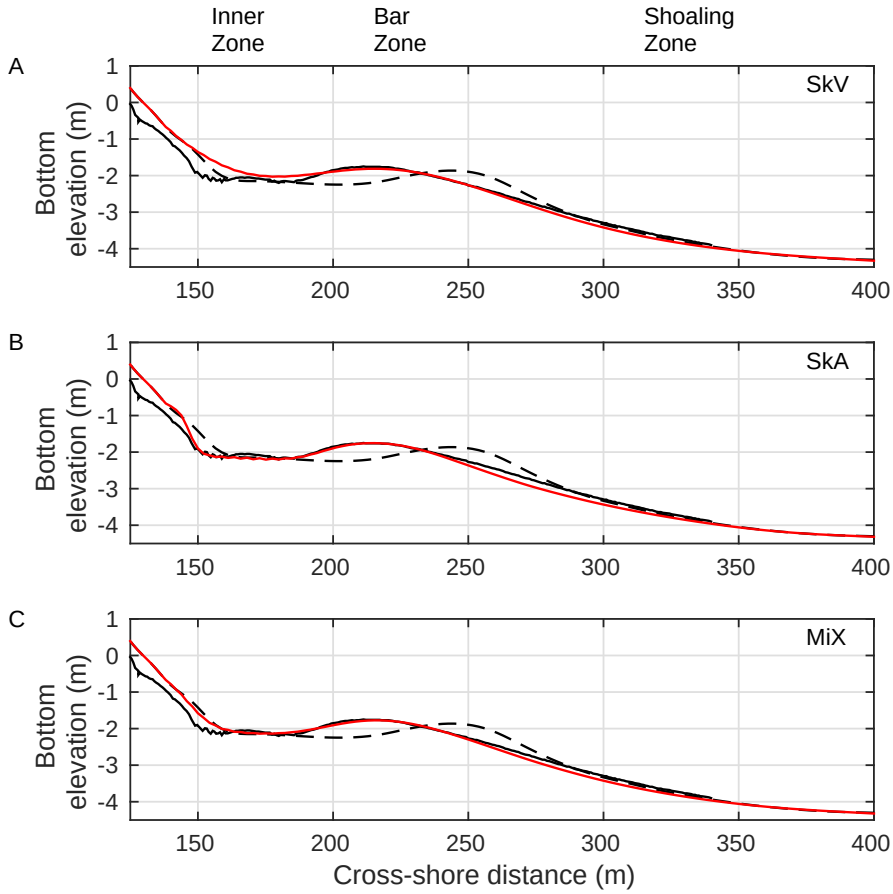

Figure 6.1: Morphological evolution (red line) of the Duck'94 onshore migration event for A) the SkV transport, B) the SkA transport, and C) the MiX transport. The initial measured profile (21^{st} September, black dashed line), final measured profile (28^{th} September, black solid line) are shown in each panel.

Beach profile evolution for the Duck94 onshore event is also computed using the MiX transport. To quantify the role of velocity skewness (α_V) and acceleration skewness (α_A) on the mixed transport formula, Figure 6.2 displays the maximum skill in modeling the bar zone (S_{bar}) as a function of α_V and α_A.

Considering the best fits for the MiX transport, the model reproduces accurately the crest position and depth of the sandbar and trough shape (Figure 6.1C). The best fit is given by $\alpha_V = 0.45$ and $\alpha_A = 0.45$ and has a maximum skill of $S_{bar}^{MiX} = 0.981$, larger than the SkV and the SkA skill values. Furthermore, when the rest of the profile is considered (see S_{in}, S_{out} and S_{tot} in Table 6.1) the MiX transport achieves the overall best performance. The bed

Table 6.1: Summary of the maximum model skill S and the corresponding $[\alpha_V, \alpha_A, \beta, \gamma]$ parameters at the bar, inner and offshore zones and the total profile, for the SkV, SkA and MiX transport.

	bar	inner zone	offshore zone	full profile	α_V	α_A	β	γ
	S_{bar}	S_{in}	S_{off}	S_{tot}				
(x_1, x_2)	$(185, 265)$	$(155, 185)$	$(265, 335)$	$(155, 335)$				
SkV	0.965	0.623	**0.876**	0.604	1.00	0.00	1.00	1.00
SkA	0.955	**0.927**	0.742	0.744	0.00	1.00	1.00	1.00
MiX	**0.981**	0.893	0.851	**0.816**	0.45	0.45	0.40	1.00

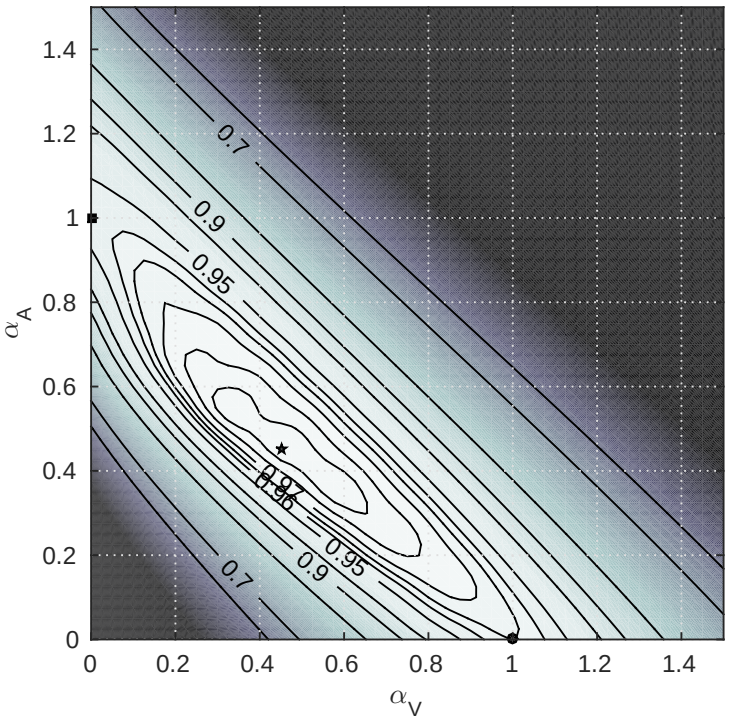

Figure 6.2: Maximum model skill S_{bar} in the $[\alpha_V, \alpha_A]$ space. Squared mark shows the position of the pure 'SkA' transport ($[0.0, 1.0, 1.0, 1.0]$); circular mark points the position of the pure 'SkV' transport ($[1.0, 0.0, 1.0, 1.0]$); star mark points the 'MiX' transport ($[0.45, 0.45, 0.40, 1.00]$)

changes due to the MiX transport captures the best trends of the ones related to the SkA and the SkV transports, collecting both behaviors on modeling the inner surf-zone and shoaling zone shapes (see Figure 6.1C). In this sense, their joint action is essential to model accurately the evolution of the entire profile during this onshore sandbar migration event.

This is further evidenced by analyzing the contribution of each term of the MiX transport in the bottom change (see Figure 6.3). At the Duck94 onshore sandbar migration event, the bottom evolution modeled with the MiX transport is characterized by a continuous onshore bar migration (Figure 6.3 E), as a result of an ongoing erosion at the seaward face of the bar and the deposition at the shoreward face (Figure 6.3 F). The main drivers of the erosion-deposition pattern in the vicinity of the bar crest are the velocity and acceleration terms of the MiX transport, Q_V and Q_A (first and second terms on the RHS of Equation 6.6). The bottom changes of both components show a similar cross-shore pattern (Figure 6.3 G and H). The bed changes driven by the divergence of the sediment transport due to currents Q_C (third term of Equation 6.6) are weaker (an order of magnitude lower than the Q_V and Q_A terms), and correspond to erosion in the inner face of the sandbar and accretion in the outer zone (Figure 6.3 I). The diffusive transport term Q_D (fourth term of Equation 6.6) produces the flattening of the sandbar (Figure 6.3 J). During this event the suspended-load transport components of the MiX transport are more relevant than the bed-load transport terms (see Appendix C). Summarizing, our third relevant finding is that both velocity skewness and acceleration skewness should be accounted for on the sediment transport modelling.

Our fourth important finding is that the morphodynamics of the shoaling zone is mainly driven by the velocity skewness (related to bed-shear stresses), while the morphodynamics of the inner surf zone is mainly controlled by acceleration skewness (related to pressure gradients, see Foster *et al.*, 2006). This could be expected because in the shoaling zone, wave-induced velocities become skewed, as wave surface changes from a sinusoidal to a pitched-forward face shape; onshore velocities are stronger than offshore velocities, and the sediment is then driven onshore. Indeed, field experiments (Marino-Tapia *et al.*, 2007) have shown that velocity skewness is the main transport mechanism in the shoaling zone. On the other hand, as the waves approach the breaking point, usually near the bar crest, wave velocity asymmetry increases producing strong accelerations that move sediment onshore. The action of near-bed accelerations driving sediment onshore has been analyzed by Foster *et al.* (2006). They provided field evidence that the incipient sediment motion is induced by fluid accelerations driven by pressure gradients. In addition to the pressure forces, an asymmetry in bed shear stress is another physical driver of sediment transport under acceleration-skewed waves. Therefore, both velocity skewness and acceleration skewness can act together in nature and provide the physical background of the MiX transport.

To substantiate our fourth point, the wave-averaged magnitudes of the Shields parameter θ' and the Sleath parameter Sl are considered. They are given by

$$\theta' = \frac{\frac{1}{2}\rho f_{cw}\langle|\vec{U}_t||U_{t,x}|\rangle}{(\rho_s-\rho)gd_{50}} \tag{6.6}$$

and

$$Sl = \frac{\rho\langle(\partial|U_{t,x}|/\partial t)\rangle}{(\rho_s-\rho)gd_{50}} \tag{6.7}$$

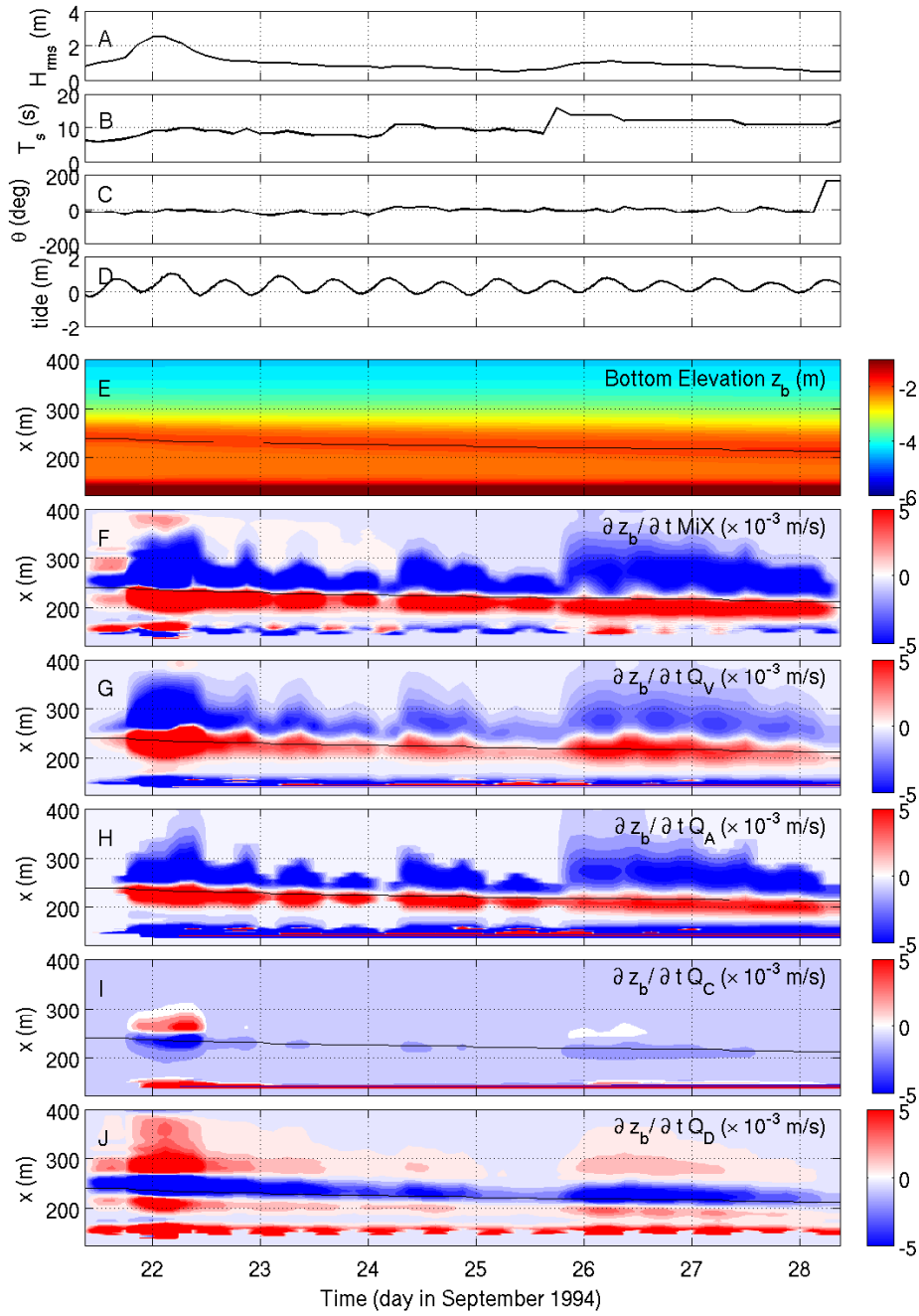

Figure 6.3: Time series of the observed offshore wave height H_{rms}, period T_p, angle of incidence θ and tide level (panels A to D). Panel E: Bottom evolution z_b during the Duck94 experiment for the MiX transport; panel F: Bottom changes driven by the MiX transport; panels from G to J: Bottom changes driven by each terms of the MiX transport: Q_V, Q_A, Q_C and Q_D respectively. Black solid line indicates the position of the bar crest.

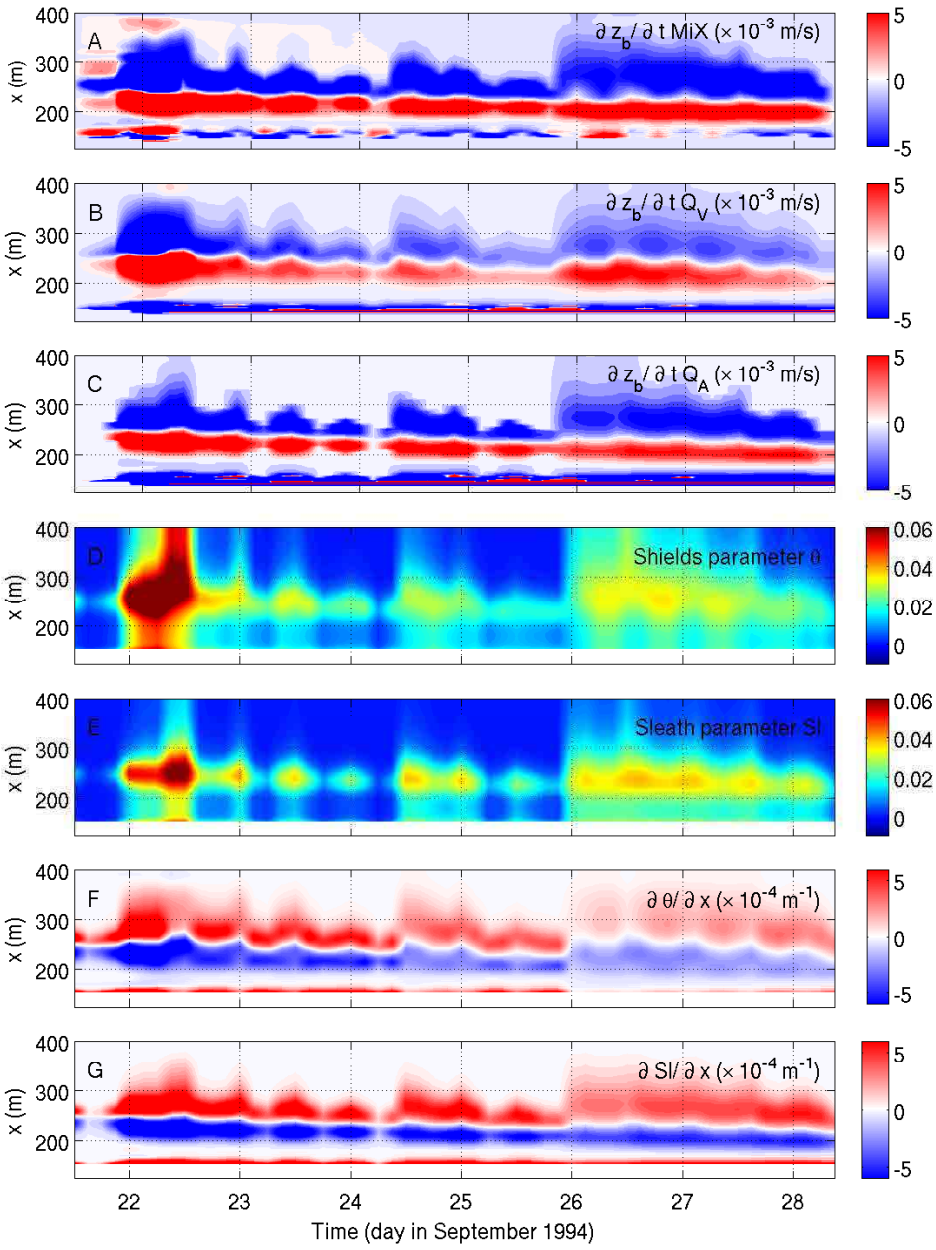

Figure 6.4: Time series of the bottom changes for the MiX transport, the Q_V term and the Q_A term (panels A to C). Panel D: Shields parameter θ' during the event; panel E: Sleath parameter Sl; panel F: spatial derivative of θ', $\partial\theta'/\partial x$; and panel G, spatial derivative of the Sl, $\partial\theta'/\partial x$.

where, ρ is the water density, ρ_s is the sediment density and f_{cw} is the wave and current friction factor (set to 0.02). The Shields parameter θ' (non-dimensional bed-shear stress) is related to the magnitude of the near-bottom velocity, and therefore, to the SkV transport. The Sleath parameter is related to the local derivative of the near-bottom velocity and thus, to the SkA transport. THe values of the bottom changes, the θ' and Sl parameters and their corresponding gradients during the event are shown in Figure 6.4. During all the event, the bed-shear stress action in the outer zone of the profile correlate with in the bottom changes in this zone (Figure 6.4 A, B, D and F). Eventually, under the high energy conditions during 22nd September (Figure 6.3), pressure gradients increase in the outer zone. At low energy conditions (from 23rd to 26th September), the bottom change in the offshore zone is dominated by the action of bed-shear stresses. In the bar crest, both bed-shear stresses and pressure gradients are present, showing the back and forth action of the pressure gradients as tides rise or fall, respectively. This is consistent with the fact that during the low tide, the bar is in the inner surf zone while during the high tide it is in the shoaling zone. Finally the results of the last stage (moderate wave heights conditions) clearly show that Sl is dominant respect to the action of θ' in the inner surf zone ($155\ \mathrm{m} < \mathrm{x} < 185\ \mathrm{m}$). On the contrary, in the the outer zone ($x > 265\ \mathrm{m}$) bed-shear stresses are dominant.

It should be noted that additional experiments, in which the acceleration $\vec{a}(t)$ is computed as the total time derivative of $\vec{U}_t$ instead of using the local time derivative, lead to similar results.

6.3.2 VALIDATION OF THE INTRA-WAVE NEAR-BOTTOM VELOCITY

In the previous section, it has been demonstrated that the wave velocity and acceleration skewness play a key role on modeling the onshore sandbar migration. Now, the modeled intra-wave motion is compared with measurements of the currentmeters during the Duck94 experiment in terms of these characteristics.

Measurements of the cross-shore near-bottom velocity have been provided by the currentmeter data sets from 21^{st} September 1994 1300 EST to 28^{th} September 1994 1600 EST during the Duck94 experiment (Figure 6.5 A). The currentmeters provided the 2 Hz sampled data of the intra-wave near-bottom velocities in sets of 3 hours that have been filtered by a 0.5 Hz low-pass filter. On the other hand, the model is driven by the 3-hour averaged wave conditions provided by the 8 m-depth pressure gauges and solves the depth and wave-averaged hydrodynamic variables to obtain the 3 hour-average representation of the intra-wave near-bottom velocities. Therefore, the direct comparison of the modelled intra-wave motions with the instantaneous measured velocities is not feasible.

To compare model and data, we have considered instead the skewness of the intra-wave near-bottom velocities and corresponding acceleration. These magnitudes are the essential wave characteristics that have been used in the model to compute sediment fluxes. The dimensional velocity skewness is computed as $Sk_U = \langle U_{tx}^3 \rangle$ where $\langle\rangle$ represents the time-averaging operator and U_{tx} is the intra-wave cross-shore velocity. Similarly, the dimensional acceleration skewness is computed as $Sk_A = \langle a_x^3 \rangle$.

The velocity and acceleration skewness from both measurements and model results show a similar spatial pattern during the event, see Figure 6.5. They increases gradually from the offshore zone to the bar crest and decays to a local minimum near the trough. Although the cross-shore patterns are similar, the model overestimates the values of velocity and accelera-

tion skewness, particularly under high energy conditions (first hours of 22^{nd} September 1994 and during 26^{th} September 1994).

A source of these differences is that currentmeters were located at different heights above the bed, see upper panel in Figure 6.6. Most of the currentmeters were deployed far above the wave boundary layer. The parameterization of Ruessink *et al.* (2012) provides in the model the intra-wave oscillatory velocity at the edge of the wave boundary layer and, thus, wave velocity skewness and asymmetry are computed at this depth. In this sense, this direct comparison of both skewness of the model results with those related to the measurements is not consistent. To avoid this problem, the intra-wave velocities of the model have been also computed at the depth of the currentmeters. Figure 6.6, panels A to L, show respectively the values of the velocity ans acceleration skewness of measurements and model results at the boundary layer and at the depth of the currentimeters at 6 stages during the event. Broadly, the velocity skewness of the model results decreases on being computed at the depth of the currentimeters, getting closer to the values given by the measurements. Under the high energy wave conditions (Figure 6.6 panel A), the differences are still noticeable, specially on the bar and on the inner-surf zone. However, the cross-shore patterns of both skewness remain similar. The acceleration skewness computed at the depth of the currentimeters is slightly overestimated, specially under high energy conditions (Figure 6.6 panel G). Nevertheless, its cross-shore patterns is similar to the one of the measurements.

Summarizing, althought there are quantitative differences between model results and measurements, the cross-shore patterns of both velocity and acceleration skewness, which lead to bottom changes, are very similar.

6.4 CONCLUSIONS

With the help of a full process-based morphodynamic model, it has been shown that accounting for the joint action of both velocity and acceleration skewnesses causes major improvement of the modeled onshore bar migration, and it is essential to accurately model the evolution of the entire cross-shore bottom profile. The sediment transport has a remarkable spatial dependence with regard to the wave propagation along the profile. Two regions should be distinguished: the shoaling zone, where the velocity skewness dominates the sediment transport that is mainly induced by bed-shear stresses, and the breaking and inner-surf zones, where the acceleration skewness dominates and sediment transport is mainly induced by pressure gradients.

Moreover, model results confirm that sediment transport based either solely on velocity skewness or acceleration skewness achieve to accurately reproduce the onshore sandbar migration, yet they can lead to significant mismatches away from the bar zone. Therefore, results in which sediment transport was computed from the observed velocities and for which both the velocity (Hsu *et al.*, 2006) and acceleration (Hoefel & Elgar, 2003) skewness can cause the onshore sandbar migration are confirmed. In order to achieve good results in process-based modelling, it is necessary to describe realistically (Abreu *et al.*, 2010; Ruessink *et al.*, 2012) the intra-wave orbital motion.

All these findings are subject to some limitations to be considered. One of the main assumptions on beach profile evolution models is the alongshore uniformity. In this sense, the alongshore variations in bathymetry induce variations in the wave properties and in the currents,

affecting the cross-shore transport and originating gradients in the longshore transport, and this has been disregarded. Moreover, the results presented here are, like the previous works of Hoefel & Elgar (2003) and Hsu *et al.* (2006), site-specific and are focused on one short event with mostly normal wave incidence. On the other hand, on testing the model under high energy conditions to reproduce an offshore migration event, the model can simulate the seaward migration linked to the sandbar decay but not a pure offshore migration. Further research should validate the present findings regarding the effects of velocity and acceleration skewness on sediment transport for different geomorphic settings and wave conditions.

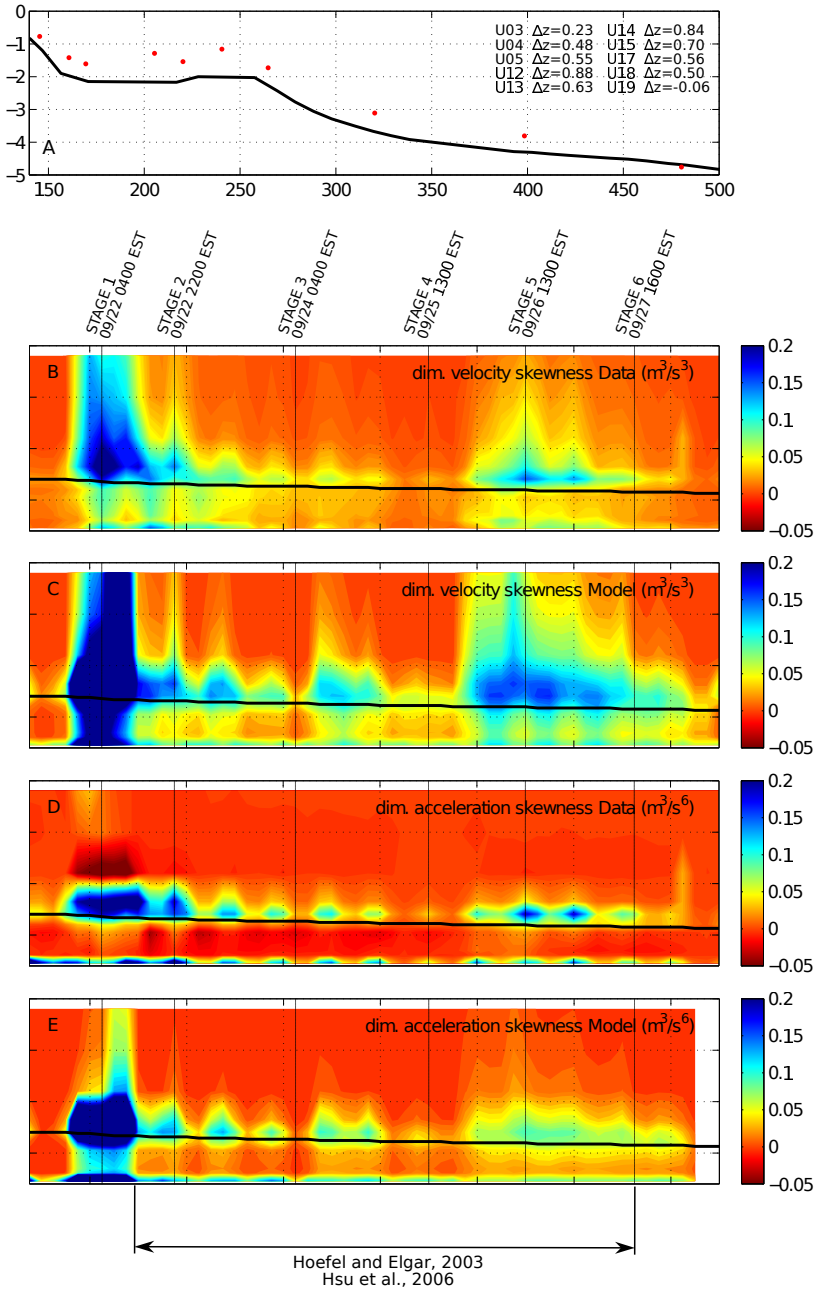

Figure 6.5: Upper panel A: Currentimeters position at 21st September 1994 1900 EST (black solid line, CRAB Survey bathymetry; red points, currentimeters position) and their elevation above the bed Δz. Dimensional velocity and acceleration skewness as a function of time and cross-shore position of the data, panels B and D respectively, and dimensional velocity and acceleration skewness of the model results, panels C and E, respectively. Vertical lines indicates the stages selected in Figure 6.6. Black solid line shows the position of the bar crest.

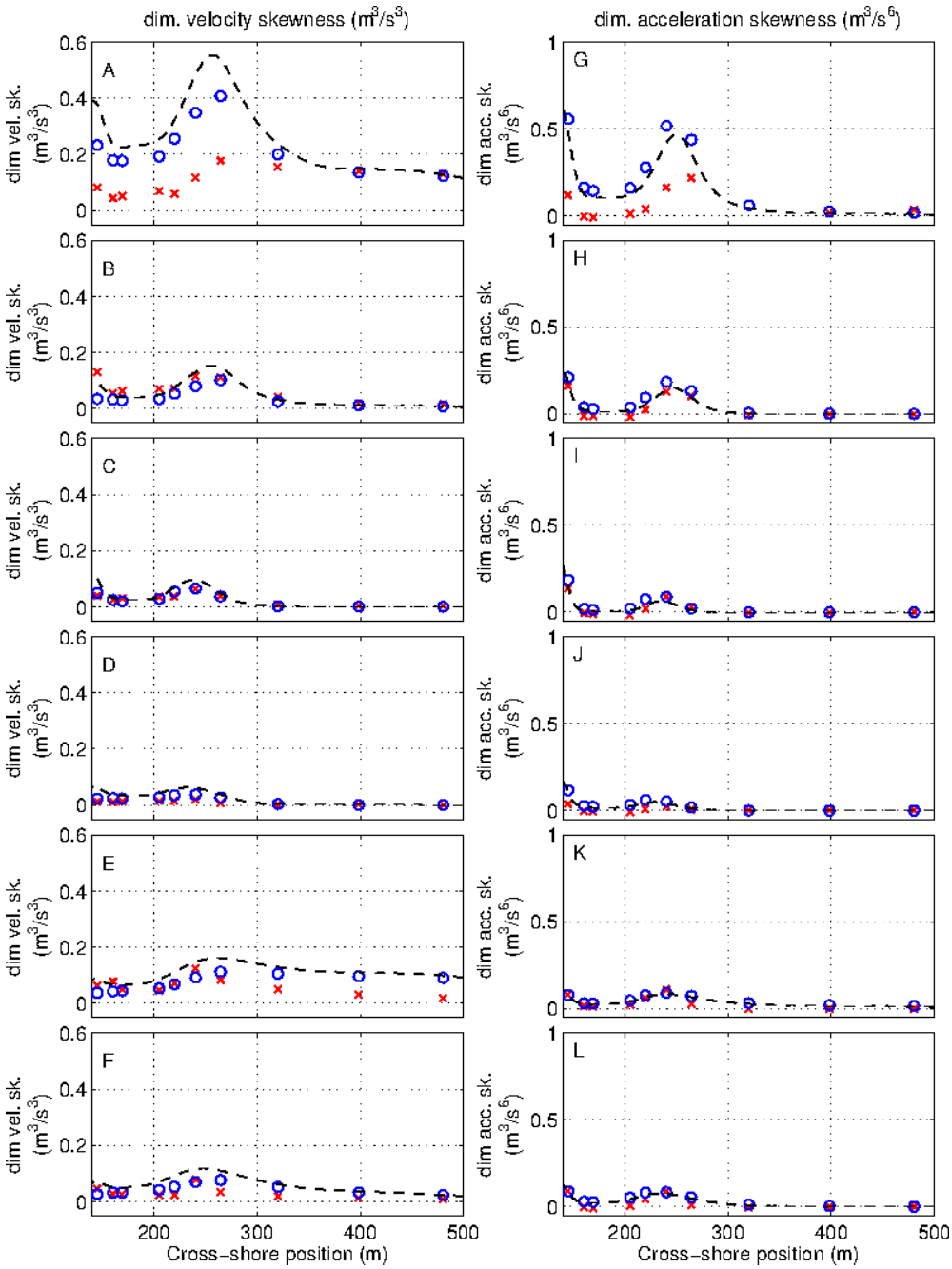

Figure 6.6: Panels A to F: Dimensional velocity skewness along the profile for each stage (model results, black dashed line; data values, red crosses; and model approximation in the currentmeters depth (blue circles). Panels G to L: Dimensional acceleration skewness along the profile for each stage (model results, black dashed line; data values, red crosses; and model approximation in the currentmeters depth (blue circles)

CHAPTER 7

VELOCITY SKEWNESS APPROXIMATION TO WAVE-INDUCED SUSPENDED SEDIMENT TRANSPORT[i]

7.1 INTRODUCTION

It has been stated in previous chapters that both velocity and acceleration skewness are essential to properly predict cross-shore morphodynamics. Hoefel & Elgar (2003) proved the relevance of the acceleration skewness on cross-shore morphodynamics by considering the transport formula of Drake & Calantoni (2001), that is a proxy to the wave-induced bed-load transport of Bailard & Inman (1981). They directly related sediment transport to the dimensional acceleration skewness $\langle a(t')^3 \rangle$. Also based in the Bailard & Inman (1981) formula, Hsu *et al.* (2006) separated the wave action from the current action in this formulation, and thus, relating the sediment transport rate to the dimensional velocity skewness $\langle U_0(t')^3 \rangle$.

This chapter addresses the dependence of the energy-based sediment transport of Hsu *et al.* (2006) on the wave shape in terms of wave velocity and acceleration skewness. A proxy for the sediment transport due to waves is formulated in terms of the wave velocity skewness and it is tested for several bathymetries and waves conditions and for the evolution of two real cases. First, the methodology and the experimental set-up is described. Second, the sediment transport is analyzed term by term and compared with velocity skewness and asymmetry. Following, the proxy is validated with real cases. Finally, conclusions are given.

7.2 NUMERICAL MODELING AND EXPERIMENTAL SET-UP

The AMORFO70 model, detailed in Chapter 2, is used to compute the cross-shore hydrodynamics and sediment transport for a set of fixed bathymetries and offshore wave conditions. The sediment transport rate is computed as the combination of an advective term Q_{ADV} and a diffusive term Q_D. The advective term is computed through the Hsu *et al.* (2006) parameterization (see Equations 3.2, 3.3 and 3.4 in Chapter 3). The diffusive transport is computed by

[i]This chapter is based on the work presented in the River, Coastal and Estuarine Morphodynamics'2013 conference held in Santander (Spain), 9th - 13th June with the title:'Waves skewness and asymmetry effects on beach profile morphodynamics'.

considering the Bagnold type diffusive transport detailed also in Chapter 3 (Equation 3.27).

The sediment transport has been computed by considering a wide range of wave conditions and bathymetric configurations. Offshore wave conditions ranged from low to high waves and from short to long periods (H_{rms} from 0.5 to 3 m, and T_s from 5 to 15 s). A four set of synthetic profiles have been considered, following the approximation of Yu & Slinn (2003) for longshore uniform barred beach profiles:

$$z_b(x) = a_1 \left(1 - \frac{\beta_2}{\beta_1}\right) \tanh\left(\frac{\beta_1 x}{a_1}\right) + \beta_2 x - a_2 \exp\left[-W_b \left(\frac{x - x_b}{x_b}\right)^2\right] \tag{7.1}$$

where x_b is the position of the bar crest, β_1 and β_2 are the nearshore and the offshore slope, respectively, a_1 is the bar width and a_2 is the bar amplitude. Figure 7.1 and Table 7.1 show the model profiles and the corresponding parameters, respectively.

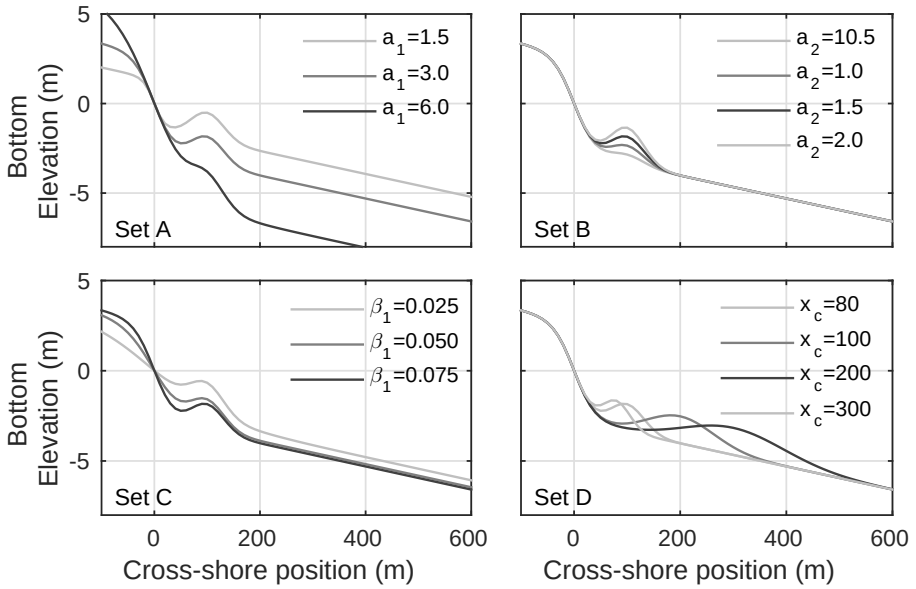

Figure 7.1: Experimental profiles: A, Set A: variation of the shape parameter a_1; B, Set B: variation of the shape parameter a_2; C, Set C: variation of the shoreline slope β_1; and D, variation of the bar crest position x_c.

7.3 RESULTS

7.3.1 TRANSPORT CONTRIBUTORS

The Hsu *et al.* (2006) sediment transport formula is divided in two terms: the 'waves' related transport, Q_W, and the 'waves plus currents' related transport, Q_C (see Chapter 3). Figure 7.2

Table 7.1: Characteristics of the beach profiles.

		a_1	a_2	β_1	β_2	x_c
Set A	Profile 1	1.5	1.5	0.075	0.0064	100
	Profile 2	3	1.5	0.075	0.0064	100
	Profile 3	6	1.5	0.075	0.0064	100
Set B	Profile 4	3	0.5	0.075	0.0064	100
	Profile 5	3	1.0	0.075	0.0064	100
	Profile 6	3	1.5	0.075	0.0064	100
	Profile 7	3	2.0	0.075	0.0064	100
Set C	Profile 8	3	1.5	0.025	0.0064	100
	Profile 9	3	1.5	0.050	0.0064	100
	Profile 10	3	1.5	0.075	0.0064	100
Set D	Profile 11	3	1.5	0.075	0.0064	80
	Profile 12	3	1.5	0.075	0.0064	100
	Profile 13	3	1.5	0.075	0.0064	200
	Profile 14	3	1.5	0.075	0.0064	300

shows the Q_{ADV} and the corresponding Q_W and Q_C for different periods and the same wave height $H_{rms} = 1$ m (for an example, Profile 2 of the Set A is shown). On analyzing which of the terms is the main contributor on the advective transport Q_{ADV}, it is found that the wave stirring term Q_W prevails over Q_C in the different cases in terms of transport rates and in the distribution along the profile. On extending this analysis to the rest of the experiments, shown in Figure 7.3, Q_W has the same order of magnitude and direction than Q_{ADV} for almost all the points and is aligned around the $1:1.25$ fitting line.

In their turn, the waves and waves plus currents terms can be split on their corresponding suspended-load and bed-load transport modes as follows

$$Q_W = \underbrace{\frac{C_w}{(s-1)g}\left(\frac{\varepsilon_B}{\tan\varphi}\langle|\vec{U}_0|^2 U_{0,x}\rangle\right)}_{Q_{W,B}} + \underbrace{\frac{C_w}{(s-1)g}\left(\frac{\varepsilon_S}{W_0}\langle|\vec{U}_0|^3 U_{0,x}\rangle\right)}_{Q_{W,S}} \tag{7.2}$$

$$Q_C = \underbrace{\frac{C_c}{(s-1)g}\left(\frac{\varepsilon_B}{\tan\varphi}\langle|\vec{U}_t|^2\rangle U_x\right)}_{Q_{C,B}} + \underbrace{\frac{C_c}{(s-1)g}\left(\frac{\varepsilon_S}{W_0}\langle|\vec{U}_t|^3\rangle U_x\right)}_{Q_{C,S}} \tag{7.3}$$

where the calibration parameters C_w and C_c are set equal to the values given by Hsu *et al.* (2006). Figure 7.4 shows the advective transport Q_{ADV} and the sediment transport terms $Q_{W,B}$, $Q_{W,S}$, $Q_{C,B}$ and $Q_{C,S}$ for the same profiles and wave conditions of Figure 7.2. Figure 7.5 shows the different transport terms respect to the advective transport for all the cases. On analyzing which of the two transport modes for each transport term Q_W and Q_C are the main driver of the total advective transport, it is found that the wave-related suspended-load term $Q_{W,S}$ is the main contributor of the advective sediment transport (Figure 7.5 panel C).

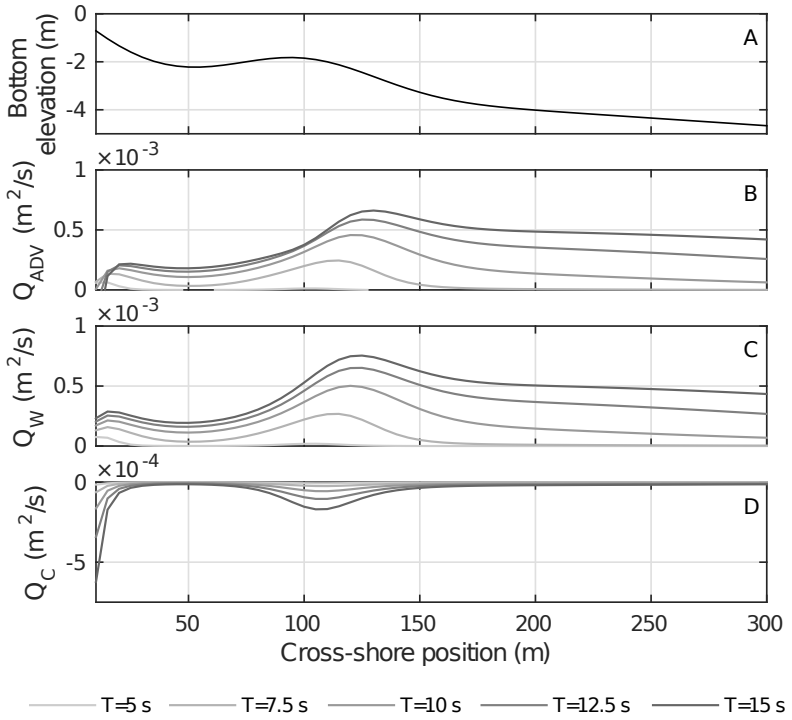

Figure 7.2: Results of sediment transport rates for the profile 2 (panel A) under $H_{rms} = 1$ m and different periods T: B, advective sediment transport Q_{ADV}; C, wave-related term Q_W; and D, waves plus currents term Q_C.

7.3.2 WAVE-INDUCED TRANSPORT SPLIT UP

It has been found that the wave-related transport terms of the Hsu *et al.* (2006) transport formula are the main drivers of sediment transport. These terms are directly related to the third and the fourth moments of the near-bottom velocity $\vec{U}_0$ (Equation 5.1). Following Abreu *et al.* (2010), the intra-wave near-bottom velocity is expressed as the product of the near-bottom velocity amplitude U_δ times a shape function $f(t')$ as $U_0(t) = U_\delta f(t')$, where $f(t')$ is

$$f(t') = \sqrt{1-r^2}\frac{\left[\sin(\omega t') + \frac{r\sin\phi}{1+\sqrt{1-r^2}}\right]}{[1 - r\cos(\omega t' + \phi)]} \tag{7.4}$$

and r and ϕ are related to the non-linearity and the phase of wave velocity respectively (detailed in Chapter 5).

Similarly to the previous section, the results of a single profile are analyzed for different periods and the same wave height ($H_{rms} = 1$ m) in Figure 7.6 (Profile 2 of Set A). On observing the position of the local maximum of Q_W, between $100 < x < 150$ m, there

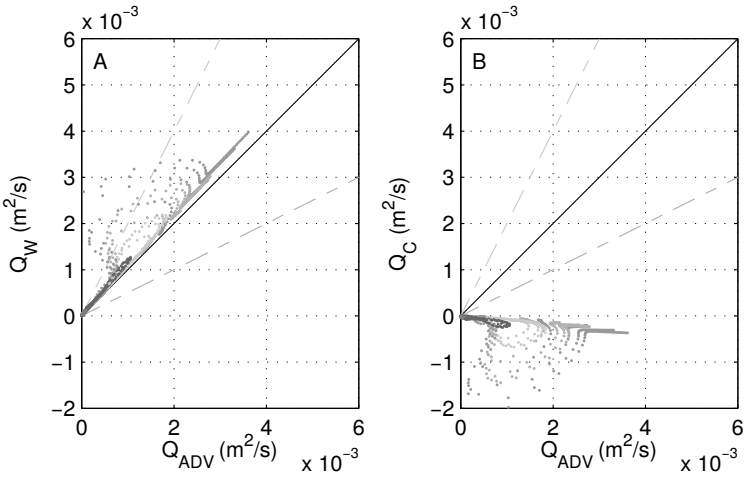

Figure 7.3: Comparison of: A, wave-related term Q_W respect to Q_{ADV} and B, wave plus currents-related term Q_C respect to Q_{ADV}, for all the combinations of bathymetries and wave conditions.

is an offshore shift with respect to the position of the corresponding local maximum of U_δ^4 ($x \approx 120$ m) (see Figure 7.6 B and C). This shift is related to the effect of the shape function $\langle f(t') \rangle$ on the sediment transport formula (Figure 7.6 D). However, at first sight, there is no straightforward observable relation between Q_W and $\langle f(t') \rangle$ (Figure 7.6 B and D).

The function $f(t')$ controls the shape of the near-bottom velocity along the profile, increasing the velocity and acceleration skewness as waves approach the shoreline. It has been stated in previous chapters (Chapters 5 and 6) that both characteristics are essential for sediment transport. Thus, they have also been compared with Q_W (Figure 7.6 B, E and F). A strong relation between the velocity skewness Sk_V, the position of the local maximum and the overall shape of Q_W along the profile is found. From this, it can be stated that the wave-related sediment transport Q_W is a function of (U_δ^4, Sk_V). In fact, the function $\{ = U_\delta^4 Sk_V$, shown in Figure 7.7 C, follows the same trend that Q_W. Thus, it is found that $U_\delta^4 Sk_V$ provides an approximation to the wave-induced sediment transport as

$$Q_W \approx Q_P = C_P U_\delta^4 Sk \tag{7.5}$$

in which C_P is a constant scaling factor ($m^{-2}s^3$) of the order $\mathcal{O}(-4)$.

7.3.3 PROXY VALIDATION

The sediment transport proxy Q_P has been validated with the estimated Q_W for all the experimental bathymetries and wave conditions. To quantify the agreement of Q_P with Q_W, the correlation coefficient R^2 and the normalized mean squared error NMSE are computed. The

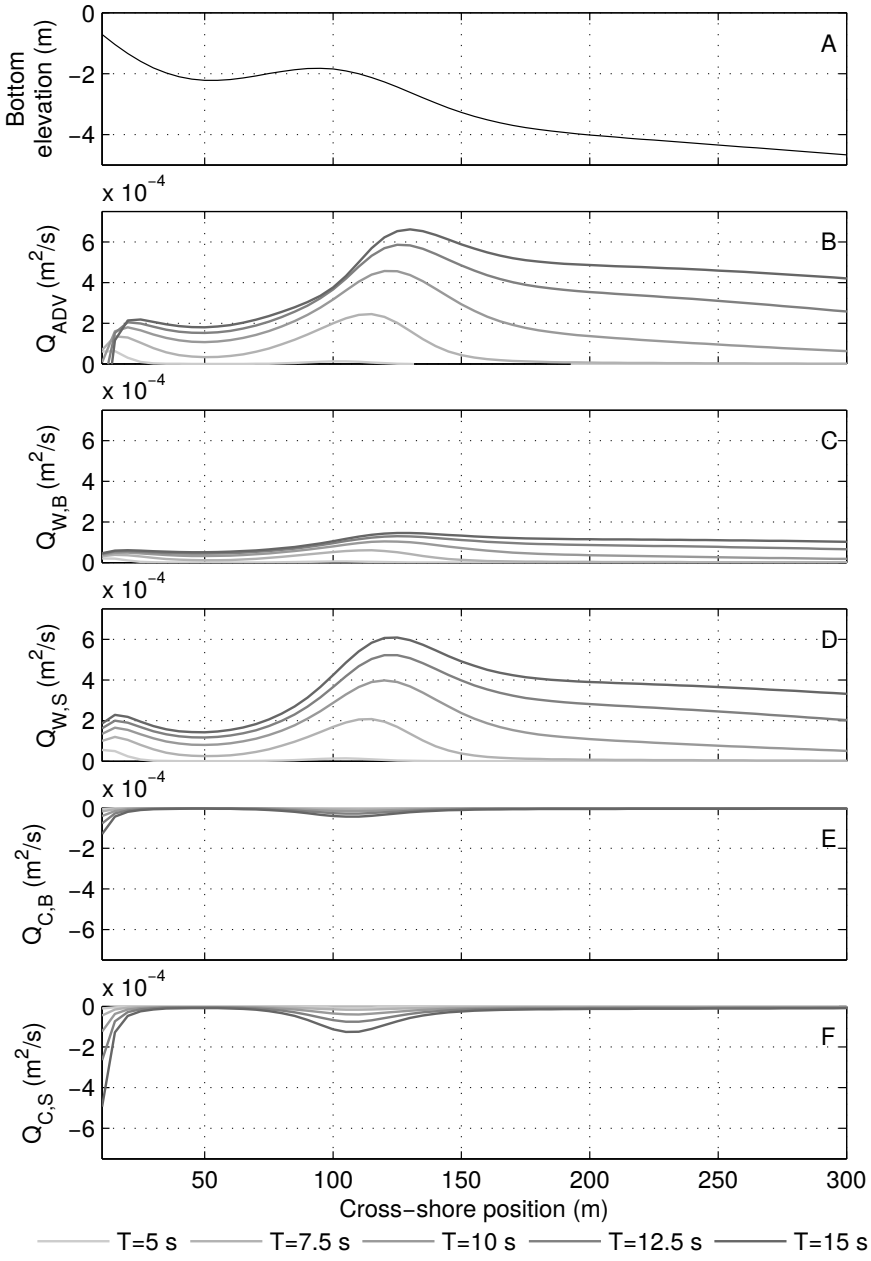

Figure 7.4: Results of sediment transport rates for the profile 2 (panel A) under $H_{rms} = 1$ m and different periods T: B, advective sediment transport Q_{ADV}; C, wave-related bed-load term $Q_{W,B}$; D, wave-related suspended-load term $Q_{W,S}$; E, current-related bed-load term $Q_{C,B}$; and F, current-related suspended-load term $Q_{C,S}$.

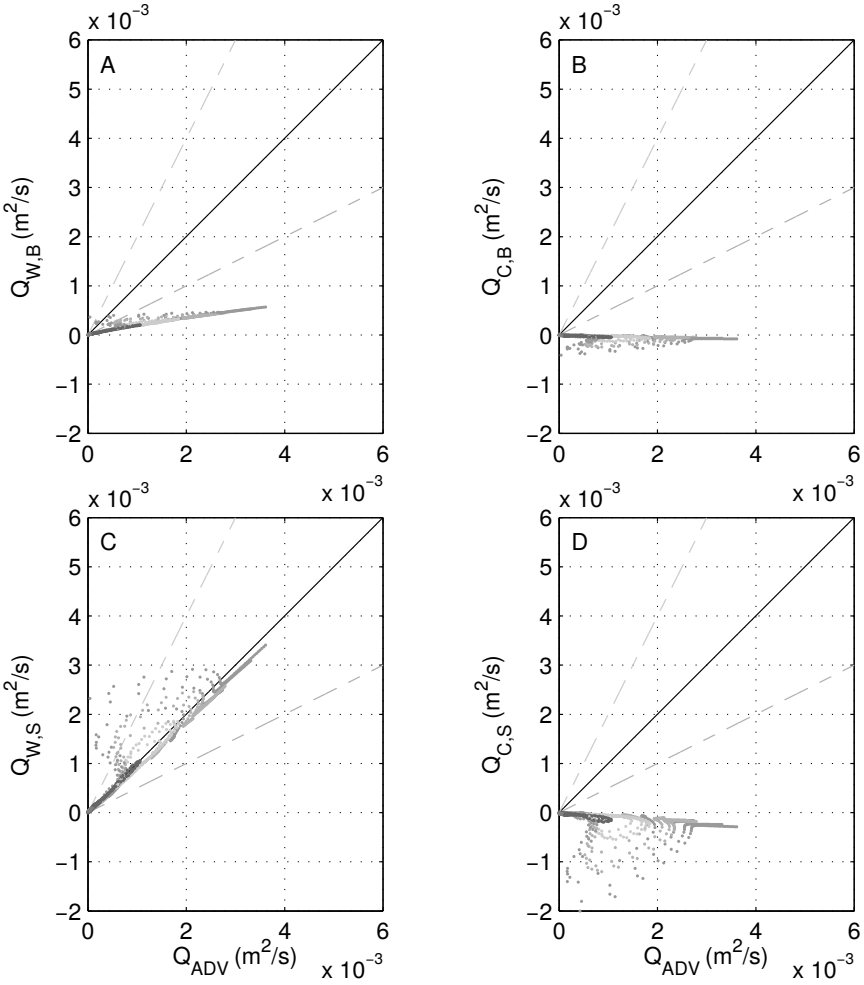

Figure 7.5: Comparison of: A, wave-related bed-load term Q_W respect to Q_{ADV}; B, current-related bed-load term $Q_{C,B}$ respect to Q_{ADV}; C, wave-related suspended-load term $Q_{W,B}$ respect to Q_{ADV}; and D, current-related suspended-load term $Q_{C,S}$ respect to Q_{ADV}, for all the combinations of bathymetries and wave conditions.

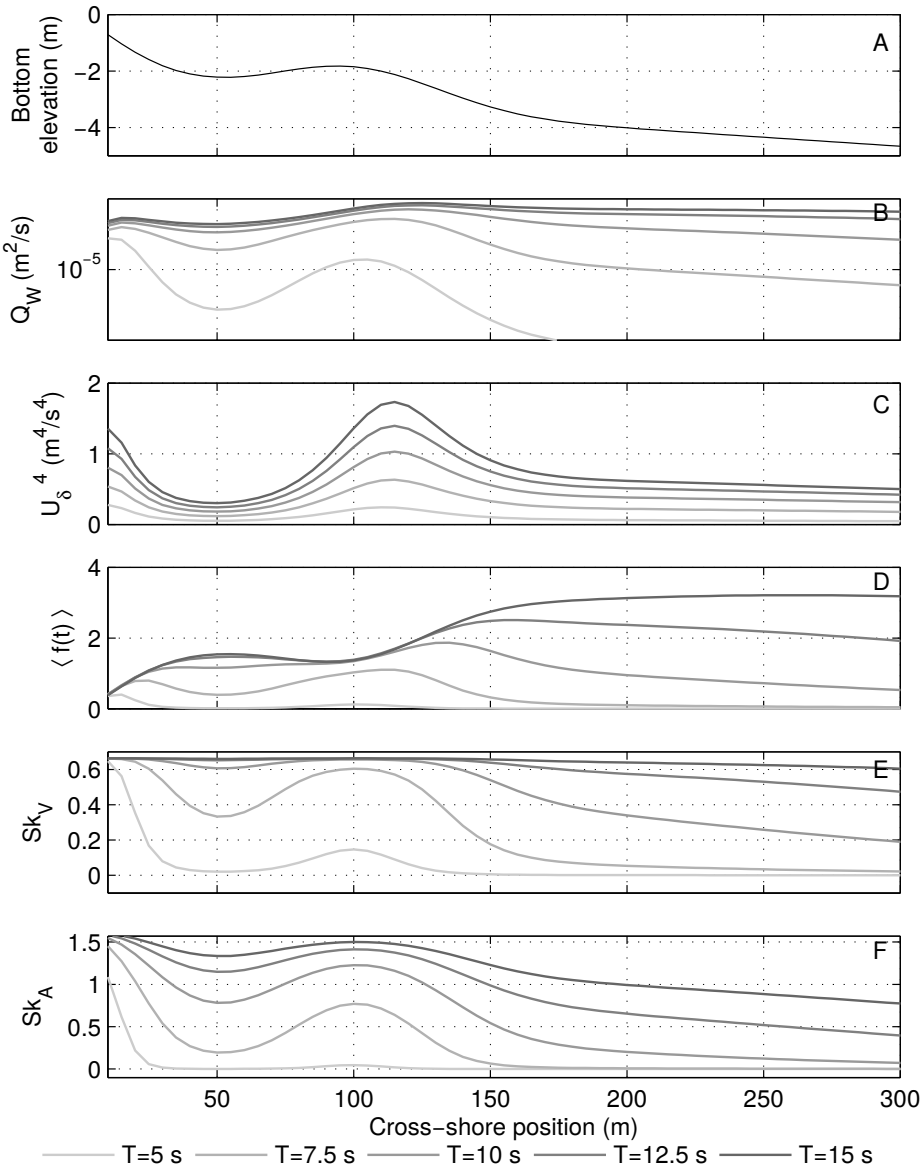

Figure 7.6: Results of sediment transport rates for the profile 2 (panel A) under $H_{rms} = 1$ m and different periods T: B, wave-related sediment transport Q_W; C, near-bottom velocity amplitude U_δ; D, wave-averaged shape function values $\langle f(t') \rangle$; E, near-bottom velocity skewness Sk_V; and F, near-bottom acceleration skewness Sk_A.

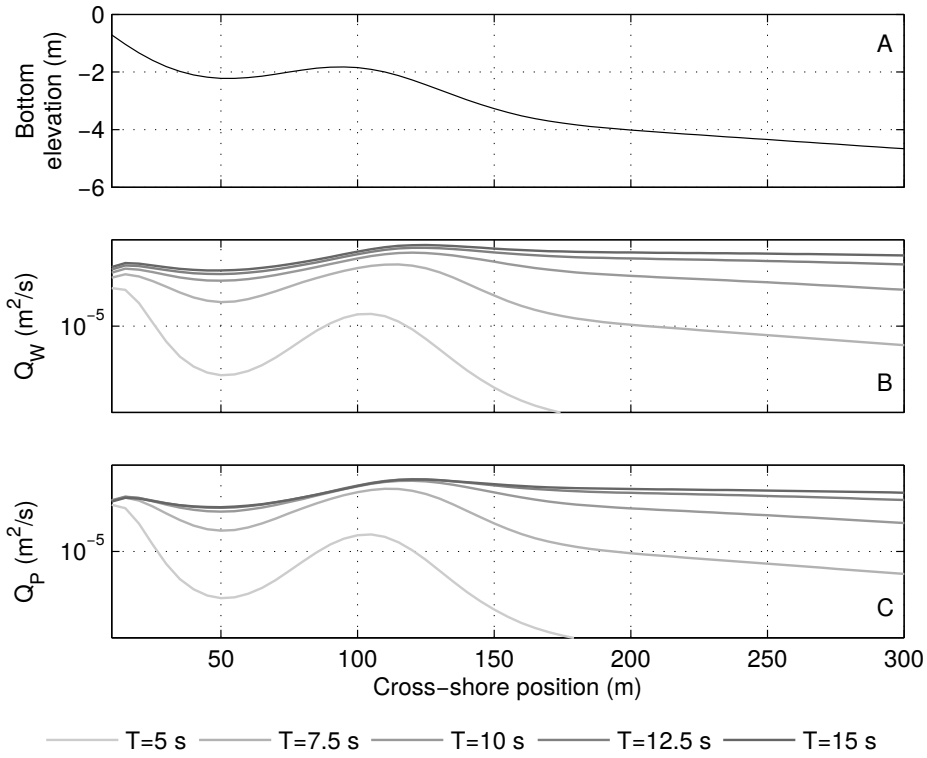

Figure 7.7: Results of sediment transport rates for the profile 2 (panel A) under $H_{rms} = 1$ m and different periods T: B, wave-related sediment transport Q_W; and C, the velocity skewness proxy Q_P (C_P set to 0.75×10^{-4}).

correlation coefficient R^2 is given by:

$$\mathrm{R}^2 = 1 - \frac{\sum_{\mathrm{i}}^{\mathrm{n}} (\mathrm{Q_{W,i}} - \mathrm{Q_{P,i}})^2}{\sum_{\mathrm{i}}^{\mathrm{n}} (\overline{\mathrm{Q_{W,i}}} - \mathrm{Q_{W,i}})^2} \tag{7.6}$$

and the root mean squared error RMSE is given by:

$$\mathrm{NMSE} = \frac{1}{\mathrm{n}} \sum_{1}^{\mathrm{n}} \frac{(\mathrm{Q_{W,i}} - \mathrm{Q_{P,ii}})^2}{(\mathrm{Q_{W,i}})^2} \tag{7.7}$$

in which $Q_{W,i}$ and $Q_{P,i}$ are the wave-related sediment transport and the proxy transport respectively, at point i, and n is the number of points.

Figure 7.8 compares the sediment transport proxy with the wave-related sediment transport for all the bathymetries and wave conditions. Table 7.2 summarizes the correlation coefficients and the root mean squared error for each bathymetry set and their mean values. Results show

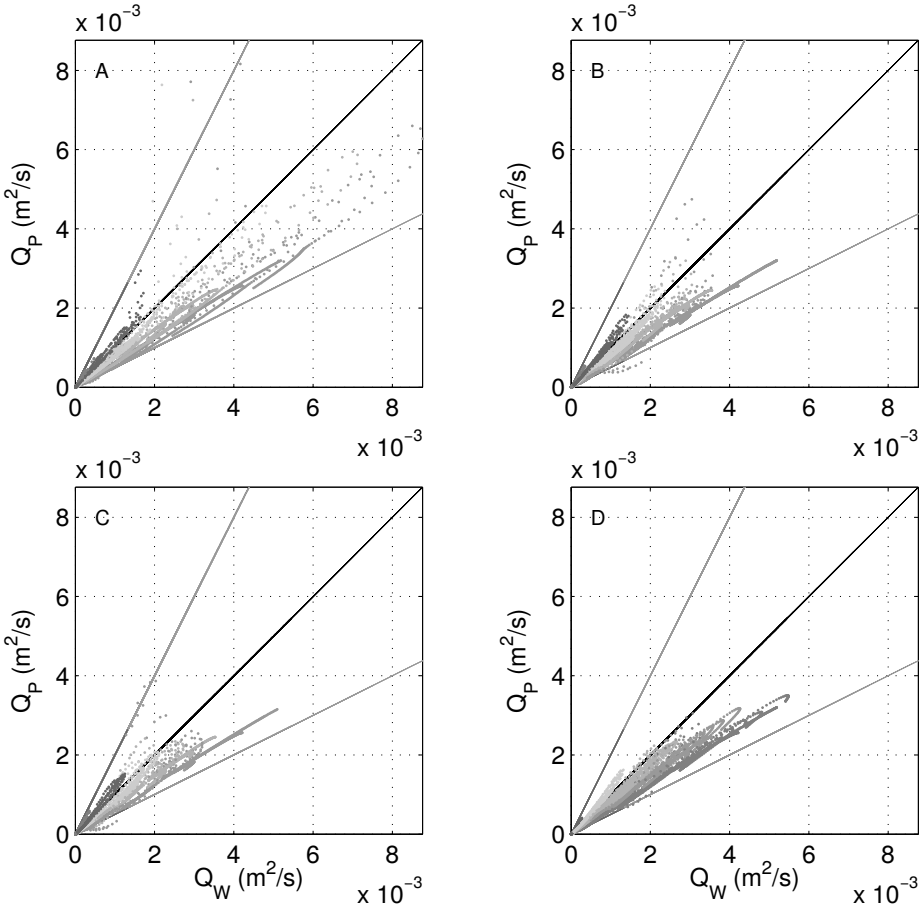

Figure 7.8: Comparison of the velocity skewness approximation Q_P with the wave-related sediment transport Q_W for: A, the set A bathymetries; B, the set B bathymetries; C, the set C bathymetries; and D, the set D, bathymetries.

Table 7.2: Correlation coefficient R^2 and normalized mean squared error NMSE of Q_P respect to Q_W for each bathymetry set considering the complete experimental wave conditions set.

Experimental set	R^2	NMSE
Set A	0.88	0.09
Set B	0.80	0.15
Set C	0.70	0.18
Set D	0.88	0.08
Mean	0.81	0.12

a good agreement between the proxy Q_P and the predicted wave-related sediment transport Q_W of the Hsu *et al.* (2006) formula.

We have also examined the morphodynamical evolution capabilities of the velocity skewness transport proxy. First, the model has been initialized with the cross-shore profile bathymetries and has been driven with the different steady offshore wave conditions at 8 m water depth and 1000 m from the shoreline, considering the total transport given by $Q_{ADV} + Q_D$ and $Q_P + Q_D$. Hydrodynamics, sediment transport and the corresponding morphological changes are computed each 300 s over a non-uniform grid during 1 h. The bottom changes $\Delta z_{b,P}$ driven by the velocity skewness proxy are compared with the bottom changes driven by the $Q_{ADV} + Q_D$ transport. Figure 7.9 compares the bottom change rates for both transport formulas. Results show a good agreement between bottom changes, with a correlation coefficient $\mathrm{R}^2 = 0.85$ and a $\mathrm{NMSE} = 0.006$. This shows that the total transport proxy $Q_P + Q_D$ provides a good approximation on simulating bottom changes.

Furthermore, the model has also been tested for two real events in which wave stirring conditions prevail (low energy conditions). The first test period consists in the onshore sandbar migration event during the Duck94 field experiment at the Field Research Facility (FRF) at Duck, NC (Gallagher *et al.*, 1998; Elgar *et al.*, 2001), detailed in Chapter 6. The second period is related to the SandyDuck97 field experiment, also at the Field Research Facility (FRF) at Duck, NC, and consists of a short onshore migration event from 6th to 9th September 1997. It is defined by a double bar system with an onshore migration of 10 m of the outer bar and a 20 m onshore migration of a shallow inner bar.

The model has been initialized with the cross-shore profile bathymetry of 21st September 1994 and the 6th September 1997 respectively. For the first case (Duck94), the model is driven with the corresponding data sampled by the 8-m water depth and 925 m offshore FRF pressure gauges, that supplied the RMS wave heights, period and direction each 3 hours during the Duck94, and the water level was given by the NOAA pressure gauge at the tip of the FRF pier (sampled each 6 minuts). For the second case (SandyDuck97), the model is driven with the corresponding offshore wave conditions given by the 17.4 m depth and 3000 m offshore wave-rider buoy that supplied the RMS wave heights, period and direction each 3 hours and the water level was also given by the NOAA pressure gauge at the tip of the FRF pier (sampled each 6 minuts). Hydrodynamics, sediment transport and bottom changes are computed each 300 s over a non-uniform grid with the time-series of wave and tide conditions.

Figure 7.10 displays the temporal evolution of each sequence. Respect to the Duck94 event (Figure 7.10 top panel), the onshore bar migration is very well predicted. Regarding the SandyDuck97 event (lower panel of Figure 7.10), the onshore migration of the outer bar is properly modeled and the position of the crest of the inner sandbar too, but the inner bar shape is poorly modeled. Table 7.3 summarizes the correlation coefficient R^2 and the NMSE of both simulations respect to the observed bathymetries. Overall, the proxy performs quite well for both events.

7.4 CONCLUSIONS

In this chapter, the dependence of sediment transport on wave velocity skewness has been studied. First, we have examined the relevance of the transport terms of the sediment transport formula of Hsu *et al.* (2006). The wave-induced sediment transport term is dominant respect

to the current terms, and particularly, the suspended-load transport term $Q_{W,S}$. Since Q_W is directly related to the near-bottom velocities, a direct linear relation between the wave-related sediment transport and the velocity skewness is found. This direct relation has been used to define a simple proxy for the wave-induced sediment transport that has been compared with several predictions of wave-related sediment transport rates and the corresponding bottom changes under several conditions. An overall good agreement between the proxy and Hsu *et al.* (2006) formula predictions is found. Furthermore, the sediment transport proxy has been tested against two real events with variable wave conditions. The proxy results in quite good predictions for both real events. Note that the sediment transport proxy Q_P is valid for the conditions of wave forcing and bathymetries here considered. Further work should be addressed to compare direct measurements of transport rates with the results of the proxy.

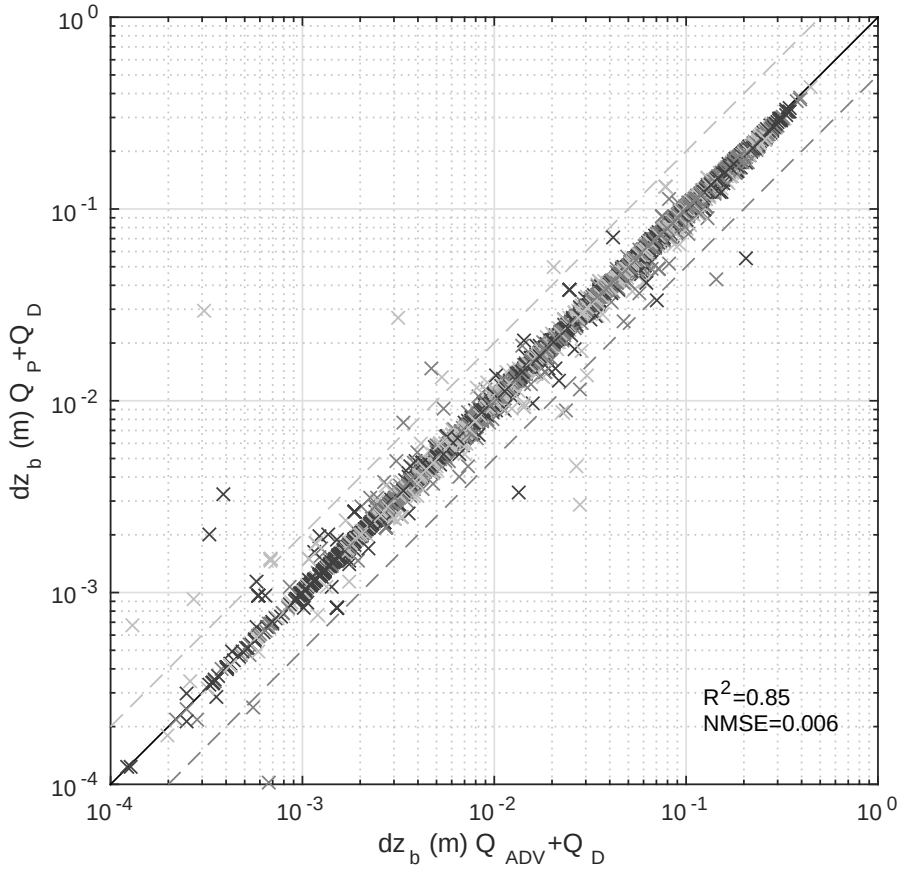

Figure 7.9: Comparison of the 1-hour bottom changes of the $Q_P + Q_D$ respect to the results of $Q_{ADV} + Q_D$ for the 420 combinations ow wave conditions and bathymetries.

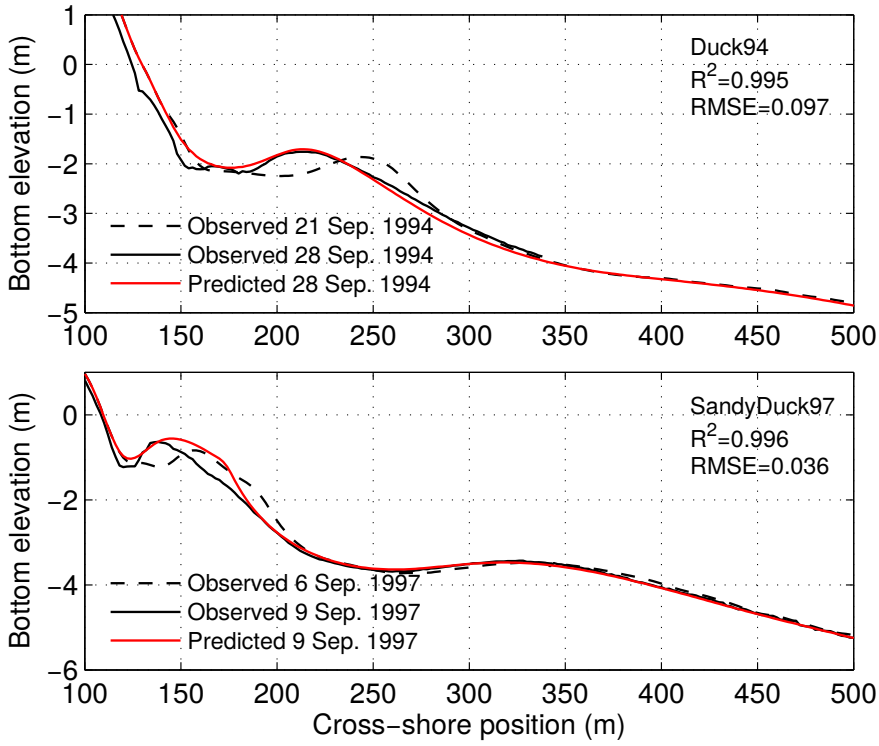

Figure 7.10: Temporal evolution predicted by using $Q_P + Q_D$ in the AMORFO70 model for: upper panel, the Duck94 onshore events; and lower panel, the SandyDuck97.

Table 7.3: Correlation coefficient R^2 and normalized mean squared error NMSE of the Duck94 and SandyDuck97 onshore migration events considering the $Q_P + Q_D$ approach to sediment transport. [a]

	R^2	NMSE
Duck94	0.98	0.007
SandyDuck97	0.99	0.019

[a] The R^2 and the NMSE are computed from $x = 150$ to $x = 335$ m for the Duck94 experiment, and from $x = 120$ to $x = 450$ m for the SandyDuck97 experiment.

CHAPTER 8

MORPHODYNAMICAL PREDICTION OF SEDIMENT TRANSPORT FORMULAS [i]

8.1 INTRODUCTION

The accurate and reliable prediction of beach morphology evolution under wave forcing is still an important challenge in coastal morphodynamic modeling. Many efforts have been made during the last decades to improve morphodynamic models which have become increasingly complex by incorporating more physical processes in the description of waves and currents. However, all these models essentially rely on sediment transport formulas to properly predict bottom changes and there are at present many different formulations to compute the sediment fluxes driven by waves and currents. Then, a crucial shortcoming of morphodynamic modeling is that under the same hydrodynamic conditions different formulas may predict very different sediment transport rates. The reasons for it is that: i) these formulas have been developed under different assumptions and different underlying physics and ii) they have been calibrated and tested under different conditions.

There are a number of studies where different transport formulas are compared with laboratory and field measurements. For example, Davies & Villaret (1997) tested four turbulent transport models against flume data. Although there was a high scater regarding the intra-wave sediment concentrations they found a good agreement between model results and data in terms of net transport rates. However, it is known that transport rates predicted for the same hydrodynamic conditions with different formulas may differ in orders of magnitude (Van Rijn *et al.*, 2001). In particular, Davies & Villaret (2002) compared the transport rates predicted by research and practical models for different hydrodynamic forcing. They also compared model outputs with field data. Their results show a large divergence between the predictions of the different models and also indicate that untuned models are in general not able to reproduce field measurements of sediment transport. Camenen & Larson (2005) studied the limitations of five sediment transport formulas (Bailard & Inman, 1981; Bijker, 1968; Dibajnia & Watanabe, 1992; Van Rijn, 1989; Ribberink, 1998) in terms of their sensitivity to wave orbital velocity, period, grain size and current. They also found diverging behaviors of the

[i] This chapter is based on the work in Fernandez-Mora *et al.* (2015*a*): Fernandez-Mora, A., Calvete, D. and Falques, A. 2015. Morphodynamical prediction of sediment transport formulas. Coastal Engineering (under review)

sediment transport rates under the same sediment and hydrodynamic conditions.

Thus, the disparity of sediment transport rate predictors has been amply put forward by the existing studies where different formulas have been compared between them and with laboratory and field measurements. However, the effects of this disparity on morphological change predictions have not been studied. First of all, it is important to stress that what is really relevant for morphodynamic modeling is not the amount of transport but the relative behavior of the transport rates along the profile, particularly, the shape of the spatial derivative of the sediment flux, Q_x, that is directly related to the bottom change rate $\partial z_b/\partial t$ (Davies & Villaret, 2002). Secondly, the practical morphodynamical models such as DELFT3D, MIKE, TELEMAC, SYSYPHE and ROMS among others (Deltares-Delft Hydraulics, 2007; DHI, 2004; Villaret & Davies, 2004; Haidvogel *et al.*, 2008), which are widely used in coastal engineering, are based on different physics and different numerical schemes (Amoudry & Souza, 2011). As a result, the differences between models such as assumptions, hydrodynamics, numerical methods and coding, that affect directly the computation of sediment transport rates, make difficult to discern which is the effect of the differences in sediment transport description on the beach evolution output.

In this chapter, the main differences between the beach profile morphodynamic predictions coming out of ten widely-used sediment transport formulas are investigated. This is done at two levels: i) by comparing the resulting initially incipient bottom changes where the morphodynamic feedback (hydrodynamics-morphology) is not yet present and ii) by comparing the long-term predicted evolutions of the cross-shore beach profile where the morphodynamic feedback is fully active. To this end, the AMORFO70 model is used to simulate the beach profile evolution with ten different sediment transport formulas. This ensures that all the sediment transport rates are computed with the same hydrodynamical model. Four synthetic cases inspired on the Short (1999) conceptual model are considered: two related to the accretionary sequence and two related to the erosive sequence. The sediment transport formulas and their effects on beach profile morphodynamics are compared in terms of the sediment transport rates and the morphological changes that they predict. THe summary of sediment transport formulas here considered is in Section 8.2. The details of the experiments and the model setup are in Section 8.3. Section 8.4 contains the comparison of the results in terms of the sediment transport rates, the incipient bottom changes and the long-term evolution of the profile of the sediment transport formulas for each sequence. Further discussions and conclusions of the results are given in Sections 8.5 and 8.6.

8.2 NUMERICAL MODELING

The intercomparison of the morphodynamic effects of sediment transport formulas has been developed by using the AMORFO70 model, detailed in Chapters 2 and 3. The model is complemented with several sediment transport formulas to compute the cross-shore directed sediment transport rate Q_x (see Chapter 3). Ten formulas have been considered, divided in four main groups:

i) energy-based (EN) formulas: the Hoefel & Elgar (2003) formula (hereinafter, EN-HE), the Hsu *et al.* (2006) formula (EN-HS), and the Fernandez-Mora *et al.* (2015*b*) combination (EN-FM);

ii) bed-load (BL) transport formulas: the Ribberink (1998) formula (BL-RB) and the Camenen & Larson (2005) formula (BL-CL);

iii) suspended-load (SL) transport formulas: the Van Rijn (1993) formula (SL-VR), the Camenen & Larson (2008) formula (SL-CL); and

iv) total-load (TL) transport formulas (bed-load plus suspended load transport): the Ribberink (1998) and Van Rijn (1993) combination (hereinafter, TL-RB+VR), that is a widely used total transport formula (Ruessink *et al.*, 2007; Van der A *et al.*, 2010*b*), the Camenen & Larson (2005) and Camenen & Larson (2008) combination (hereinafter, TL-CL), used by Nam *et al.* (2011), and the Soulsby (1997) total transport formula (TL-SB).

8.3 CASE STUDIES AND EXPERIMENTAL SET-UP

8.3.1 CASE STUDIES

Sediment transport formulas and their effects on beach profile morphodynamics are examined by exploring the temporal evolution in four scenarios that reflect common cross-shore beach profile morphodynamic processes: the sandbar formation sequence S1, the onshore sandbar migration S2, the offshore sandbar migration S3, and the dissipative state sequence S4. These sequences are inspired in the accretionary and erosive sequences of the conceptual model of Short (1999) by assuming that beach states can change by varying wave conditions and thus the offshore Dean number $\Omega_D = H_0/(\omega_s T)$.

1. The sandbar formation sequence (S1)

   Surf-zone sandbars may appear in dissipative beaches ($\Omega_D > 6$) under the mid-term forcing of intermediate wave conditions ($2.5 < \Omega_D < 5$). These conditions enhance the formation of sandbars by the erosion of the inner-surf zone and the accretion in the vicinity of the breaking zone. This sequence is inspired in the first stage of the accretionary sequence of the Short (1999) conceptual model.

2. The onshore and offshore sandbar migration sequences (S2 and S3)

   Longshore sandbars show a relevant temporal variability, as they tend to move onshore or offshore and even disappear depending on the wave conditions. Under the action of low waves (low Ω_D), longshore sandbars usually grow and migrate onshore, and if the forcing is long enough, they eventually can attach to the shoreline to finally reach a reflective beach state (hereinafter sequence S2). The common bottom change pattern is characterized by the erosion of the seaward face of the sandbar and the accretion of the shoreward face. Under high energy conditions (higher Ω_D), longshore sandbars usually migrate offshore and even decay, by the erosion of their inner face and accretion of the seaward face (hereinafter sequence S3). These sequences are related to the accretionary and erosive sequences of Short (1999) model, respectively.

3. The dissipative state sequence (S4)

   Intermediate terrace profiles forced by high wave conditions (large Ω_D) evolve towards the dissipative state. During the transition the profile becomes smoother by the accretion

of the shallower part of the terrace. A sandbar can be developed in the seaward point of the terrace an even migrate and decay further offshore.

The initial profiles of each sequence have been computed through the approximation given by Yu & Slinn (2003) for longshore uniform barred profiles:

$$z_b(x) = a\left(1 - \frac{\beta_2}{\beta_1}\right)\tanh\left(\frac{\beta_1 x}{a}\right) + \beta_2 x - A_b \exp\left[-W_b\left(\frac{x - x_b}{x_b}\right)^2\right] \tag{8.1}$$

where x_b is the position of the bar crest,β_1 and β_2 are the nearshore and the offshore slope, respectively, A_b is the bar amplitude and W_b is the bar width. Table 8.1 summarizes the parameters values that build the initial bathymetries of each beach state. Figure 8.1 shows the initial profiles of the different sequences. The steady offshore wave conditions for each sequence and the corresponding offshore Dean number $\Omega_D = H_0/(\omega_s T)$ are summarized in Table 8.2

Table 8.1: Characteristics of the beach profiles.

Sequence	β_1	β_2	a	x_b (m)	A_b (m)	W_b (m)
S1	0.025	0.0070	2.0	150	1.5	0.1
S2-S3	0.075	0.0064	2.5	200	1.5	10.0
S4	0.015	0.0080	3.0	350	1.5	5.0

8.3.2 MODEL SET-UP

The hydrodynamics, sediment transport, bottom changes ans bottom updating are computed every 300 s over a non-uniform grid that extend from the shoreline $x = 0$ m to $x = 1000$ m. The temporal evolution of the profile is computed considering the different time-scales of each sequence (summarized in Table 8.2).

The calibration parameters of each sediment transport formula are set to the values given by the corresponding authors (detailed in Appendix A). Sand grain diameter is considered constant along the profile and set to $d_{50} = 0.2$ mm.

8.4 INTERCOMPARISON OF SEDIMENT TRANSPORT FORMULAS

In this section, sediment transport formulas are evaluated for each sequence in terms of transport rates and morphological changes. Sediment transport rates are compared at the initial stage ($t = 0$ s). Morphological changes are analyzed at the initial stage ('incipient bottom change' $(\partial z_b/\partial t)|_0$) and at the end of the sequence ('long-term bottom changes'). Results of each sediment transport formula and sequence are shown in Figures 8.2 to 8.5. Tables 8.3 and 8.4 summarize the behavior of the incipient and the long-term bottom changes of each sediment transport formula respect to each sequence.

8.4.1 THE SANDBAR FORMATION SEQUENCE S1

On comparing the sediment transport rates for the S1 sequence, most sediment transport rates exhibit a local maximum onshore transport in the vicinity of the breaking point ($x \approx 300$ m) but differ in the amount of transport, that ranges from 10^{-5} to 10^{-4} $\mathrm{m^2 s^{-1}}$ (column A of Figure 8.2). Particularly, the EN-HS and EN-FM formulas, the BL-RB and BL-CL formulas, the SL-VR and SL-CL formulas and their corresponding combinations follow this main trend. This trend is not followed by the predictions of the EN-HE and TL-SB formulas.

In the case of the incipient bottom change $(\partial z_b/\partial t)|_0$ (see column B of Figure 8.2), there is a general trend on the predictions that describes an accretionary zone onshore of the breaking point, and an erosive zone offshore of the breaking point. This pattern leads to the formation of a terrace by steepening the shoaling zone ($x > 250 - 300$ m) and flattening the inner-surf zone ($x < 250$ m). The incipient bottom changes that follows this trend are given by the EN-HS and the EN-FM formulas, the bed-load formulas BL-RB and BL-CL, the suspended-load formulas SL-VR and SL-CL and their corresponding combinations (TL-RB+VR and TL-CL). The main differences between results rely in the position of the transition point from the accretive to the erosive zones (positive and negative values of the $(\partial z_b/\partial t)|_0$, respectively), that ranges from 250 to 300 m and the amount of the bottom change rates (that ranges from 10^{-5} to 10^{-4} m/s). Further differences are given in the case of the SL-CL formula that leads to an accretive zone further seaward than the rest of formulas (Figure 8.2 B3). On the contrary, the EN-HE formula results in the opposite pattern of the incipient bottom change by describing

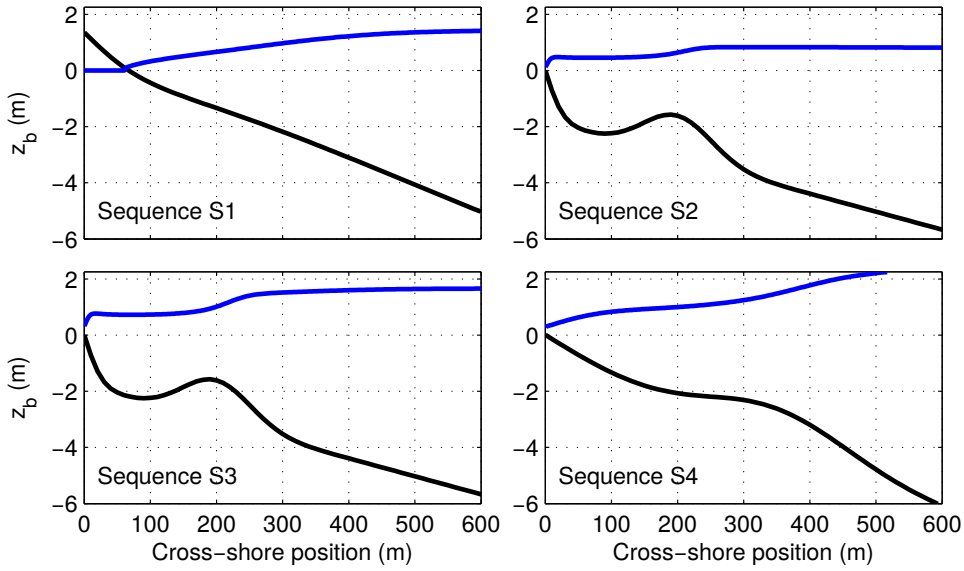

Figure 8.1: Initial bathymetries (black solid line) and wave height H (blue solid line) at $t = 0$ s of the four sequences: A, bar formation sequence S1; B, onshore sandbar migration sequence S2; C, Offshore sandbar migration S3; and D, dissipative state sequence S4.

Table 8.2: Offshore wave conditions for each sequence.

Sequence	H_0 (m)	T (s)	t (days)	Ω_D
S1	1.5	6	60	4.7
S2	0.75	8	30	2.4
S3	1.5	10	5	3.8
S4	2.5	10	10	6.3

the erosion of the inner-surf zone (Figure 8.2 B1). In its turn, the TL-SB formula leads only to an erosive incipient bottom change in the shoaling zone. In all cases, the incipient bottom change does not reflect the expected trend in the sandbar formation sequence.

Similarly to the accretionary sequence of the conceptual model of Short (1999), the final profile of the S1 sequence is defined by the long-shore bar-through profile (LBT). Consistently, it is found that many of the sediment transport formulas lead to barred profiles in their long-term evolution (shown in Figure 8.2 column D), although the predicted profiles differ in the shape and the position of the sandbars respect to the shoreline. Particularly, the EN-HS and the EN-FM formulas lead to a terrace profile with a breaker bar attached at the end of the terrace (at $x \approx 200$ m and at $x \approx 150$ m receptively). The BL-CL and SL-CL formulas and their combination TL-CL lead to the formation of steep-faced sandbars, specially in the case of the SL-CL formula and the total-load combination. On the other hand, the long-term profile of the BL-RB formula depicts a 100 m long shallow terrace. The EN-VR formula also leads to a terrace.shape profile with an incipient breaker bar at $x \approx 250$ m. The long-term evolution considering the BL-RB+SL-VR combination leads to a well defined 150 m long terrace. On the contrary, the EN-HE and the TL-SB formulas results on steep beach faces with an exponential profile shape due to the erosion of the inner-surf zone.

8.4.2 THE ONSHORE SANDBAR MIGRATION SEQUENCE S2

In this sequence there is a significant resemblance between the resulting transport rates (column A of Figure 8.3). Most of the sediment transport formulas match in the position of the local maximum onshore transport rates close to the the bar crest (ranging from $x \approx 200$ to $x \approx 250$ m), but they may differ in one order of magnitude. On the contrary, the TL-CL combination, that leads to a maximum onshore transport above the sandbar crest and a maximum offshore transport in the seaward face of the sandbar, and the TL-SB formula, that leads to a maximum offshore rate over the sandbar crest.

In terms of the incipient bottom change, most of the results mirrors the onshore migration pattern related to this sequence (column B of Figure 8.3), differing in the position of the local minimum-maximums, the rate of bottom changes that ranges from 10^{-4} to 10^{-3} ms^{-1}, and the position of the erosion-accretion transition point. In the case of the energy-based formulas and the bed-load transport formulas, the accretive zone is located above and in the shoreward face of the sandbar. Suspended-load formulas, specially the SL-VR formula, and the TL-

Table 8.3: Summary of the incipient bottom changes for each sediment transport formula regarding the cross-shore evolution sequences.

Sequence	S1	S2	S3	S4
	Bar formation	Onshore migration	Offshore migration	Dissipative state
EN-HE - Hoefel & Elgar (2003)	×	✓	×	✓
EN-HS - Hsu *et al.* (2006)	×	✓	✓	✓
EN-FM - Fernandez-Mora *et al.* (2015*b*)	×	✓	✓	✓
BL-RB - Ribberink (1998)	×	✓	×	✓
BL-CL - Camenen & Larson (2005)	×	×	✓	✓
SL-VR - Van Rijn (1993)	×	✓	✓	✓
SL-CL - Camenen & Larson (2008)	×	✓	✓	✓
TL-RB+VR - Ribberink (1998); Van Rijn (1993)	×	×	✓	✓
TL-CL - Camenen & Larson (2005, 2008)	×	✓	×	✓
TL-SB - Soulsby (1997)	×	×	✓	×

RB+VR combination result in an accretive zone that is located slightly seaward of the sandbar crest position. This pattern enhances the growth of the sandbar. In its turn, the TL-SB formula leads to the opposite pattern, by the accretion of seaward face of the sandbar, leading to the offshore migration of the sandbar.

This sequence reflects the progressive onshore migration of longshore sandbars, also present in the Short (1999) accretionary sequence. It is found that most of the sediment transport formulas simulate the onshore migration of the sandbar (column D of Figure 8.3). Particularly, energy-based models lead to a clear onshore migration and growth of the sandbar (Figure 8.3 D1), that is also described by the TL-CL combination. The BL-RB, the BL-CL and the SL-CL formulas describe the growth of the sandbar but not the onshore migration process. The SL-VR formula and the TL-RB+VR combination lead to the accretion of the immediately seaward point of the sandbar crest due to the erosion of the seaward face of the sandbar. On the contrary, the TL-SB formula results on the offshore migration and decay of the sandbar (Figure 8.3 D4).

It is worth pointing out that the simulations of the BL-CL, the SL-VR and the TL-RB+VR formulas stopped prematurely due to high gradients in the hydrodynamics because of unrealistic bottom shapes.

8.4.3 THE OFFSHORE SANDBAR MIGRATION S3

In this sequence, initial sediment transport rates differ noticeably in terms of the direction. The energy-based models, the bed-load transport BL-CL, the suspended-load transport SL-VR and the combinations TL-RB+VR and TL-CL results on onshore directed transport rates, while the rest are off-shore directed. However, the position of the local maximum-minimum is located in the vicinity of the bar-crest.

By comparing the incipient bottom changes, it is shown that the BL-RB formula, the suspended-load formulas, and the TL-RB+VR and TL-SB formulas agree with the offshore migration pattern in terms of the accretive-erosive zones along the profile (positive-negative values of the incipient bottom change), although some differences are evidenced in terms of the bottom change rates (Figure 8.4 B). On the contrary, energy-based models and the BL-Cl transport formula predict the accretion of the sandbar, differing in the position of the accretion maximum. Specially, this is evidenced on comparing the incipient bottom changes related to the EN-HE, EN-HS and the EN-FM formulas.

During this sequence, the shoreward face of the sandbar is eroded and sediment moves offshore infilling the seaward face. The sandbar position moves offshore and decay or even disappear. (column D in Figure 8.4). In case of the energy-based formulas, since the EN-HS formula simulates the off-shore accretion of the bar crest, the EN-HE and the EN-FM formulas result in the growth and a slight onshore sandbar migration. The BL-RB formula the sandbar decays, but does not migrate offshore. On the contrary, the BL-Cl formula results in an unrealistic growth of the sandbar. Both suspended load-transport formulas lead to the offshore decay of the sandbar. Similarly, the TL-RB+VR combination and the TL-SB formula lead to offshore decay shape. The TL-CL combination leads to the growth of the sandbar.

8.4.4 THE DISSIPATIVE PROFILE SEQUENCE S4

For this sequence, most sediment transport rates are defined by a local minimum at the breaking zone that is located in the seaward face of the terrace. Panels in Figure 8.5 column A show the initial sediment transport rates of each sediment transport formula. Differences between results rely in the position of the local minimum that ranges from $x \approx 400$ to $x \approx 500$ m.

Regarding the incipient bottom changes, the main pattern is characterized by accretion along the terrace zone and erosion in the seaward face of the terrace (column B of Figure 8.5). In this sense, most sediment transport formulas follow the Short (1999) conceptual model. The EN-HS and EN-FM formulas, the bed-load formulas, the SL-CL formula and the TL-CL combination lead to very similar shapes of the incipient bottom change function, differing in the amount of the maximum accretion point (located at $x \approx 350$ m), that ranges from 10^{-3} to 10^{-2} m/s. The EN-HE and the SL-VR formulas and the TL-RB+VR combination, that also lead to the infilling of the terrace zone, diverge from the rest of formulas in the position of the maximum accretion point. In the case of the EN-HE formula, this point is located further shoreward, and in the case of the SL-VR formula and the TL-RB+VR combination, this point is located further seaward. On the contrary, the TL-SB formula results in an incipient bottom change that depicts the erosion of the terrace and the accretion of the shoaling zone (Figure 8.5 column B4).

This state synthesizes the evolution of the terrace-shape profile towards the dissipative beach state under high energy conditions. Most of the sediment transport formulas are not able to describe this progression, but they reproduce part of the sequence, i.e., the formation and/or further offshore migration and decay of the breaker sandbar attached to the terrace. This process is reproduced by the EN-HS and EN-FM formulas, the BL-RB formula, the SL-VR formula and the TL-RB+VR combination. The EN-HS formula, the EN-FM and the EN-RB formulas lead to the formation of an incipient sandbar at the end of the terrace. Also they reproduce the shallowing of the inner-surf zone. The SL-VR formula and the TL-RB+VR

Table 8.4: Summary of long-term beach states for each sediment transport formula regarding the cross-shore evolution sequences.

Sequence	S1	S2	S3	S4
	Bar formation	Onshore migration	Offshore migration	Dissipative state
EN-HE - Hoefel & Elgar (2003)	×	✓	×	×
EN-HS - Hsu *et al.* (2006)	✓	✓	✓	✓
EN-FM - Fernandez-Mora *et al.* (2015*b*)	✓	✓	✓	✓
BL-RB - Ribberink (1998)	×	×	×	✓
BL-CL - Camenen & Larson (2005)	×	✓	×	×
SL-VR - Van Rijn (1993)	×	×	✓	✓
SL-CL - Camenen & Larson (2008)	×	×	✓	×
TL-RB+VR - Ribberink (1998); Van Rijn (1993)	×	×	✓	✓
TL-CL - Camenen & Larson (2005, 2008)	×	✓	×	×
TL-SB - Soulsby (1997)	×	×	✓	×

combination result in the formation of a sandbar at the end of the terrace and its further offshore migration. The EN-HE formula results also in the formation of a sandbar at the end of the terrace that migrates onshore. Similarly, the BL-CL and SL-CL formulas lead to an unrealistic growth of a sandbar attached to the terrace. The TL-CL combination lead to the formation of a sandbar and the incipient infilling of the inner-surf zone. On the contrary, the TL-SB formula results in the erosion of the terrace, and the further steepening the profile.

8.5 DISCUSSION

8.5.1 SEDIMENT TRANSPORT RATES

On comparing the initial predictions of sediment transport rates of the different sediment transport formulas, it is found that, under the same hydrodynamic conditions, they differ in two or three orders of magnitude. This is consistent with the findings of previous studies on the intercomparison of sediment transport rates driven by different sediment transport formulas (Bayram *et al.*, 2001; Van Rijn *et al.*, 2001; Davies & Villaret, 2002; Davies *et al.*, 2002; Camenen & Larroude, 2003). For all the cases, the formulas that predict to higher transport rates are the EN-HS formula, the BL-RB and BL-CL bed-load formulas, the SL-VR formula and the TL-RB+VR combination.

The physical processes that are considered in each formula are fitted against real flume and/or field data through coefficients that weight the action of these processes in the sediment transport, affecting directly to the spatial gradients that determine the bottom changes. In this sense, each sediment transport formula accounts for the different processes and transport modes in one way or another, but usually one process prevails over the rest. Besides, these coefficients are also used to compensate the errors derived by the lack of the description of some processes

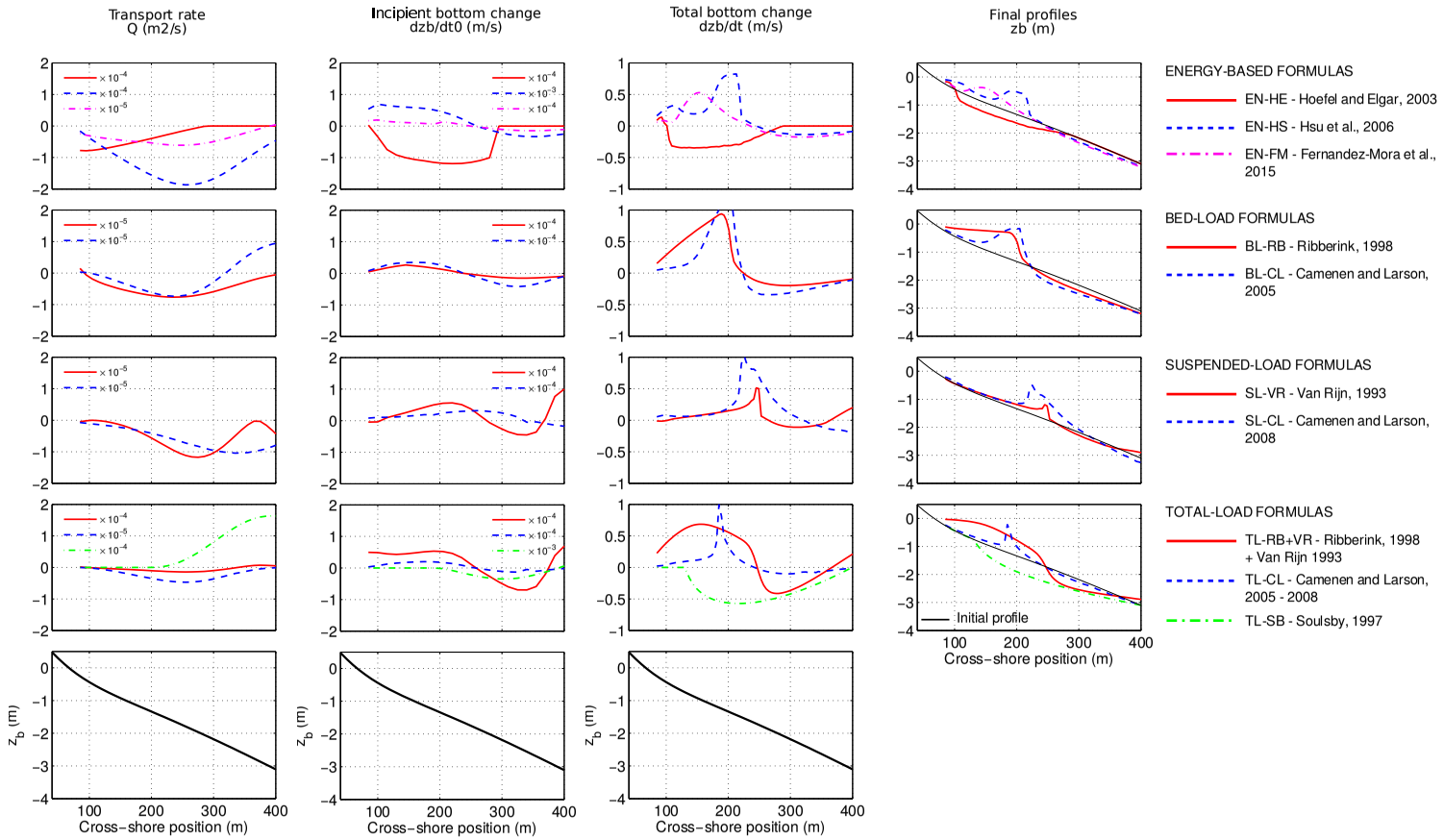

Figure 8.2: Results of the bar formation sequence S1 of the different sediment transport formulas: column A, Incipient cross-shore sediment transport Q_x, column B, incipient bottom change $\frac{dz_b}{dx}|_0$, column C, total bottom change $\frac{dz_b}{dx}|_{\text{inf}}$, and column D, final profile $z_{b,\text{inf}}$.

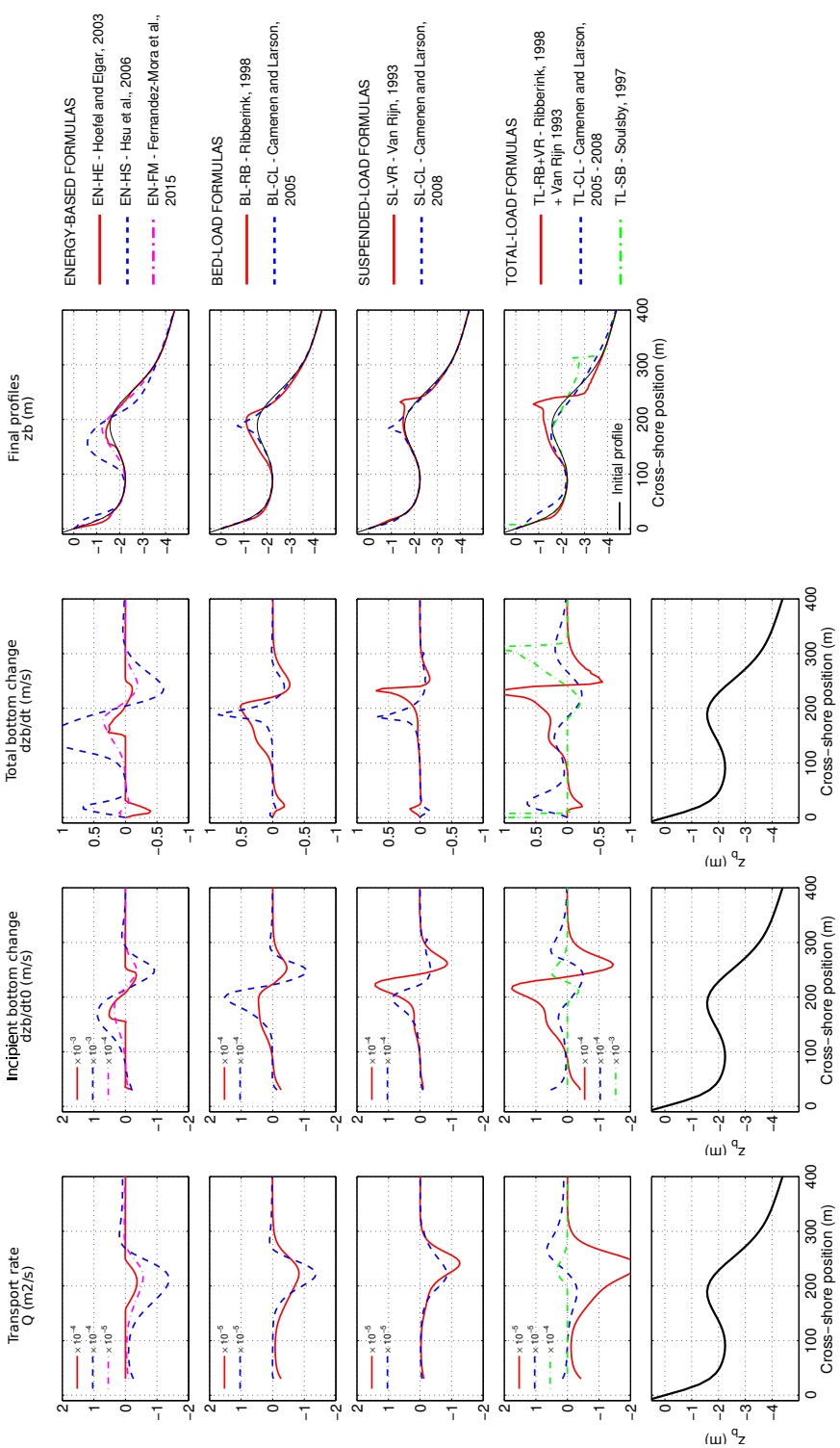

Figure 8.3: Idem Figure 8.2 for the onshore migration sequence S2.

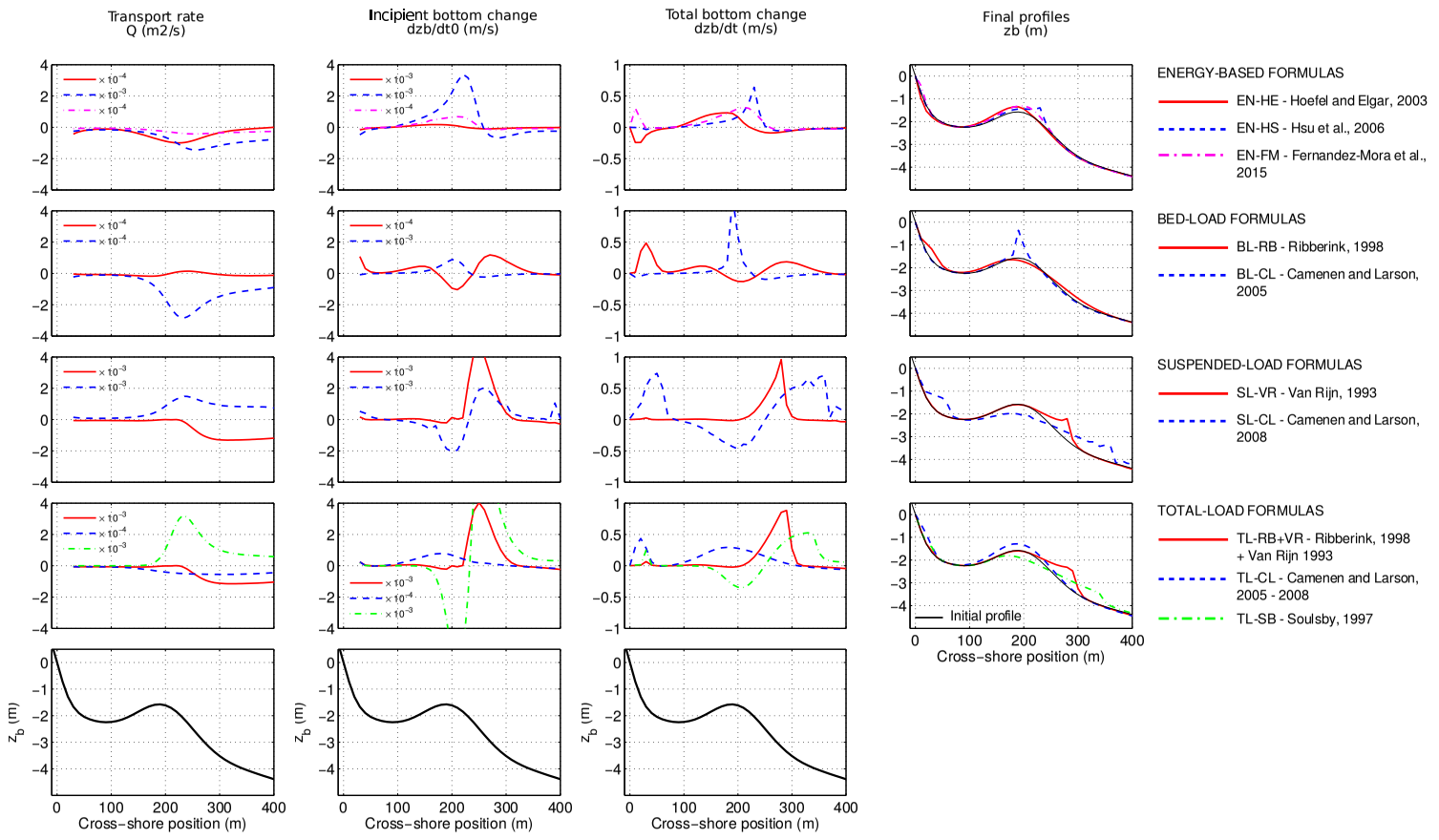

Figure 8.4: Idem Figure 8.2 for the offshore migration sequence S3.

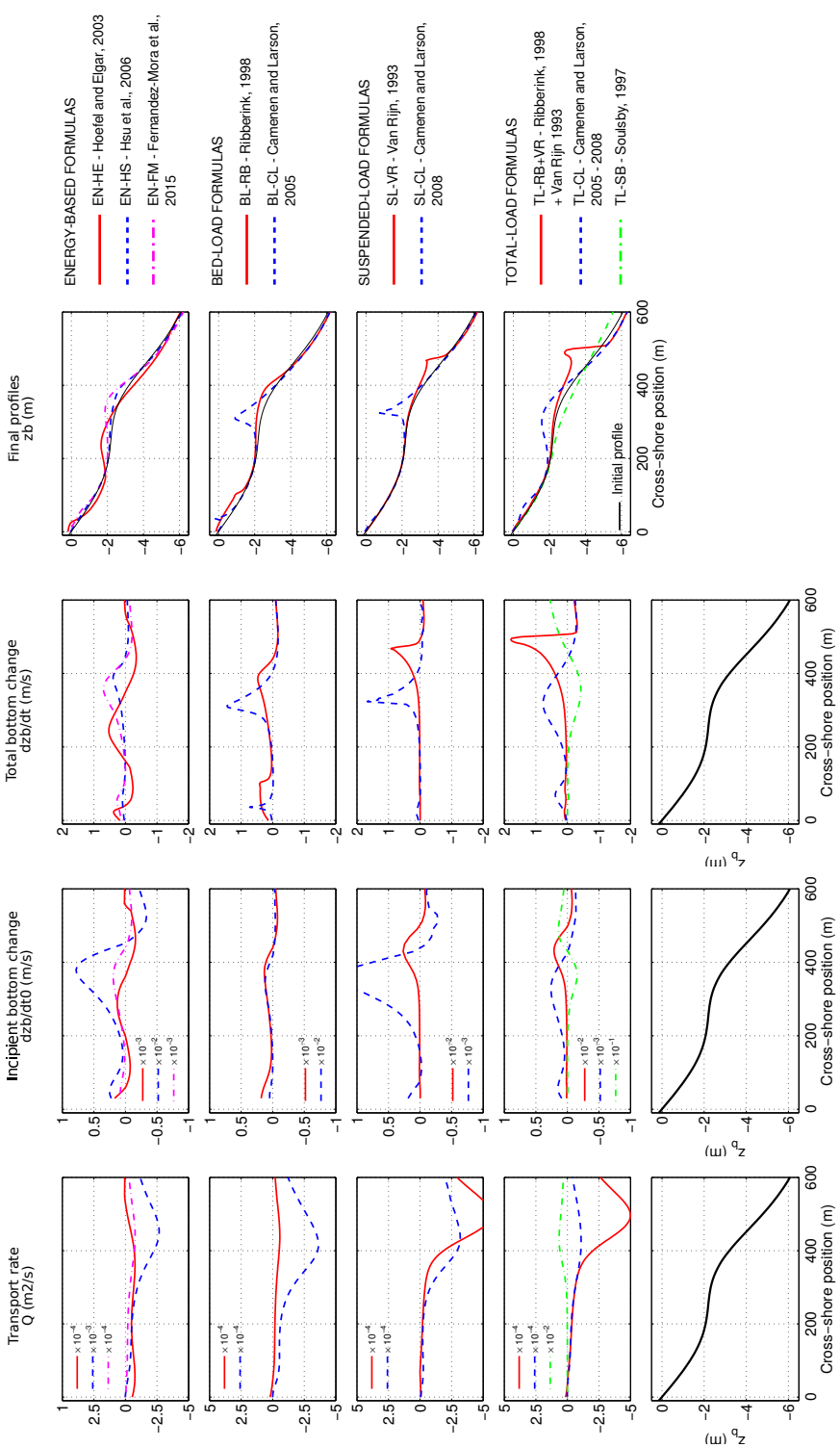

Figure 8.5: Idem Figure 8.2 for the dissipative state sequence S4.

by the formulas. Sediment transport formulas predict properly the transport rates for the conditions in which they were developed, but they often fail under different conditions, and this explains the differences between the predicted transport rates in the sequences.

8.5.2 INCIPIENT BOTTOM CHANGES

By comparing the incipient bottom change, it is found that formulas based on the same physical concepts show relatively similar incipient bottom changes for each sequence. For instance, the EN-HS and the EN-FM formulas and the bed-load transport formulas, which are based on similar physical concepts (wave skewness in the case of the energy-based formulas, and bed-shear stresses in the case of the bed-load formulas), drive qualitatively similar incipient bottom changes for all the sequences, differing only in the magnitude of bottom change rate. In case of the suspended-load transport formulas, each one is related to different physical concepts, and the discrepancies between results are further evidenced. The TL-SL formula, that does not account for the wave action in the transport process, results in opposite patterns of bottom changes in all the sequences. On the other hand, the incipient bottom change of the TL-RB+VR and the TL-CL combinations are generally highly influenced by their suspended-load component, specially under high energy conditions (sequences S3 and S4).

8.5.3 LONG-TERM EVOLUTION OF BEACH PROFILES

Regarding the long-term evolution profiles, is it evidenced that the resulting profiles of each sequence are considerably different. This fact points out the strong dependence of the results on the sediment transport formula that is used.

In terms of the cross-shore morphodynamic sequences, it is found a significant matching between predictions and the conceptual model profiles, specially for the accretionary sequences S1 and S2. In the case of the S1 sequence (Figure 8.2), in which a sandbar should be developed, most sediment transport formulas achieve a final barred profile. However, the predicted bar formation process does not capture the expected morphodynamic evolution. Following Short (1999), under these conditions, two erosive zones, the first related to the erosion of sediment from the inner-surf zone towards the breaking point and the second related to the erosion of the shoaling zone towards the breaking point, limit an accretive zone near the breaking point. This pattern produces the formation of the sandbar. However, the mechanism described by the sediment transport formulas in the model differs from this process. In general, most sediment transport formulas develops, in a first instance, a terrace from the shoreline to the breaking point ($x \approx 200$ m). In these conditions, wave breaks close to the turning point of the terrace, which implies a sudden decrease of wave energy. Thus, in the vicinity of the breaking point, the bottom change pattern develops a local maximum near the terrace turning point. This process feedbacks the growth of a breaker bar.

For the S2 sequence, most of the sediment formulas are able to simulate the onshore sandbar migration for this sequence (except the TL-SB formula). Recently, it has been shown that accounting for bed-shear stresses and/or horizontal pressure gradients is essential to properly model the onshore migration of sandbars (Fernandez-Mora *et al.*, 2015*b*). In this sense, the sediment transport formulas that accounts for one (or both) of these processes can reproduce the onshore sandbar migration event (all the formulas except the TL-SB formula).

The final profiles of the S3 and S4 sequences evidence the discrepancies between using the different sediment transport formulas as they lead to significant different beach profiles. This two sequences are characterized by high-energy wave conditions, and under these conditions, mean currents action becomes more relevant than the wave action, or even prevails, enhancing the offshore sediment transport. In this sense, the way that current action is considered in each transport formula affects the final predictions. In the case of the S3 sequence, final profiles show different trends. Most of them predict onshore sandbar migration, while the expected offshore sandbar migration is reproduced by few formulas. In the case of the S4 stage, most of the formulas can not achieve the dissipative state, but they describe part of the process, particularly the offshore sandbar formation and further migration and decay. Formulas that dismiss the action of current (e.g., EN-HE formula), reproduce the opposite sandbar migration, as they enhance the onshore wave-induced transport.

This supports again the idea that sediment transport formulas account for the different processes and transport modes formulas in different ways depending on the coefficients that weight the action of these processes in the sediment transport.

A relevant issue to analyze is the unrealistic profile shapes predicted by some sediment transport formulas in some sequences, i.e., the BL-CL and BL-CL formulas predictions in the S2, the S3 and the S4 sequences (Figures 8.3, 8.4 and 8.5). These unrealistic shapes are characterized by bottom slopes that surpasses the equilibrium slope for non-cohesive sediments (30^0). These results support the relevance of accounting for the effects of gravity and turbulence on the morphodynamic modeling of the beach profile. Accounting for these processes ensures that the bottom slopes do not exceed the equilibrium slope for non-cohesive sediments so unrealistic bottom shapes are avoided.

Another issue to point out concerning the long-term behavior associated to some formulas is that the equilibrium state is reached during the sequences. Under steady mean wave conditions, the spatial derivative $\partial Q/\partial x$ tends to 0 due to the accommodation of the bottom to the incoming waves. This state, in which there is no bottom change, is generally called 'equilibrium profile'.

8.5.4 INCIPIENT BOTTOM CHANGES VS LONG-TERM PREDICTIONS

On comparing the $dzb/dt|_0$ with the final predictions, it is found that the incipient bottom change does not always determine the long-term evolution of the profile. Figures 8.2 to 8.5 panels B and C show the incipient and the long-term bottom changes for each stage ($dzb/dt|_0$ and $dzb/dt|_\infty$, respectively).

The shift in the behavior of the bottom changes during the evolution of the profile is due to the morphodynamic coupling. The profile accommodates to the incoming waves by changing the shape that in its turn affects the hydrodynamics. This fact points out the relevance of keeping in mind the morphodynamic coupling on modeling the beach profile evolution and the sediment transport rates.

8.5.5 THE RELEVANCE OF THE PHYSICAL PROCESSES

The difficulty of properly predict the morphodynamic changes of beach profile relies on the way the processes involved in the sediment transport are accounted for on computing transport

rates.

In the case of the models of EN-HS and EN-FM, they account directly for the action of the near-bottom motions in terms of bed-shear stresses (velocity skewness). However, both formulas consider both transport modes, but, while the EN-HS formula enhances the bed-load mode, the more relevant driver of sediment transport in the EN-FM formula is the suspended-load component. Furthermore, the EN-FM combination also considers the action of acceleration skewness. In this way, this combination enhances the action of intra-wave oscillatory velocity. Regarding the bed-load formulas, and including here the EN-HE bed-load transport, while the BL-RB and the BL-CL formulas are related to the velocity skewness through the bed-shear stresses, the EN-HE formula is directly related to the acceleration skewness (pressure gradients). Furthermore, the BL-RB and the BL-CL formulas account for the non-linear interaction of waves and currents, while the EN-HE formula just accounts for the acceleration skewness (related to waves stirring). The SL-VR formula accounts for the Stokes drift by the parameterization of the vertical distribution of the mass flux. On the other hand, the TL-SB formula, that was developed for conditions in which currents action prevails over waves action, dismisses the orbital motion due to waves.

8.6 CONCLUSIONS

In the present work, some of the most widely used sediment transport formulas are qualitatively compared in terms of the sediment rate and the morphodynamic evolution that they describe.

Results point out that sediment transport rates may differ two orders of magnitude for each sequence, which supports the findings of previous works on the comparison of sediment transport rates (Van Rijn *et al.*, 2001; Davies & Villaret, 2002). Besides, sediment transport formulas that account for similar processes, agree in the shape of the corresponding 'incipient bottom changes'. However, this usually mismatches with the representative expected behavior for each sequence, particularly for the high energy sequences (S3 and S4), and the final predicted profile for each sequence clearly mismatch between formulas. This indicates that the prediction of long-term beach profiles depends on the sediment transport formula used in the morphodynamic model. Besides, the incipient bottom changes do not always reflect the final overall changes in the profile, which enhances the relevance of the morphodynamic coupling.

Comparing the results with the expected behavior at each sequence, some trends are captured by some of the formulas, specially in the accretionary sequences. Particularly the formulas that account directly for the effects of velocity an acceleration skewness, such as Ribberink (1998); Hsu *et al.* (2006); Fernandez-Mora *et al.* (2015*b*) result in the best predictions for most of the sequences.

Note that the results presented in this work are limited to the sequences under idealized condition (steady mean wave conditions, longshore uniformity and synthetic topographies). Further efforts should be done to determine differences between the predictions of different transport formulas for real cases, that involve variable wave conditions, tide effects, 3D dynamics and the differences between the morphodynamics derived from each sediment transport formulas should be examined in a quantitative way. Furthermore, it would be interesting to extend the comparison to recent sediment transport formulas that account for the effects of pressure gradients in the bed-shear stress definition or the phase lag in suspended-load (Van der A *et al.*,

2010*b*; Abreu *et al.*, 2013).

CHAPTER 9

CONCLUSIONS

9.1 OVERALL CONCLUSIONS

The main objective of this thesis has been to get more insight into the physical processes involved in the cross-shore beach profile morphodynamics through numerical modeling. To this end, a process-based model for the evolution of the profile has been developed.

The AMORFO70 model is based on: 1) phase-averaged wave description, 2) mean depth-averaged hydrodynamics, 3) cross-shore sediment flux computation and 4) bed updating according to sediment mass conservation. In this way waves, mean hydrodynamics and bed evolution are fully coupled. The mean hydrodynamics is given by the depth- and wave- averaged momentum and mass balance equations. The wave description uses the wave and roller energy balance, Snell's law and the dispersion relation. It has been proven that the model is able to reproduce short- and mid-term events with substantial accuracy.

During the development of this thesis, a new parameterization for the intra-wave near-bottom velocity came out (Abreu *et al.*, 2010; Ruessink *et al.*, 2012). Previous studies had evidenced the relevance of the intra-wave processes in the sediment transport and morphodynamic processes and, particularly, the shape on the intra-wave near-bottom velocity and acceleration (Hoefel & Elgar, 2003; Hsu *et al.*, 2006). The addition of this novel parameterization to the process-based model improved substantially the morphodynamical prediction of the model. What is more relevant is that it provided new research lines to the thesis, such as the analysis of the effects of the shape of the intra-wave near-bottom velocities and accelerations on cross-shore morphodynamics. Accounting for both velocity and acceleration skewness in the sediment transport is essential to properly simulate onshore sandbar migration and the entire profile. Results have shown a strong spatial dependence of sediment transport along the profile, in such a way that the shoaling zone transport is mostly driven by bed-shear stress (velocity skewness) and the breaking and inner-zone transport is dominated by pressure gradients (acceleration skewness).

In order to analyze the differences between the morphodynamic predictions related to different sediment transport formulas for different wave conditions and bathymetries, the AMORFO70 model has been complemented with several transport parameterizations. Results evidenced several differences between the predicted transport rates and also between the predicted in-

cipient bottom changes related to the different sediment transport formulas. Remarkably, it is found that the cross-shore morphodynamic predictions strongly depend on the sediment transport formula that is used. Besides, not all the morphodynamic predictions related to the sediment transport formulas capture the expected trends for the studied sequences. Particularly, formulas that account directly for the effects of wave velocity and acceleration skewness lead to the best predictions, specially for accretionary sequences.

9.2 SPECIFIC ANSWERS TO THE RESEARCH QUESTIONS

1. **Which is the morphodynamic prediction of beach profile evolution by using different sediment transport formulas? Which are the main differences and resemblances? Do the different predictions match with the expected trends for accretionary and erosive sequences?**

   Several sediment transport formulas have been compared in terms of the predicted transport rates, the incipient bottom changes and the beach profile evolution for four representative beach profile evolution sequences: the sandbar formation, the onshore and offshore sandbar migration and the terrace shaping. Results have evidenced that predicted sediment transport rates may differ by two orders of magnitude. This supports previous works on the comparison of predicted rates of sediment transport formulas with data-driven models. Also, this evidences that sediment transport formulas are developed and calibrated for rather limited conditions, for which they properly predict the sediment transport rates. However, they can fail on the prediction for other wave conditions, which enhances the idea that they have to be calibrated for each case. Despite the difference in magnitude, it is found an overall agreement in the shape of the distribution of Q_x along the profile and in the corresponding incipient bottom change. Nevertheless, it has been demonstrated that the long-term prediction of the evolution of the cross-shore beach profile depends on the sediment transport formula that is used in the morphodynamic model. Interestingly, the incipient bottom changes do not always reflect the final overall changes in the profile. This enhances the relevance of morphodynamic coupling on modeling beach morphodynamics.

   Comparing the model results with the expected behavior for each sequence, some formulas capture the corresponding trends. It is found that sediment transport formulas that accounts directly for the effects of wave velocity skewness (bed-shear stresses) and/or acceleration skewness (pressure gradients), lead to better predictions (i.e., the energy-based formulas of Hsu *et al.* (2006) formula and the Fernandez-Mora *et al.* (2015*b*) combination, and the Ribberink (1998) bed-load formula), particularly in the accretionary sequences.

   However, erosive sequences are not properly predicted. The recent improvements on hydrodynamic modeling, particularly the addition of the intra-wave near-bottom velocity parameterization, have brought to light that the undertow values predicted by the available parameterizations are too weak to balance the net onshore velocities driven by the the near-bottom velocities. A way to avoid this problem and properly predict erosive sequences is through a specific calibration of the sediment transport formulas to enhance the action of currents respect to the wave oscillatory flow (Dubarbier *et al.*, 2015).

2. **In which way the addition of the intra-wave near-bottom velocities that account for the wave velocity and acceleration skewness improves cross-shore morphodynamics modeling? Which is the effect of wave velocity and acceleration skewness on nearshore morphodynamics?**

   The addition of this novel parameterization on the process-based model has helped to improve the morphodynamics and provided new research lines to the thesis, such as the analysis of the effects of the shape of the intra-wave near-bottom velocities and accelerations on cross-shore morphodynamics. Previous studies had pointed out previously the relevance of the intra-wave processes in the sediment transport and the morphodynamic processes, specially, the shape of the intra-wave near-bottom velocity and acceleration (Hoefel & Elgar, 2003; Hsu *et al.*, 2006). It is found that an accurate description of the near-bottom velocity is essential to properly predict cross-shore beach profile morphodynamics, and particularly the degree of skewness of the near-bottom velocity and acceleration. Accounting for either one or the other process on sediment transport computing allows to properly simulate onshore sandbar migration events, although they can lead to significant mismatches away from the bar zone. Nevertheless, the joint action of both velocity and acceleration skewnesses effects improves the predictions of the onshore sandbar migration and it is essential to accurately model the evolution of the entire cross-shore profile.

   Also, it is found that the sediment transport has a remarkable spatial dependence related to the wave propagation along the profile, and thus, respect the cross-shore distribution of wave velocity and acceleration skewness. In the shoaling zone, wave velocity skewness, directly related to bed-shear stresses, dominates the sediment transport. On the contrary, the breaking and inner-surf zone are dominated by the wave acceleration skewness and sediment transport is mainly induced by pressure gradients.

   Additionally, bearing in mind that the Hoefel & Elgar (2003) parameterization is a proxy of the energy-based bed-load transport directly related to the acceleration skewness, we have found a proxy of the energy-based suspended-load transport that is linearly related to the wave velocity skewness.

3. **Can we neglect alongshore variability on modeling the short-, mid- and long-term cross-shore profile evolution?**

   The hypothesis that the alongshore processes can be neglected for the prediction of the mean profile evolution has been analyzed through the simulation of a long-term (150 days) event that comprises an onshore sandbar migration stage, a 'terrace-shaping' stage and an offshore sandbar migration stage. The analysis has been done for multiple profiles along the beach and the corresponding mean profile (method A) has been compared with the average of the evolution of the individual profiles (method B).

   It is found that the model is able to reproduce the short-term onshore migration event for all the cases. The introduction of the effects of wave velocity and acceleration skewness through the Abreu *et al.* (2010) parameterization allows to simulate net onshore sediment transport fluxes and thus, the onshore migration of the sandbar. For the mid-term evolution, the average of the evolution of the individual profiles (method B) results in the best prediction. This method is a way to account for the longshore variability of the cross-shore beach profiles. In the long-term, although the predictions of the individual

profiles and the methods A and B agree with the measurements, the morphodynamics described by the model are not realistic. This stresses that the simulated morphodynamics during the long-term evolution should be analyzed in terms of the temporal evolution to avoid mistakes in the interpretation of model capabilities. These differences between real and modeled morphodynamics can be due to dismissing swash-zone and inter-tidal processes that cause the formation of inter-tidal sandbars and their further migration towards the surf-zone. The addition of inter-tidal dynamics in the model might improve the long-term predictions.

Previous works on the long-term evolution of the profile (Ruessink *et al.*, 2003; Ruessink, 2005; Ruessink *et al.*, 2007; Dubarbier *et al.*, 2015) use to recalibrate the model and update the bathymetry at some intermediate dates during the simulations. This helps to correct errors during long-term simulations. In our approach, the model has neither been calibrated for the conditions of the event, nor updated in intermediate dates, leaving the free parameters set to the original values given by the authors.

9.3 FURTHER RESEARCH

9.3.1 THE UNDERTOW PROBLEM

Previously to the introduction of wave velocity and acceleration skewness in beach profile evolution models, accretionary sequences were difficult to simulate, as predicted offshore directed velocities related to the undertow were stronger than predicted onshore velocities. This prevented to correctly simulate onshore-directed transport fluxes. To be able to simulate accretionary sequences, morphodynamic models included transport parameterizations or were calibrated in order to enhance the onshore directed transport.

The recent approximations of the intra-wave near-bottom velocity (i.e. Isobe & Horikawa, 1992; Elfrink *et al.*, 2006; Abreu *et al.*, 2010; Ruessink *et al.*, 2012) have become an essential tool for morphodynamic models but also have revealed that the current parameterizations of the undertow used by wave- and depth-averaged models are not accurate enough to compensate the onshore directed velocities given by the novel intra-wave approximations. In this sense, process-based models can simulate accretionary sequences at present but not erosive sequences (i.e., offshore sandbar migration) if they are not specifically calibrated.

The parameterizations of undertow have been usually developed and tested for flume conditions in which there is a control of the processes and the longshore uniformity is mostly ensured. In nature, the bi-dimensional flow patterns and their complex interaction can not be captured by these parameterizations. In this sense, further work should be focused to improve (derive) the current(new) parameterizations of the undertow.

9.3.2 COMPARISON OF SEDIMENT TRANSPORT FORMULAS IN REAL CONDITIONS

In this thesis, the differences of the morphodynamic prediction of different sediment transport formulas have been analyzed for synthetic conditions. A next step should be the comparison of predicted sediment transport rates and morphodynamics associated to different sediment transport formulas with respect to flume/field measurements.

9.3.3 IMPROVEMENTS IN THE MODEL

An interesting improvement to implement in the model should be to upgrade it to a 2DV model by adding the vertical dimension to the radiation stress and the velocity field in the momentum conservation equations (hydrodynamic module). This can improve the prediction of the Stokes drift and avoid using undertow parameterizations. Regarding the sediment transport module, it would be interesting to complement the model with more recent sediment transport formulas that account for the phase lag effects or pressure gradients effects on the bed-shear stress.

BIBLIOGRAPHY

AAGAARD, T., KROON, A., HUGHES, M. G. & GREENWOOD, B. 2008 Field observations of nearshore bar formation. *Earth Surface Processes and Landforms* **33** (7), 1021–1032.

ABREU, T., MICHALLET, H., SILVA, P., SANCHO, F., VAN DER A., D. & RUESSINK, B. 2013 Bed shear stress under skewed and asymmetric oscillatory flows. *Coastal Eng* **73**, 1–10.

ABREU, T., SILVA, P. A., SANCHO, F. & TEMPERVILLE, A. 2010 Analytical approximate wave form for asymmetric waves. *Coastal Eng.* **657**, 656–667.

AMOUDRY, L. O. & SOUZA, A. J. 2011 Deterministic coastal morphological and sediment transport modeling: A review and discussion. *Reviews of Geophysics* **49** (2), n/a–n/a.

AUSTIN, M., MASSELINK, G., O'HARE, T. & RUSSELL, P. 2009 Onshore sediment transport on a sandy beach under varied wave conditions: Flow velocity skewness, wave asymmetry or bed ventilation? *Marine Geology* **259**, 86–101, doi:10.1016/j.margeo.2009.01.001.

BAGNOLD, R. A. 1963 Mechanics of marine sedimentation. In *The Sea* (ed. M. Hill), pp. 507–528. New York, U.S.A.: Wiley–Interscience.

BAILARD, J. A. & INMAN, D. L. 1981 An energetics bedload model for a plane sloping beach: local transport. *J. Geophys. Res.* **86** (C3), 2035–2043.

BATTJES, J. A., SOBEY, R. J. & STIVE, M. J. F. 1990 Nearshore circulation. In *The Sea: Ocean Engineering Science,* vol. 9, pp. 469–493. John Wiley & Sons, Inc.

BAYRAM, A., LARSON, M., MILLER, H. C. & KRAUS, N. C. 2001 Cross-shore distribution of longshore sediment transport: comparison between predictive formulas and field measurements. *Coastal Eng.* **44** (2), 79–99.

BIJKER, E. W. 1967 Some considerations about scales for coastal models with movable bed. *Tech. Rep.* 50. Delft Hydraulics Laboratory.

BIJKER, E. W. 1968 Littoral drift as function of waves and current. In *Coastal Engineering Proceedings 1968*, pp. 415–435. Am. Soc. of Civ. Eng.

BIRKEMEIER, W., LONG, C. & HATHAWAY, K. 2001 Delilah, duck94 and sandyduck: Three nearshore field experiments. In *Coastal Engineering Proceedings 2001*, , vol. 1.

BLONDEAUX, P. 2001 Mechanics of coastal forms. *Ann. Rev. Fluid Mech.* **33**, 339–370.

BOSBOOM, J., AARNINKHOF, S., RENIERS, A., ROELVINK, J. & WALSTRA, D. 2000 Unibest-tc 2.0, overview of model formulations. *Tech. Rep.*. WL Delft Hydraulics.

BOWEN, A. J. 1980 Simple models of nearshore sedimentation: Beach profiles and longshore bars. In *The Coastline of Canada* (ed. S. B. McCann), pp. 1–11 (Paper 80–10). Otawa, Canada: Geological Survey of Canada.

CABALLERIA, M., FALQUÉS, A., COCO, G. & HUNTLEY, D. A. 2001 A morphodynamic mechanism for transverse bars in the nearshore. In *Coastal Dynamics 2001*, pp. 1058–1067. Am. Soc. of Civ. Eng.

CALVETE, D., COCO, G., FALQUÉS, A. & DODD, N. 2007 (un)predictability in rip channel systems. *Geophysical Research Letters* **34** (5), n/a–n/a, l05605.

CALVETE, D., DODD, N., FALQUÉS, A. & VAN LEEUWEN, S. M. 2005 Morphological development of rip channel systems: Normal and near-normal wave incidence. *Journal of Geophysical Research: Oceans* **110** (C10), n/a–n/a, c10006.

CAMENEN, B. & LARROUDE, P. 2003 Un modèle morphologique côtier pour la création de barres rythmiques. *Revue Française de génie civil* **7/9**, 1099–1116.

CAMENEN, B. & LARSON, M. 2005 A general formula for non-cphesive bed load sediment transport. *Estuarine, coastal and Shelf Science* **63** (doi:10.1015/j.ecss.2004.10.019), 249–260.

CAMENEN, B. & LARSON, M. 2008 A general formula for noncohesive suspended sediment transport. *J. Coastal Res.* **24** (3), 615–627.

CASTELLE, B., MARIEU, V., BONNETON, P., BRUNEAU, N. & GRASSO, F. 2010*a* Modelling beach profile evolution. *La Houille Blanche* **1**, 104–110.

CASTELLE, B., RUESSINK, B., BONNETON, P., MARIEU, V., BRUNEAU, N. & PRICE, T. 2010*b* Coupling mechanisms in double sandbar systems. part 1: Patterns and physical explanation. *Earth Surf. Process. Landforms* **35** (doi: 10.1002/esp.1929), 476–486.

DAVIES, A., VAN RIJN, L., DAMGAARD, J., VAN DE GRAAF, J. & RIBBERINK, J. 2002 Intercomparison of research and practical sand transport models. *Coastal Eng.* **46** (1), 1–23.

DAVIES, A. & VILLARET, C. 1997 *Oscillatory flow over rippled beds: Boundary layer structure and wave-induced Eulerian drift.. Gravity Waves in Water of Finite Depth, Advances in Fluid Mechanics* . Southampton, UK: Computational Mechanics Publications.

DAVIES, A. & VILLARET, C. 2002 Prediction of sand transport rates by waves and currents in the coastal zone. *Continental Shelf Res.* **22** (18–19), 2725 – 2737, physics of Estuaries and Coastal Seas, Volume II: Proceedings of the tenth biennial conference, Norfolk, Virginia, USA, 7-11 October 2000.

DEAN, R. G. 1991 Equilibrium beach profiles: characteristics and application. *J. Coastal Res.* **7** (1), 53–84.

DEAN, R. G. 2002 *Beach nourishment. Theory and practice*. Singapore: World Scientific.

DELTARES-DELFT HYDRAULICS 2007 Delft3d-flow: Simulation of multi-dimensional hydrodynamic flows and transport phenomema, including sediments. *Tech. Rep.*. Deltares, Delft, The Netherlands.

DHI 2004 Recommendations for nourishment strategies. *Tech. Rep.*. HUMOR project, DHI water and environment.

DIBAJNIA, M. & WATANABE, A. 1992 Sheet flow under nonlinear waves and currents. *Coastal Engineering Proceedings 1992* **1** (23).

DOERING, J. & BOWEN, A. 1995 Parametrization of orbital velocity asymmetries of shoaling and breaking waves using bispectral analysis. *Coastal Eng.* **26** (1–2), 15 – 33.

DRAKE, T. G. & CALANTONI, J. 2001 Discrete particle model for sheet flow sediment transport in the nearshore. *J. Geophys. Res.* **106** (C9), 19859–19868.

DUBARBIER, B., CASTELLE, B., MARIEU, V. & RUESSINK, G. 2013 Numerical modelling of pronounced sloping beach profile evolution: comparison with the large-scale BARDEX II experiment. *J. Coastal Res.* **SI 65** (1762-1767), iSSN 0749-0208.

DUBARBIER, B., CASTELLE, B., MARIEU, V. & RUESSINK, G. 2015 Process-based modeling of cross-shore sandbar behaviour. *Coastal Eng.* **95**, 35–50.

ELFRINK, B., HANES, D. M. & RUESSINK, B. G. 2006 Parameterization and simulation of near bed orbital velocities under irregular waves in shallow water. *Coastal Eng.* **53**, 915–927.

ELGAR, S. 1987 Relationships involving third moments and bispectra of a harmonic process. *IEEE Transactions on Acoustics, Speech, and Signal Processing* **ASSP-35**, 1725–1726.

ELGAR, S., GALLAGHER, E. L. & GUZA, R. T. 2001 Nearshore sandbar migration. *J. Geophys. Res.* **106** (C6), 11623–11628.

FALQUÉS, A., IRANZO, V. & MONTOTO, A. 1993 Resonance of longshore currents under topographic forcing. *Physics Fluids A* **5** (12), 3071–3084.

FALQUÉS, A., MONTOTO, A. & IRANZO, V. 1996 Bed-flow instability of the longshore current. *Cont. Shelf Res.* **16** (15), 1927–1964.

FEDDERSEN, F., GUZA, R. T., ELGAR, S. & HERBERS, T. H. C. 2000 Velocity moments in alongshore bottom stress parameterizations. *J. Geophys. Res.* **105** (C4), 8673–8686.

FERNANDEZ-MORA, A., CALVETE, D., FALQUES, A., RIBAS, F. & IDIER, D. 2013 On the predictability of mid-term cross-shore profile evolution. *J. Coastal Res.* **SI 65** (476-481), iSSN 0749-0208.

FERNANDEZ-MORA, A., CALVETE, D. & FALQUÉS, A. 2015*a* Morphodynamical prediction of sediment transport formulas. *Coastal Eng.* Under review.

FERNANDEZ-MORA, A., CALVETE, D., FALQUÉS, A. & DE SWART, H. E. 2015*b* Onshore sandbar migration in the surf zone: New insights into the wave induced sediment transport mechanisms. *Geophysical Research Letters* pp. n/a–n/a.

FOSTER, D. L., BOWEN, A. J., HOLMAN, R. A. & NATOO, P. 2006 Field evidence of pressure gradient induced incipient motion. *J. Geophys. Res.* **111** (C05004), doi:10.1029/2004JC002863.

FREDSOE, J. & DEIGAARD, R. 1992 *Mechanics of Coastal Sediment Transport*, 1st edn. Singapore: World Scientific.

GALLAGHER, E., ELGAR, S. & GUZA, R. T. 1998 Observations of sand bar evolution on a natural beach. *J. Geophys. Res.* **103** (C2), 3203–3215.

GARNIER, R., CALVETE, D., FALQUÉS, A. & DODD, N. 2008 Modelling the formation and the long-term behavior of rip channel systems from the deformation of a longshore bar. *J. Geophys. Res.* **113** (C07053), doi:10.1029/2007JC004632.

GRASSO, F., MICHALLET, H. & BARTHELEMY, E. 2011 Sediment transport associated with morphological beach changes forced by irregular asymmetric, skewed waves. *J. Geophys. Res.* **116** (C03020).

HAIDVOGEL, D., ARANGO, H., BUDGELL, W., CORNUELLE, B., CURCHITSER, E., LORENZO, E. D., FENNEL, K., GEYER, W., HERMANN, A., LANEROLLE, L., LEVIN, J., MCWILLIAMS, J., MILLER, A., MOORE, A., POWELL, T., SHCHEPETKIN, A., SHERWOOD, C., SIGNELL, R., WARNER, J. & WILKIN, J. 2008 Ocean forecasting in terrain-following coordinates: Formulation and skill assessment of the regional ocean modeling system. *Journal of Computational Physics* **227** (7), 3595 – 3624.

HENDERSON, S. M., ALLEN, J. S. & NEWBERGER, P. A. 2004 Nearshore sandbar migration predicted by an eddy-diffusive boundary layer model. *J. Geophys. Res.* **109** (C06024), doi:10.1029/2003JC002137.

HOEFEL, F. & ELGAR, S. 2003 Wave-induced sediment transport and sandbar migration. *Science* **299**, 1885–1887.

HSU, T., ELGAR, S. & GUZA, R. T. 2006 Wave-induced sediment transport and onshore sandbar migration. *Coastal Eng.* **53**, 817–824.

ISOBE, M. & HORIKAWA, K. 1992 Study on water particle velocities of shoaling and breaking waves. *Coastal Engineering in Japan* **25**, 109–123.

KURIYAMA, Y. & NAKATSUKASA, T. 2010 A one-dimensional model for undertow and longshore current on a barred beach. *Coastal Eng.* **10**, 39–58.

LONGUET-HIGGINS, M. S. 1952 On the statistical distribution of the heights of sea waves. *J. Marine Res.* **XI** (3), 245–266.

LONGUET-HIGGINS, M. S. & STEWART, R. W. 1964 Radiation stresses in water waves: a physical discussion with applications. *Deep Sea Res.* **11**, 529–562.

MADSEN, O. S. & GRANT, W. D. 1976 Sediment transport in the coastal environment. *Tech. Rep.*. MIT Ralph M. Parsons Lab., Cambridge, USA.

MARINO-TAPIA, I., RUSSELL, P., O'HARE, T., DAVIDSON, M. & HUNTLEY, D. 2007 Cross-shore sediment transport on natural beaches and its relation to sandbar migration patterns: 1. field observations and derivation of a transport parameterization. *J. Geophys. Res.* **112** (C03001), doi:10.1029/2005JC002893.

MEI, C. C. 1989 *The Applied Dynamics of Ocean Surface Waves*, *Advanced Series on Ocean Engineering*, vol. 1. Singapore: World Scientific.

MEYER-PETER, E. & MUELLER, R. 1948 Formulas for bed-load transport. In *IAHR*. Stockholm.

NAM, P. T., LARSON, M., HANSON, H. & HOAN, L. X. 2009 A numerical model of nearshore waves, currents, and sediment transport. *Coastal Eng.* **56**, 1084–1096.

NAM, P. T., LARSON, M., HANSON, H. & HOAN, L. X. 2011 A numerical model of beach morphological evolution due to waves and currents in the vicinity of coastal structures. *Coastal Eng.* **58** (9), 863–876.

NAM, P. T., OUMERACI, H., LARSON, M. & HANSON, H. 2013 Modeling undertow due to random waves. In *Extended Abstracts of Coastal Dynamics 2013* (ed. P. Bonneton & T. Garlan), pp. 1655–1666.

NICHOLSON, J., BROKER, I., ROELVINK, J., PRICE, D., TANGUY, J. & MORENO, L. 1997 Intercomparison of coastal area morphodynamic models. *Coastal Eng.* **31** (1–4), 97 – 123, doi:10.1016/S0378-3839(96)00054-3.

NIELSEN, P. 1992 *Coastal Bottom Boundary Layers and Sediment Transport*, *Advanced Series on Ocean Engineering*, vol. 4. World Scientific.

PAPE, L., PLANT, N. G. & RUESSINK, B. G. 2010 On cross-shore migration and equilibrium states of nearshore sandbars. *J. Geophys. Res.: Earth Surface* **115** (F3), n/a–n/a, f03008.

PLANT, N. G., HOLLAND, K. T. & HOLMAN, R. A. 2006 A dynamical attractor governs beach response to storms. *J. Geophys. Res.* **33** (L17607), 25575–25587, doi:10.129/2006GL027105.

RAKHA, K., DEIGAARD, R. & BROKER, I. 1997 A phase-resolving cross-shore sediment transport model for beach profile evolution. *Coastal Eng.* **31**, 231–261.

RENIERS, A. J. H. M., ROELVINK, J. A. & THORNTON, E. B. 2004 Morphodynamic modeling of an embayed beach under wave group forcing. *J. Geophys. Res.* **109** (C01030), doi:10.1029/2002JC001586.

RIBAS, F. 2004 On the growth of nearshore sand bars as instability processes of equilibrium beach states. PhD thesis, Appl. Physics Dept., Univ. Politècnica de Catalunya, Barcelona, Spain.

RIBAS, F., DE SWART, H. E., CALVETE, D. & FALQUÉS, A. 2011 Modelling waves, currents and sandbars on natural beaches: the effect of surface rollers. *J. Marine Syst.* **88**, 90–101, doi:10.1016/j.jmarsys.2011.02.016.

RIBBERINK, J. S. 1998 Bed-load trasport for steady flows and unsteady oscillatory flows. *Coastal Eng.* **34**, 59–82.

ROCHA, M., SILVA, P., MICHALLET, H., ABREU, T., MOURA, D. & FORTES, J. 2013 Parameterizations of wave nonlinearity from local wave parameters: a comparison with field data. *J. Coastal Res.* **SI 65** (374–379), iSSN 0749-0208.

ROELVINK, J. A. & BROKER, I. 1993 Cross-shore profile models. *Coastal Eng.* **21**, 163–191.

ROELVINK, J. A. & STIVE, M. J. F. 1989 Bar-generating cross-shore flow mechanisms on a beach. *J. Geophys. Res.* **94** (C4), 4785–4800.

ROELVINK, J. & RENIERS, A. 1995 Report h2130. lip 11d delta flume experiments. a data set for profile model validation. *Tech. Rep.*. Delft Hydraulics, The Netherlands.

RUESSINK, B. G. 2005 Predictive uncertainty of a nearshore bed evolution model. *Continental Shelf Res.* **25**, 1053–1069.

RUESSINK, B. G., COCO, G., RANASINGHE, R. & TURNER, I. L. 2007 Coupled and noncoupled behavior of three-dimensional morphological patterns in a double sandbar system. *J. Geophys. Res.* **112** (C07002), doi:10.1029/2006JC003799.

RUESSINK, B. G., MILES, J. R., FEDDERSEN, F., GUZA, R. T. & ELGAR, S. 2001 Modeling the alongshore current on barred beaches. *J. Geophys. Res.* **106** (C10), 22451–22463.

RUESSINK, B. G., RAMAEKERS, G. & VAN RIJN, L. C. 2012 On the parameterization of the free-stream non-linear wave orbital motion in nearshore morphodynamic models. *Coastal Eng.* **85**, 56–63.

RUESSINK, B. G., WALSTRA, D. J. R. & SOTHGATE, H. N. 2003 Calibration and verification of a wave model on barred beaches. *Coastal Eng.* **48**, 139–149.

SHORT, A. D. 1999 *Handbook of Beach and Shoreface Morphodynamics*. Chichester: John Wiley & Sons, Ltd.

SHORT, A. D. & AAGAARD, T. 1993 Single and multi-bar beach change models. *J. Coastal Res.* **SI 15**, 141–157.

SILVA, P. A., ABREU, T., VAN DER A, D. A., SANCHO, F., RUESSINK, B. G., VAN DER WERF, J. & RIBBERINK, J. S. 2011 Sediment transport in nonlinear skewed oscillatory flows: Transkew experiments. *Journal of Hydraulic Research* **49** (sup1), 72–80.

SOULSBY, R. L. 1997 *Dynamics of Marine Sands*. London, U.K.: Thomas Telford.

STIVE, M. J. F. 1986 A model for cross-shore sediment transport. In *Coastal Engineering Proceedings 1986*, pp. 1550–1564. Am. Soc. of Civ. Eng.

SVENDSEN, I. 1984 Mass flux and undertow in the surf zone. *Coastal Eng.* **8**, 347–365.

SVENDSEN, I. A. & PUTREVU, U. 1995 Surf-zone hydrodynamics. *Tech. Rep.* Res. Report CACR-95-02. University of Delaware.

THORNTON, B. & GUZA, R. T. 1983 Transformation of wave height distribution. *J. Geophys. Res.* **88** (10), 5925–5938.

THORNTON, B. & HUMISTON, R. T. 1996 Bar/trough generation on a natural beach. *J. Geophys. Res.* **101** (C5), 12097–12110.

VAN DER A, D. A., O'DONOGHUE, T. & RIBBERINK, J. S. 2010*a* Measurements of sheet flow transport in acceleration-skewed oscillatory flow and comparison with practical formulations. *Coastal Eng.* **57** (3), 331 – 342.

VAN DER A, D., RIBBERINK, J., DER WERF, J. V. & O'DONOGUE, T. 2010*b* New practical model for sand transport induced by non-breaking waves and currents. In *Proceedings 30th International Conference on Coastal Engineering*.

VAN RIJN, L. 1989 Handbook sediment transport by currents and waves. *Tech. Rep.* Rep. H461. Deltares, Delft, The Netherlands.

VAN RIJN, L. C. 1993 *Principles of Sediment Transport in Rivers, Estuaries and Coastal Seas*. Amsterdam, The Netherlands: Aqua Publications.

VAN RIJN, L. C. 2007*a* Unified view of sediment transport by current and waves, i: initiation of motion, bed roughness and bed-load transport. *J. Hydraul. Eng.* **133**, 649–667.

VAN RIJN, L. C. 2007*b* Unified view of sediment transport by current and waves, ii: suspended transport. *J. Hydraul. Eng.* **133**, 668–689.

VAN RIJN, L. C., DAVIES, A. G., VAN DE GRAAFF, J. & RUESSINK, B. G. 2001 *Sediment Transport Modelling in Marine Coastal Environments*. Amsterdam, The Netherlands: Aqua Publications.

VAN RIJN, L. C., WALSTRA, D. J. R., GRASMEIJER, B., SUTHERLAND, J., PAN, S. & SIERRA, J. P. 2003 The predictability of cross-shore bed evolution of sandy beaches at the time scale of storms and seasons using process-based profile models. *Coastal Eng.* **47**, 297–327.

VILLARET, C. & DAVIES, A. G. 2004 Numerical modeling of litoral sand transport. In *Coastal Engineering Proceedings 2004*, pp. 1678–1689. Am. Soc. of Civ. Eng.

DE VRIEND, H., CAPOBIANCO, M., CHESHER, T., DE SWART, H., LATTEUX, B. & STIVE, M. 1993 Special issue coastal morphodynamics: Processes and modelling approaches to long-term modelling of coastal morphology: A review. *Coastal Eng.* **21** (1), 225 – 269.

VAN DER WERF, J., NOMDEM, H., RIBBERINK, J., WALSTRA, D. & KRANENBURG, W. 2012 Application of a new sediment transport formula within the cross-shore morphodynamic model unibest-tc. In *Proceedings 33rd International Conference on Coastal Engineering*.

WRIGHT, D., BOON, J., KIM, S. & LIST, J. 1991 Modes of cross-shore sediment transport on the shoreface of the Middle Atlantic Bight. *Mar. Geol.* **96**, 19–51.

WRIGHT, L. & SHORT, A. 1984 Morphodynamic variability of surf zones and beaches: A synthesis. *Marine Geology* **56** (1), 93 – 118.

YU, J. & SLINN, D. N. 2003 Effects of wave-current interaction on rip currents. *J. Geophys. Res.* **108** (C33088), doi:10.1029/2001JC001105.

APPENDIX A

HYDRODYNAMICS CALIBRATION

The hydrodynamics module of the AMORFO70 model, detailed in Chapter 2, contains semi-empirical parameterizations to describe the hydrodynamic processes that involve calibration parameters which condition. Cross-shore distribution of wave height, set-up/set-down and currents deppend on the calibration of these parameterizations. The calibration parameters are principally B, that controls the wave breaking geometry, the normalized wave height γ_b and the bed roughness z_0. They are related to the wave energy dissipation D_w (Equation 2.20) of Thornton & Guza (1983), the bed shear stresses (Equation 2.22) and the wave boundary layer. Thornton & Guza (1983) set the value of γ_b to 0.42 and suggested the value of $B^3 = 0.8$ for laboratory conditions and to 1.72 for field conditions. The improvements of the AMORFO70 model with respect the model of Thornton & Guza (1983), such as the addition of the wave-current interaction or the rollers effects, makes necessary to calibrate again these variables to ensure the accuracy of the hydrodynamic solution of the model.

This chapter adresses the calibration of these parameters in the AMORFO70 model. In Section A.1, the real data selected and the methodology of the calibration are described and results are summarized in Section A.2.

A.1 EXPERIMENTAL SET-UP

Hydrodynamic calibration has been done with the data provided by the FRF Field Research Facility of the USACE-ARMY at Duck, North Carolina. The bathymetric and hydrodynamic data used for the calibration was obtained at the FRF Duck facility at Duck, North Carolina, from August to November 1997 during the SandyDuck97 experiment (Birkemeier *et al.*, 2001). Wave height and long-shore currents data were obtained by the pressure gauges and currentmeters of the SPUV array during the experiment. Surveys were conducted by using the Coastal Research Amphibious Buggy (CRAB) over a serie of 36 cross-shore lines during the experiment, which extend from the dune to approximately 950 m offshore and are located over the position of the SPUV array (see Figure A.1). Offshore wave conditions were measured by a 3 km offshore wave rider buoy in service since 1986 (providing directional data since 1997). Measured tide was provided by the NOAA tide station at Duck (operating since 1981). The root mean squared wave height $H_{rms,0}$, the peak period T_p, the wave incidence

Figure A.1: Location of the FRF at Duck,NC, and position of the reference profile for the hydrodynamics calibration during the SandyDuck'97 experiment (source: Google Earth).

angle θ_0 and the tides for each bathymetry are shown in Table A.1.

For each set of data (bathymetry, waves heights, currents), more than 32.000 iterations of the hydrodynamic module have been performed for each profile, related to the combinations of the variables concerned and covering an extended space of values for each free parameter: $0.4 \leq B^3 \leq 3$, $0.4 \leq \gamma_b \leq 1$, $0.005 \leq z_0 \leq 0.1$.

The accuracy of the hydrodynamic results has been computed through the normalized mean squared error (hereinafter NMSE) as follows

$$\mathrm{NMSE_p} = \frac{1}{\mathrm{n}} \sum_{1}^{\mathrm{n}} \frac{(\mathrm{p_i^{obs}} - \mathrm{p_i})^2}{(\mathrm{p_i^{obs}})^2} \tag{A.1}$$

where p_i is the predicted value of the variable, p_i^{obs} is the measurement of the variable both at the gauge i, and n is the number of gauges along the profile. For each data set, the NMSE is computed in terms of wave height $\mathrm{NMSE_H}$, the longshore current $\mathrm{NMSE_V}$ and the total error $\mathrm{NMSE_T}$. The latter accounts for the contribution of both the wave height and longshore currents errors as follows

$$\mathrm{NMSE_T} = \sqrt{\mathrm{NMSE_H^2} + \mathrm{NMSE_V^2}} \tag{A.2}$$

The offshore wave conditions have been divided into high energy and low energy events ($H_{rms,0} > 1.5\mathrm{m}$ and $H_{rms,0} < 1.5\mathrm{m}$, respectively). In this way, the best fitting of parameters is considered for the high energy conditions, for the low energy conditions and also for both conditions.

A.2 RESULTS

Figure A.2 shows the minimum NMSE values of the model results in terms of the wave height, the longshore current and the total NMSE respect to the B^3 and γ_b parameters for the high

Table A.1: Date and offshore wave conditions of the 36 surveys during the SandyDuck97 experiment.

Date and time (Day/Hour)	H_s (m)	T_p (s)	θ_0 (deg.)	$z_{s,0}$ (m)	Data and time (Day/Hour)	H_s (m)	T_p (s)	θ_0 (deg.)	$z_{s,0}$ (m)
97/08/07 09:33	0.84	4.17	20	0.73	97/10/05 06:21	0.36	6.58	-36	0.36
97/08/15 12:54	0.39	5.23	-30	0.00	97/10/08 10:14	0.69	9.7	-10	0.54
97/08/28 08:15	0.78	8.16	0	0.25	97/10/09 09:14	0.78	8.86	-8	0.34
97/09/13 12:06	0.87	12.0	-20	0.23	97/10/12 09:31	1.01	10.72	-18	-0.19
97/09/16 12:01	0.59	10.7	-16	-0.48	97/10/13 09:35	0.71	9.7	14	0.29
97/09/22 12:42	0.81	7.55	12	0.70	97/10/14 09:54	0.49	8.86	2	0.23
97/09/23 10:19	0.57	8.16	0	0.27	97/10/17 13:51	1.54	10.72	10	-0.09
97/09/24 12:54	1.04	5.80	26	0.76	97/10/18 09:45	1.84	6.58	16	1.27
97/09/25 10:12	0.90	6.58	2	0.11	97/10/21 07:12	1.80	13.56	-6	0.26
97/09/26 10:05	0.38	7.55	6	0.07	97/10/22 11:00	1.07	12.0	-24	0.44
97/09/27 12:09	1.12	4.54	10	0.20	97/10/23 12:10	0.84	12.0	-24	0.01
97/09/28 11:29	1.05	6.58	10	0.08	97/10/24 12:53	0.35	10.72	-12	0.433
97/09/29 09:45	0.38	7.55	-40	0.01	97/10/27 11:08	0.79	8.15	-2	0.01
97/09/30 10:25	0.19	8.15	-36	0.06	97/10/28 08:33	1.56	6.58	20	0.74
97/10/01 09:52	0.50	4.54	44	0.29	97/10/29 10:41	0.43	6.58	20	-0.09
97/10/02 10:21	0.97	6.58	22	0.59	97/11/06 10:52	1.69	5.52	4	0.71
97/10/03 10:09	0.46	12.0	4	0.51	97/11/11 14:09	0.63	4.75	38	0.36
97/10/04 10:13	0.36	15.6	6	0.61	97/11/21 10:50	0.29	8.86	-8	0.08

energy, the low energy and the high+low energy events (for the best fits of the z_0 parameter for the events). Considering the $\mathrm{NMSE_H}$, higher errors result from the solutions of the high energy events (one order of magnitude higher than the $NMSE_H$ of the low and high+low energy events), and are given by high values of B^3 and low values of γ_b. On the contrary, simulations of the low energy and low+high energy events result in higher errors for low values of B^3 and high values of γ_b. In the case of the $\mathrm{NMSE_V}$, it is almost no sensitive to the variations of the B^3 and γ_b parameters for the three cases, as it is controlled by z_0.

The calibration values of the B^3, γ_b and z_0 parameters is set by considering the $\mathrm{NMSE_T}$. For the high energy events, the best fit is given by values of the $[B^3, \gamma_b, z_0]$ set to $[1.1, 0.8, 0.07]$, for the low energy conditions, the best fit is given for values $[0.5, 0.45, 0.045]$, and for the high+low energy conditions, best fit values are set to $[0.5, 0.45, 0.05]$.

Most morphodynamic models that use the Thornton & Guza (1983) formula (Van Rijn *et al.*, 2003), set the value of the B^3 to 1.1. Taking as a reference this value, the best fit of the $\mathrm{NMSE_T}$ for the high energy events is given by $\gamma_b = 0.8$ and $z_0 = 0.07$. In the case of the low energy events, and again considering the reference point $B^3 = 1.1$, the best fit is given by $\gamma_b = 0.6$ and $z_0 = 0.045$, and the best fit for the high+low events is given by $[1.1, 0.6, 0.05]$. Table A.2 summarizes the calibration values of the parameters for high, low and high+low energy conditions. In the model simulations, the value of these parameters switches from the high energy values to the low energy values depending on the off-shore wave conditions.

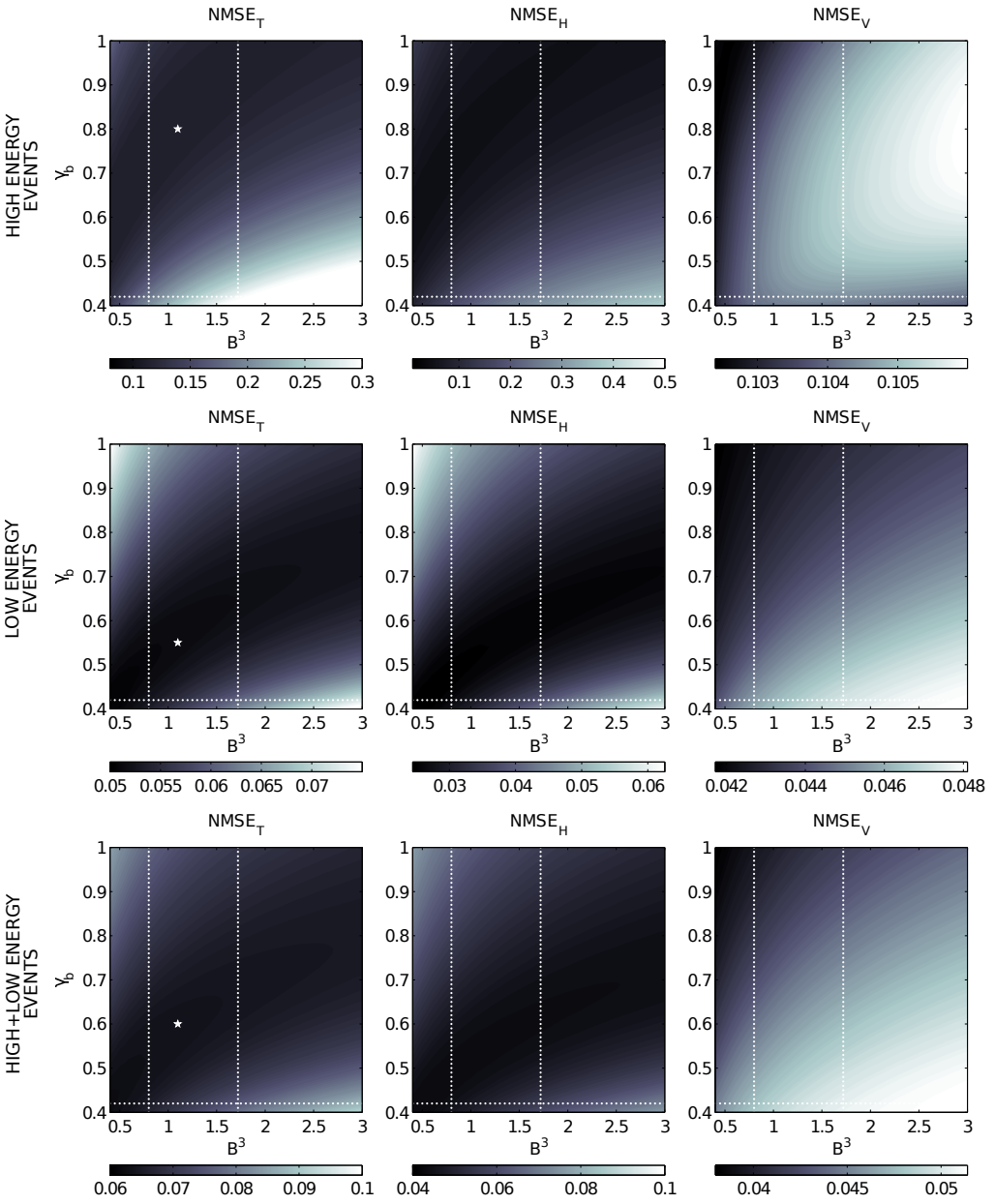

Figure A.2: Minimum normalized mean square errors $\mathrm{NMSE_T}$, $\mathrm{NMSE_H}$ and $\mathrm{NMSE_V}$, respect to the parameter z_0, in terms of the parameters B^3 and γ_b, of the High, the Low and the High+Low events. White lines depict the values of B^3 and γ_b given by Thornton & Guza (1983).

Table A.2: Best fit values of the calibration parameters B^3, γ_b and z_0 of the high energy conditions, the low energy conditions and both conditions. White stars stand for the final calibration points.

	B^3	γ_b	z_0
High energy conditions	1.1	0.8	0.07
Low energy conditions	1.1	0.5	0.045
Both conditions	1.1	0.6	0.05

APPENDIX B

EXPERIMENTAL SET-UP FOR THE RESULTS SHOWN AT CHAPTER 5

B.1 INTRODUCTION

In order to study the behaviour of the free-stream velocity and acceleration approximation of Abreu *et al.* (2010); Ruessink *et al.* (2012) (analyzed at Chapter 5), the model has been forced under several wave conditions and different bathymetries to cover a wide range of wave heights, periods and Ursell number conditions.

In this chapter these experimental conditions used at Chapter 5 are detailed in this Appendix.

B.2 WAVE CONDITIONS

The model has been forced considering normal indcidence of waves 70 ocombinations. Table B.1 summarizes the off-shore conditions considered.

B.3 BATHYMETRIES

Three different bathymetries have been selected to analize the behaviour of the free-stream velocity approximation in the AMORFO70 model: i), a barred profile, ii), a terrace profile, and iii) a exponential profile (see Figure B.1).

Table B.1: Off-shore wave conditions considered.

H (m)	0.5	0.75	1.0	1.25	1.50	1.75	2.0			
T (s)	5.0	6.0	7.0	8.0	9.0	10.0	11.0	12.0	13.0	14.0

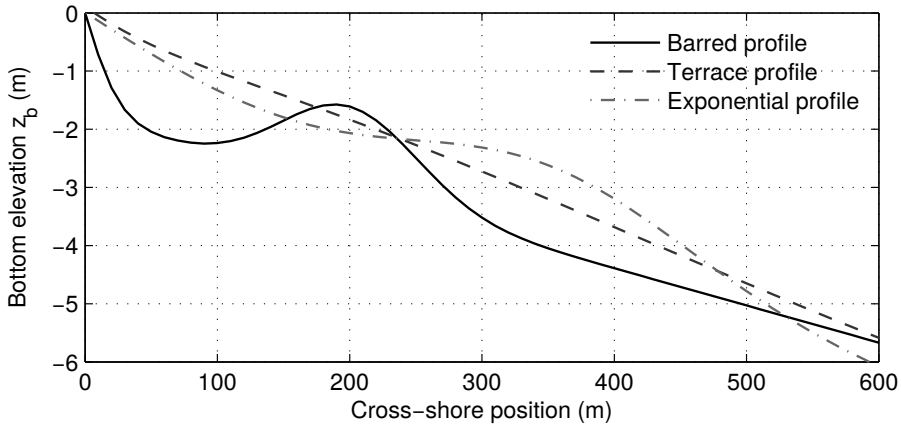

Figure B.1: Experimental bathymetries: barred, terrace and exponential profiles.

APPENDIX C

BED-LOAD AND SUSPENDED LOAD TRANSPORT CONTRIBUTIONS IN THE WAVE AND CURRENTS TRANSPORT TERMS Q_V AND Q_C

---

i

The wave related transport term Q_V given in Equation 6.2 can be split in the bed-load, $Q_{V,B}$, and in the suspended load, $Q_{V,S}$, components that read

$$\begin{cases} Q_{V,B} = \dfrac{C_w}{(s-1)g}\left(\dfrac{\varepsilon_B}{\tan\varphi}\langle|U_0|^2 U_{0,x}\rangle\right) \\ Q_{V,S} = \dfrac{C_w}{(s-1)g}\left(\dfrac{\varepsilon_S}{W_0}\langle|U_0|^3 U_{0,x}\rangle\right) \end{cases} \tag{C.1}$$

where the value of the wave friction coefficient for the best fit of the MiX transportC_w (i.e., $C_w^{MIX} = \alpha_V C_w^{SkV}$) is set to 1.7×10^{-4}. For of the currents transport term Q_C in Equation 4 its corresponding bed-load, $Q_{C,B}$, and suspended load, $Q_{C,S}$, components read

$$\begin{cases} Q_{C,B} = \dfrac{C_c}{(s-1)g}\left(\dfrac{\varepsilon_B}{\tan\varphi}\langle|U_t|^2 U_x\rangle\right) \\ Q_{C,S} = \dfrac{C_c}{(s-1)g}\left(\dfrac{\varepsilon_S}{W_0}\langle|U_t|^3 U_x\rangle\right) \end{cases} \tag{C.2}$$

where the value of the currents friction coefficient for the best fit of the MiX transport C_c (i.e., $C_c^{MIX} = \beta(\alpha_V C_c^{SkV} + \alpha_A C_c^{SkA})$) is set to 2.7×10^{-5}.

Figure C.1 shows the contributions of the different components of Q_V and Q_C in the MiX transport formula during the Duck94 event. Both components of the Q_V term (Figure C.1 B and C) lead to similar cross-shore variations of the MiX transport (Figure C.1 A). However, the $Q_{V,S}$ transport rate is one order of magnitude greater than the $Q_{V,B}$ transport rate, in particular on the vicinity of the sandbar. On the contrary, the Q_C transports are restricted to the inner-surf zone and drives the sediment in the opposite direction.

[i] This chapter is part of the work in Fernandez-Mora *et al.* (2015*b*): Fernandez-Mora, A., Calvete, D., Falques, A. and de Swart H. E. 2015. Onshore sandbar migration in the surf zone: New insights into the wave induced sediment transport mechanisms. Geophysical Research Letters, ISSN 1944-8007, DOI: 10.1002/2014GL063004

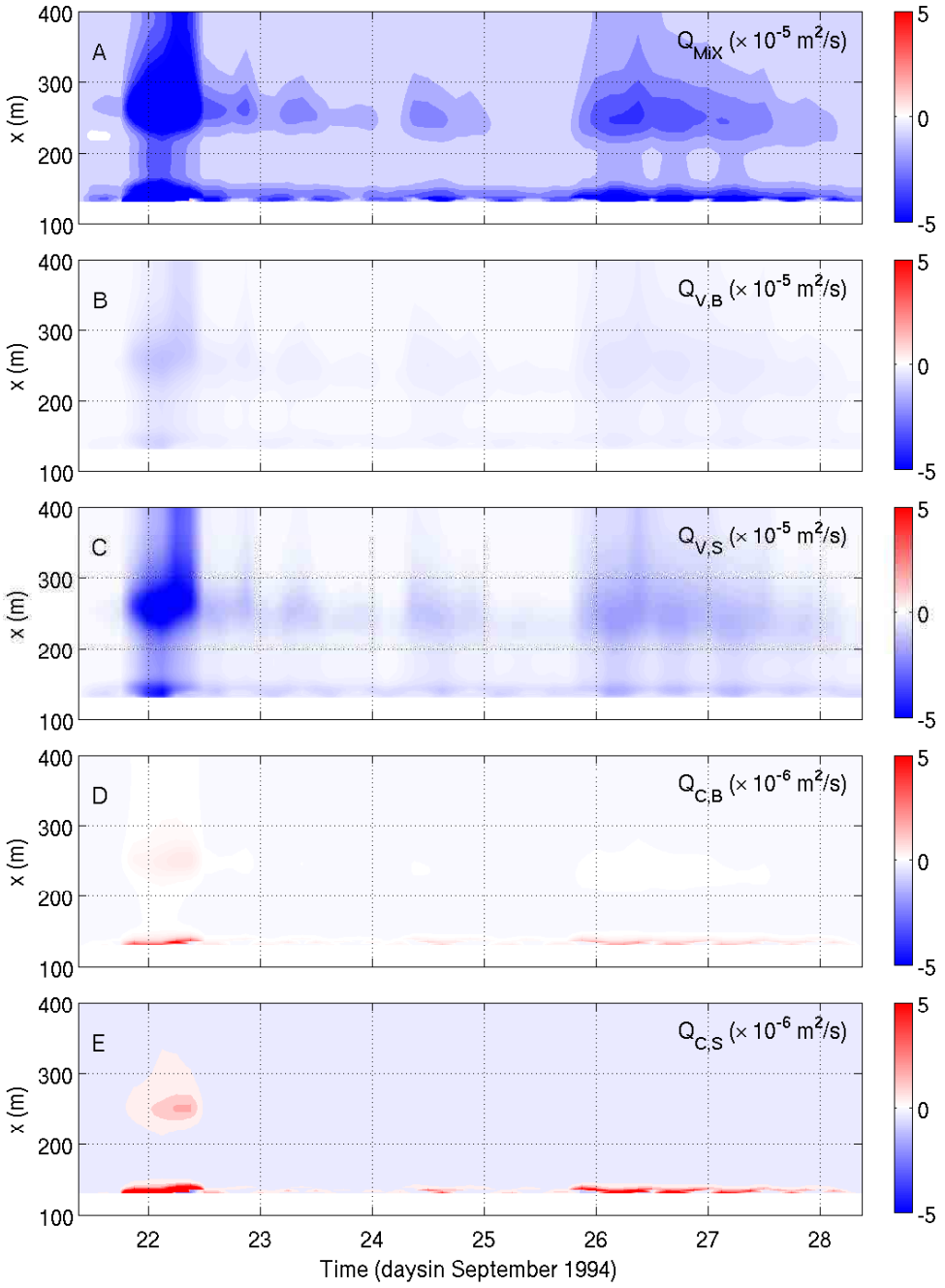

Figure C.1: Sediment transport rates (m^2/s) along the profile during the event corresponding to: A) the MiX total transport Q_{MiX}, B) the wave bead-load component Q_V, B, C) the wave suspended load component $Q_{V,S}$, D) the currents bed-load component $Q_{C,B}$, and E) the currents suspended load component $Q_{C,S}$.

Summarizing, the suspended load components of the MiX transport are larger than the bed-load components. This points out to the relevance of suspended load transport in the sediment transport process during this event. Furthermore, the wave suspended load component $Q_{V,S}$ is noticeably higher than the rest of components.